Molecular modeling of cation–π interactions and ammonium permeation in AmtB

Esam Abd El-Malek Abd-Allah Orabi

A Thesis

In

The Department

of

Chemistry and Biochemistry

Presented in Partial Fulfillment of the Requirements

for the Degree of Master of Science (Chemistry) at

Concordia University

Montreal, Quebec, Canada

April 2011

CONCORDIA UNIVERSITY

School of Graduate Studies

This is to certify that the thesis prepared

By: Esam Abd El-Malek Abd-Allah Orabi

Entitled: Molecular modeling of cation–π interactions and ammonium permeation in AmtB

and submitted in partial fulfillment of the requirements for the degree of

Master of Science (Chemistry)

complies with the regulations of the University and meets the accepted standards with respect to originality and quality.

Signed by the final examining committee:

Ann M. English ___ Chair

Gilles H. Peslherbe Examiner

Peter D. Pawelek Examiner

Guillaume Lamoureux Supervisor

Approved by _____
Chair of Department or Graduate Program Director

_____
Dean of Faculty

Date April 12, 2011

ABSTRACT

Molecular modeling of cation–π interactions and ammonium permeation in AmtB

Esam Abd El-Malek Abd-Allah Orabi

Cation–π interactions are noncovalent interactions known to play various important roles in chemical and biological systems. In proteins, such interactions usually involve Phe, Tyr or Trp in contact with inorganic cations or positively charged amino acids (Arg and Lys). AmtB is a transmembrane protein that has a high affinity for ammonium and facilitates its transport across the membrane which provides a source of nitrogen for amino acid synthesis in bacteria. The amino acid residues that line the pore of the crystallographically-identified outer binding site, S1, of AmtB (Trp148, Phe107, and Phe103) are known to stabilize NH_4^+ through cation–π interactions. However, the nature of the transported species, NH_3 or NH_4^+, and the permeation mechanism are not yet known. In this study, ab initio quantum mechanical calculations at the MP2/6-311++G(d,p) level of theory are performed on the interaction of Li^+, Na^+, K^+ and NH_4^+ with benzene monomer, dimer, and trimer in order to measure the strength of cation–π interactions in these systems and to parameterize a polarizable force field for these interactions. The resulting force field is used to investigate cation–π interactions and their effect on π–π interactions in water. Polarizable potential models for NH_3, Na^+, K^+, and NH_4^+ interacting with H_2O and with model compounds of the amino acids found along the AmtB permeation pathway are also developed based on ab initio calculations on these interactions at the same level of theory. The resulting models are used to investigate the binding selectivity of S1 toward NH_4^+ and the biologically abundant monovalent ions Na^+ and K^+. The nature of the permeable species and possible permeation mechanisms are also investigated based on molecular dynamics free energy calculations.

Acknowledgements

The present study was carried out in the Department of Chemistry and Biochemistry at Concordia University during the period 5/2009−4/2011.

I am most grateful to my supervisor, Professor Guillaume Lamoureux for the chance to work in his laboratory and for his guidance and financial support throughout the course of this research. Especially, I am indebted for his time and effort during the last, tense days.

I wish to thank Professor Gilles H. Peslherbe and Professor Peter D. Pawelek for being on my research committee and for their helpful suggestions during the course of my research.

I sincerely thank all my friends and colleagues in the laboratory of Computational Chemistry for the friendly atmosphere. I would like to express my special thanks to Dr. Shihao Wang, the postdoc in our lab for useful scientific dissections and for his help in writing a script that I used in analyzing some molecular dynamics simulations.

I would also like to thank my friend Jean-François Prieur for his encouragements and his help to set up computers and fix their problems.

Great thanks to my brother, Dr. Mohamed Orabi for his orientations, suggestions, and financial support.

I dedicate this thesis to my wife for her support, encouragement, and understanding during the course of my degree and to my daughters (Nadeen and Yasmeen), my father's spirit, mother, brothers and sisters.

Finally, the financial support from Concordia University, PROTEO, and Québec Ministry of Education and the computational facilities from CERMM and RQCHP are gratefully acknowledged.

Table of Contents

List of Figures

List of Tables

Symbols

$q(A)$	Charge of atom A
$q_c(A)$	Charge of the core particle of atom A
$q_D(A)$	Charge on the Drude particle of atom A
E	Ab initio interaction energy
E^{CP}	Ab initio interaction energy, corrected for basis set super position error
E^{MM}	Interaction energy calculated using the Drude model
E_{syn}	Synergetic stabilization energy
k_D	Force constant of the bond between the core and the Drude particle
r_D	Distance between the core and Drude particle
U	Potential energy function
k_B	Boltzmann constant
k_b	Force constant for a chemical bond
k_θ	Force constant for bond angle
k_{UB}	Urey-Bradley force constant for 1,3 atoms
$Emin_{ij}$	Lennard-Jones well depth for interaction between atoms i and j
$Rmin_{ij}$	Lennard-Jones radius for interaction between atoms i and j
α	Polarizability
ΔG_{hyd}	Free energy of hydration
$\Delta\Delta G_{hyd}$	Relative free energy of hydration
ΔG_{mut}^{wat}	Relative free energy for alchemical ligand “mutation” in water.
λ	Alchemical parameter in free energy calculations

R	Gas constant
T	Temperature
p	Pressure
X	Center of the six membered ring
Y	Equilibrium position of the cation on top of benzene center

Abbreviations

ACh	Acetylcholine
AChE	Acetylcholinesterase
Amt	Ammonia/ammonium transporter
AmtB	Bacterial ammonium transporter
Benz	Benzene
BSSE	Basis set superposition error
CDS	Cambridge Structural Database
CHARMM	Chemistry at HARvard Macromolecular Mechanics
CM	Centre of mass
DNA	Deoxyribonucleic acid
FF	Force field
H-bonded	Hydrogen bonded
His	Histidine
LJ	Lennard-Jones
MA	Methyl ammonium
MD	Molecular dynamics
MEP	Methylamine permeases
MM	Molecular mechanics
MP	Møller-Plesset
NMA	N-methylacetamide
NPT	Constant number of particles, pressure, and temperature
NVE	Constant number of particles, volume, and total energy

NVT	Constant number of particles, volume, and temperature
PDB	Protein data bank
PES	Potential energy surface
Phe	Phenylalanine
PMF	Potential of mean force
QM	Quantum mechanical
RDF	Radial distribution function
Rh	Human rhesus protein
RNA	Ribonucleic acid
Ser	Serine
SWM4-NDP	Simple water model with four sites and negative Drude polarizability
TI	Thermodynamic integration
Trp	Tryptophan
Tyr	Tyrosine
UB	Urey-Bradley
VDW	Van der Waals
WHAM	Weighted histogram analysis method

1. Introduction

1.1. Noncovalent interactions

Noncovalent interactions play major roles in stabilizing biological macromolecules, in receptor-ligand interactions, enzyme-substrate binding, and antigen-antibody recognition.[1] In contrast to covalent interactions that require overlap of partially occupied orbitals of interacting atoms, no overlap is necessary in noncovalent interactions. These interactions are generally weak, compared to covalent interactions.[2,3] While covalent bonds are generally shorter than 2 Å, noncovalent interactions function within a range of several angstroms.[2] Among noncovalent interactions are cation–π, π–π, hydrophobic effect, hydrogen-bonding, and ion-pairing (salt bridge).[1–3]

1.1.1. Cation–π interactions

Cations, from simple ions such as Li^+, Na^+, and K^+ to more complex structures like quaternary ammonium ions and acetylcholine, show strong attraction to the π electrons of organic compounds such as benzene. Such interactions between cations and π systems are generally referred to as cation–π interactions.[1] Cation–π interactions are involved in molecular recognition,[4] stabilization of protein and nucleic acid structures,[5,6] stability of protein-DNA complexes,[4,7] and protein-ligand interactions.[1,8] In addition, the investigation of these interactions can help in finding new binding sites and designing new ligands and drugs.[9] The study on cation–π interactions has thus become a research focus in many fields of chemistry and biology.

Based on the properties of the cation, cation–π interactions are classified into three types[9]: 1) The interaction of inorganic cations such as Na^+, K^+, Ca^{2+} and Mg^{2+} with aromatic systems. An example of this type is the interaction between Mg^{2+} and the sidechain of Phe in a protein crystal structure (Figure 1.1 **a**).[11] 2) The interaction between organic cations and aromatic systems. The binding of acetylcholine (ACh) to the active site of the enzyme acetylcholine esterase (AChE)[1,12] is an example for this type of cation–π interactions. The binding of ACh and other inhibitors with AChE result from the cation–π interaction between the positively charged quaternary ammonium head and the sidechain of Trp84 (Figure 1.1 **b**). 3) The interaction between atoms possessing partial positive charges (e.g. H in H_2O and NH_3) and aromatic systems.[9,10] This third class is energetically weak and can be represented by the complexes formed between NH_3 and benzene (Figure 1.1 **c**).

Although electrostatic forces are considered to play the dominant role in the overall binding,[13] different forces contribute to the total cation–π interaction energy. Thus a quantitative description of cation–π interactions requires additional terms such as polarizabilities to be included.[1] In cation–π systems, electrostatic interactions arise from ion-dipole, ion-quadrupole, and ion-induced dipoles interactions, with ion-quadrupole playing a main role in cation–π attraction. Benzene is a nonpolar molecule; it does not have a permanent dipole moment due to its symmetric charge distribution (Figure 1.2 **a**). The permanent nonspherical charge distribution of benzene (Figure 1.2 **b**) however results in a large quadrupole. Ion-quadrupole interaction is thus the main electrostatic force in cation-benzene complexes.[1,13]

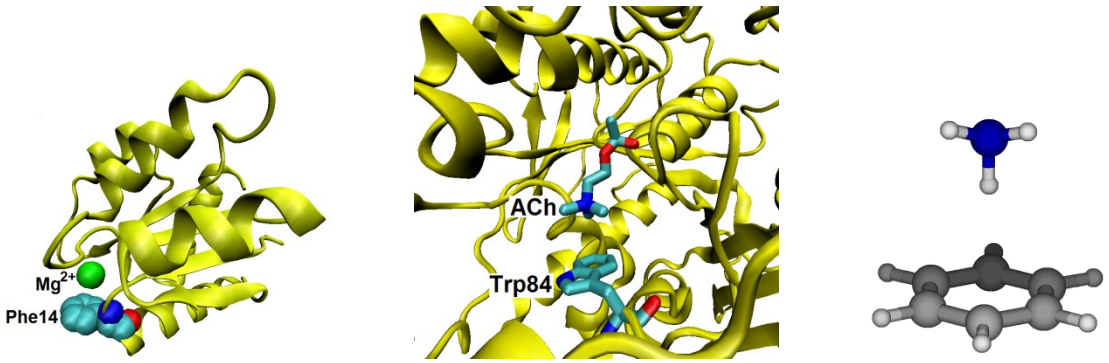

a **b** **c**

Figure 1.1. Examples of cation–π interactions: **a**, interaction between Mg^{2+} and Phe14 in the structure of CheY (PDB code: 1 CHN)[11]; **b**, interaction between ACh and Trp84 in the X-ray structure of Torpedo California AChE (PDB code: 1ACE)[12]; **c**, interaction of NH_3 with benzene.

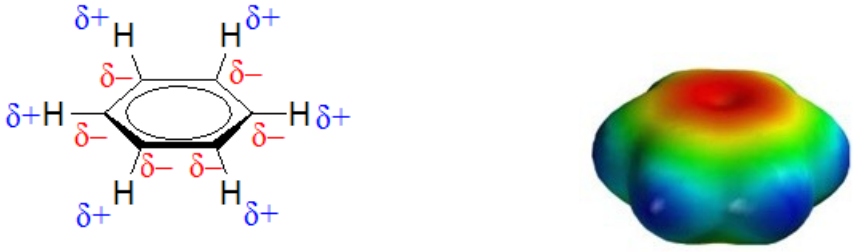

a **b**

Figure 1.2. a, distribution of partial charges in benzene; **b**, electrostatic potential surface of benzene[1] (red = negative and blue = positive).

Polarization is an important factor in determination of the strength of cation–π interaction, due to the strong electric field produced by the cation.[14–16] Other forces such as dispersion and charge transfer are weaker and their contribution to cation–π attraction is minor compared to induction and electrostatic interactions.[16]

1.1.2. π–π interactions

Interactions between aromatic groups (π–π interactions) are important noncovalent interactions.[17] About 60% of aromatic side chains in proteins have been estimated to participate in π–π interactions.[18] These interactions are known to stabilize the structures of DNA, RNA, and proteins.[18,19] π–π interactions also enhance the stability of host-guest complexes[20] and drug-DNA complexation[21]. In biological systems, π–π interactions arise from interactions between the side chains of the aromatic amino acids Phe, Tyr, and Trp. Extensive computational studies on the simplest π–π system, the benzene dimer, have thus been performed in order to understand the energetic and structural properties of these interactions.[17] Figure 1.3 shows three stable binding modes in the benzene dimer, known as: **a**, t-shaped; **b**, parallel-displaced; and **c**, sandwiched.

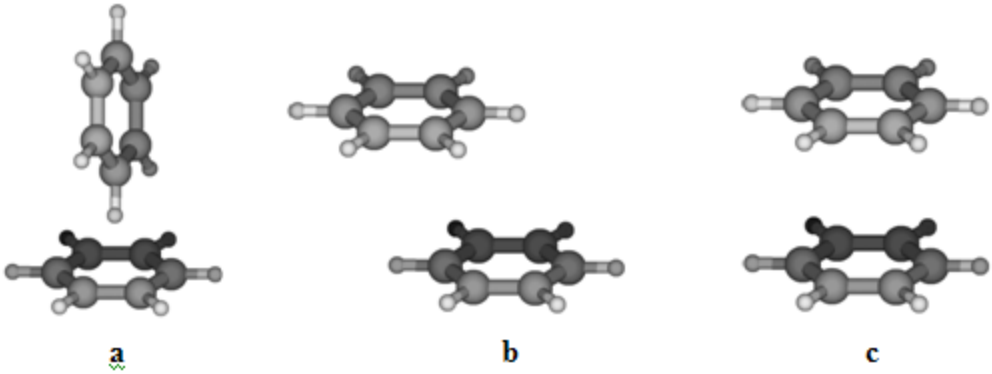

Figure 1.3. Stable configurations of the benzene dimer: **a**, t-shaped; **b**, parallel-displaced; **c**, sandwiched.

1.2. Interplay between noncovalent interactions

The interplay between different noncovalent interactions affects the net stabilization energy of the complex. For example the presence of cation–π and π–π interactions in the same complex results in extra stabilization of the complex, that is, the complexation energy is larger than the sum of the individual complexation energies.[22,23] The extra stability gained from the interplay between the two interactions is known as the cooperativity between these interactions.[22] Cooperativity has also been reported to exist between cation–π interactions and other noncovalent interactions such as H-bonding interactions.[24] Further studies on these cooperativities, especially between cation–π and π–π interactions and investigating their existence in aqueous and biological systems are thus important to elucidate their abundance and functions in biological systems.

1.3. Computational methods for studying cation–π and π–π interactions

Quantum mechanical (QM) calculations have been extensively applied in studying cation–π and π–π interactions, especially in simple complexes.[9,13–17,22–24] Quantum mechanics deals explicitly with electrons and their calculations are thus computationally expensive and become prohibitive for large systems such as biological ones. Molecular mechanics (MM) or force fields (FF), on the other hand treat electrons implicitly and hence their calculations are much faster. Aside from the limitations of FFs, their calculations are less time consuming, in addition it allows for studying large biological molecules with many thousands of atoms.

The fact that polarization represents an important contributing force to cation–π interactions,[14–16] indicates that polarizable FF will accurately model cation–π interactions compared to the additive (non-polarizable) FF. Polarization effects are included in FFs by three groups of methods: 1) Drude oscillator;[25,26] 2) fluctuating charge;[27] and 3) induced point dipole.[28]

1.3.1. Polarization based on the Drude oscillator model

Drude oscillator models, also known as shell models[29] incorporate electronic polarizability by representing a polarizable atom as a two-particle system: a core particle with charge $q_c(A)$ and a shell particle, also called Drude particle, with charge $q_D(A)$, where the sum $q_c(A) + q_D(A) = q(A)$, is the net charge of the polarizable atom.[26,30] The magnitude of both charges is fixed. The core and Drude particle are linked by a harmonic spring with a force constant k_D (Figure 1.4). Thus electronic polarization is mimicked by

relative displacement of both charges due to an external electrostatic field.[29] Atomic polarizability, $\alpha(A)$, is related to force constant k_D and the atomic charge $q(A)$ and is determined by $\alpha(A) = q_D^2(A)/k_D$. The magnitude of k_D is chosen in order to achieve small displacements of Drude particles from their corresponding atomic positions, $\mathbf{r}_D$.[26,30]

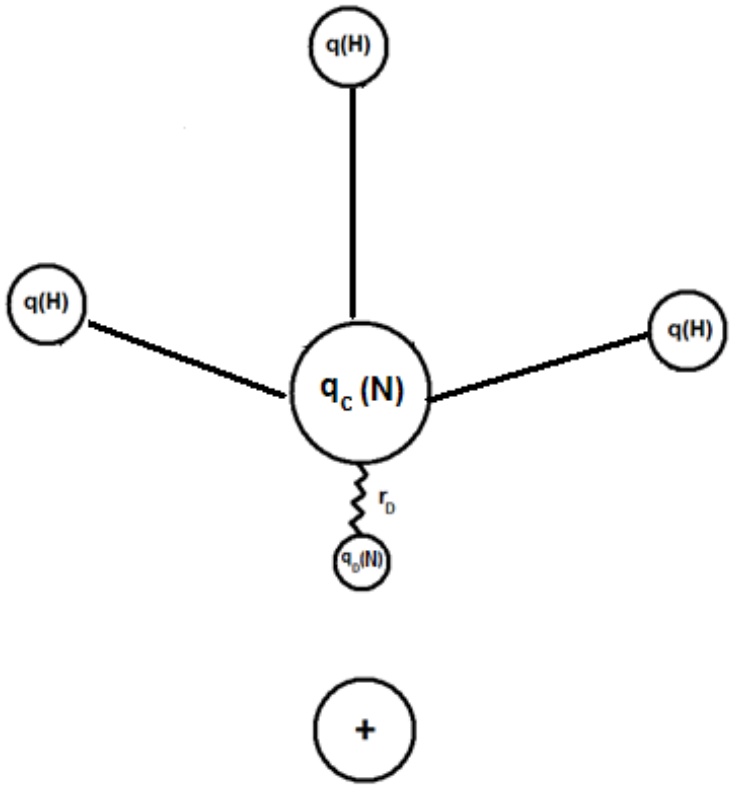

Figure 1.4. Classical Drude oscillator model using NH_3 molecule as an example. The displacement, r_D, of the Drude particle attached to the N atomic center in presence of a cation is presented.

1.4. Ammonia/Ammonium transport proteins

The transport of ammonium and/or ammonia (Amm) through cellular membranes provides a source for nitrogen for amino acid synthesis in plants and bacteria and help to maintain the acid-base equilibrium in animal and humans.[31] This transport is mediated by proteins from the Amt/MEP/Rh family. The X-ray crystallographic structures of AmtB protein from *Escherichia coli*[32,33] and the homologous protein Amt-1 from *Archaeoglobus fulgidus*[34] show that these proteins are homotrimers with one channel at the center of each monomer (Figure 1.5 **a**).

The crystal structure of AmtB determined at 1.35 Å resolution by Khademi *et al.*[32] shows an electronic density in a binding site at the periplasmic side of the channel, known as S1, in addition to electronic densities in three sites, called S2, S3, and S4, that exist in the pore lumen of AmtB (Figure 1.5 **b**). Based on the hydrophobicity of the pore and the fact that this density is observed when the protein was crystallized in presence of an ammonium salt, the authors of the structure have suggested that the electronic density at S2, S3, and S4 corresponds to NH_3 molecules.[32] Other experimental[33] and computational studies[35], on the other hand suggest that these sites are occupied by water molecules. The fact that the three species, H_2O, NH_3, and NH_4^+ are isoelectronic make them indistinguishable, unless hydrogen atoms can be resolved. The identity of the species occupying the pore sites, especially S2 have not been confirmed to date.

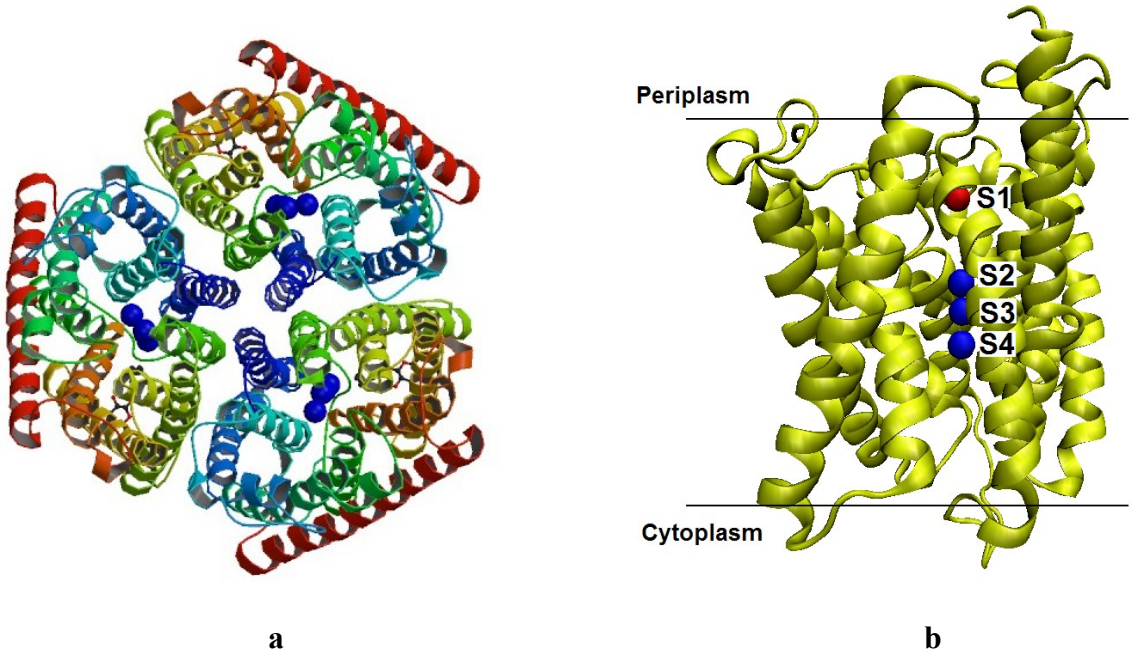

Figure 1.5. Three dimensional fold of: **a**, the AmtB trimer; **b**, the monomeric ammonia/ammonium channel in AmtB (PDB code: 1U7G).[32] The four crystallographically identified sites are presented in **b** as spheres with S1 colored red and S2, S3, and S4 colored blue.

Extracellular ammonia exists predominantly in the positively charged form under physiological pH conditions and thus S1 is known to bind NH_4^+. Experimental studies on the selectivity of Amm transport proteins[36–38] have shown that the periplasmic site of the protein (S1) is selective for NH_4^+ toward most monovalent alkali ions. The results showed that while the biologically abundant ions Na^+ and K^+ do not reach S1 and do not inhibit the protein activity,[36–38] Cs^+ can reach S1 and inhibits the protein activity.[37]

Computational investigations on the selectivity of S1 in AmtB[39,40] on the other hand, have not shown good agreement with the experiments. The results in one study[39]

showed that K^+ can reach S1, in contrast to the experiments. [36–38] In another study,[40] K^+ and Cs^+ were found to possess the same binding affinity to S1, which also does not agree with the experiment.[37] Further computational studies using more reliable FFs are thus required for investigation and understanding the selectivity of these proteins.

While NH_4^+ is known to bind S1 in AmtB, the exact transport mechanism and the identity of the transported species, NH_3 or NH_4^+, have not been identified so far. Three different transport mechanisms have been suggested, namely, the electroneutral NH_3 transport,[32,33] NH_3/H^+ cotransport,[37] and NH_4^+ transport[41].

Computational studies have shown that the free energy barrier for the diffusion of the charged species is prohibitive[42,43] and NH_4^+ has thus to deprotonate along the pathway. The position where the deprotonation occurs and the identity of the proton acceptor however, are not yet identified. Different computational studies suggest that deprotonation occurs at S1 and that NH_3 is the species that penetrates the periplasmic side toward the cytoplasmic one.[42,43] The hydrophobic pore of the channel contains two conserved histidine residues (His168 and His318) that are suggested to play a role in the deprotonation process[35] based on their high conservation[32,33] and based on mutagenesis studies.[44] NH_4^+ is thus believed to be stable enough to reach S2, where deprotonation are suggested to occurs.[35] Reliable calculation of the binding free energy of NH_4^+ in S2 in comparison to that of S1 is expected to give a clear prediction about the possibility of permeation of the ionic species to S2. Such reliable calculations require a FF that is calibrated for interactions of the ion with neighboring amino acid side chains and water molecules in the two sites. To the best of our knowledge such a FF has not been applied in computational studies of AmtB so far.

1.5. Aim of the thesis

Owing to the important roles for cation–π interactions in biological systems, and the computationally prohibitive nature of QM calculation on these systems, we aim in our work to parameterize reliable polarizable models for cation–π interactions. We aim to apply our models to investigate the strength of cation–π interactions and their interplay with π–π interactions in aqueous solutions.

In order to investigate the selectivity, transport mechanism, and the nature of the transported species in AmtB proteins, we aim to parameterize polarizable potential models for the interactions of NH_3, Na^+, K^+, and NH_4^+ with compounds that model the side chains of the amino acids that exist in the permeation pathway. We will apply our models in investigating the binding affinity and selectivity of S1 toward Na^+, K^+, and NH_4^+. The models will also be used to calculate the binding energy of NH_4^+ at S2 compared to S1, in order to investigate the identity of the species that binds S2 and to suggest the most probable deprotonation position and proton acceptor along the permeation pathway.

1.6. Research strategy

- Perform ab initio QM calculations on the interactions of Li^+, Na^+, K^+, and NH_4^+ with benzene monomer, dimer, and trimer and evaluate the strength of cation–π interactions in the gas phase and their cooperativity with π–π interactions.

- Parameterize polarizable models for NH_4^+ and for the interaction of the four cations with benzene as well as for the interaction of NH_4^+ with H_2O based on the ab initio calculations.

- Validate the NH_4^+–H_2O polarizable model by investigating the hydration structure and free energy of hydration of the ion.

- Measure the binding free energy of the four cations with benzene in water using potential of mean force calculations.

- Perform molecular dynamics simulations on $(benzene)_2$ and $NH_4^+(benzene)_2$ complexes in water in order to investigate the interplay between cation–π and π–π interactions in aqueous solutions.

- Ab initio calculations on the interaction of NH_3 with water, ammonia, ethanol, N-methylacetamide, benzene, toluene, phenol, p-methylphenol, indole, 3-methylindole, imidazole, and 4-methylimidazol.

- Parameterize polarizable models for these interactions based on their ab initio properties.

- Validate the NH_3–H_2O potential model by calculation of the free energy of hydration of NH_3.

- Validate the NH_3–NH_3 model by calculating the density, latent heat of vaporization, and the structure of liquid ammonia and comparing with experimental results.

- Ab initio calculations on the interaction of Na^+, K^+, and NH_4^+ with ethanol, N-methylacetamide, benzene, toluene, phenol, p-methylphenol, indole, 3-methylindole, imidazole, and 4-methylimidazol.

- Model the amino acids side chains that exist near S1 and S2 in AmtB with the parameterized polarizable models, using ethanol as model for Ser, toluene for Phe, 3-methylindole for Trp, and 4-methylimidazole for His.

- Investigate the binding selectivity of S1 toward NH_4^+, Na^+, and K^+, via measuring the binding free energy of each ion in S1 relative to that in bulk water.

- Measure the binding free energy of NH_4^+ in S2 relative to that in S1 and identify the identity of the species permeating from S1 to S2.

- Based on the free energy calculations, suggest the most probable position for deprotonation of ammonium along the permeation pathway and suggest the most probable proton acceptor.

1.7. Structure of the thesis

This thesis is based on three manuscripts that are currently in preparation, which are referred to in the text by their Roman numbers:

I **Esam A. Orabi and Guillaume Lamoureux** "Cation–π and π–π interactions in aqueous solution studied using polarizable potential models"

II **Esam A. Orabi and Guillaume Lamoureux** "Polarizable potential for ammonia interacting with water and with amino acid model compounds"

III **Esam A. Orabi and Guillaume Lamoureux** "Ammonium affinity and ion selectivity of the bacterial transporter AmtB studied using a polarizable force field for cation–π interactions"

2. Cation–π and π–π interactions in aqueous solution studied using polarizable potential models

Abstract

New polarizable potential models for NH_4^+ and the interactions of Li^+, Na^+, K^+, and NH_4^+ with benzene as well as for NH_4^+–H_2O interaction are parameterized based on ab initio quantum mechanical calculations at the MP2/6-311++G(d,p) level of theory. The optimized models reproduce the ab initio calculated stabilization energies and potential energy surfaces of these systems. They also reproduce the cooperativity between cation–π and π–π interactions that is observed in ab initio calculations of the four cations in complex with benzene dimer and trimer. These models are applied in investigating cation–π interactions in aqueous solutions by measuring the potential of mean force for each cation in complex with benzene in water. The results show that Li^+ and Na^+ are preferentially solvated by water and do not bind benzene while K^+ and NH_4^+ bind benzene with –1.1, and –1.4 kcal/mol, respectively. Molecular dynamics simulations on NH_4^+ in complex with two benzene molecules in water are performed in order to investigate the interplay between cation–π and π–π interactions in aqueous solutions. The results show that benzene association increases in presence of the cation, confirming the cooperativity of the two interactions in water. The NH_4^+–H_2O interaction model reproduces the experimental hydration structure and free energy of hydration of the ion without further adjustments.

2.1. Introduction

Cation–π interactions are noncovalent interactions defined as the preferential attraction between cations and the π electrons in aliphatic and aromatic compounds.[1,13,45–47] Such preferable association of cations and the π systems of organic compounds have been the subject of experimental[48–68] and computational[14–16,69–76] studies over the last two decades, and their existence has been confirmed experimentally. Experimental studies on cation–π interactions in the gas phase are showing that these interactions are competitive with the strongest known nonbonding interactions.[49,67] Extensive quantum mechanical (QM) investigations in the gas phase have also been performed at different levels of theory,[45–57,59,60,68–76] and the binding enthalpies of alkali metal ions with benzene showed good agreement with the experimental values.[76] QM calculations on cation–π interactions serve thus as a good tool for studying and understanding these interactions.

Different forces contribute to cation–π interactions with electrostatics and polarization being the dominant forces while other forces such as dispersion and charge transfer are much weaker. Dougherty and co-workers performed ab initio calculations on 11 Na^+–π complexes and found that the electrostatic energy represents 40–60% of the total interaction energy.[13] Different theoretical studies showed that polarization is an important factor in determination of the strength of these interactions due to the strong electric field produced by the cation.[14–16,69,70]

Analysis of protein structures in the PDB showed that cation–π interactions are common among protein structures[47,77] and protein-protein interfaces.[78] Cation–π

interactions make important contribution to protein stability,[5,6] stability of protein-DNA complexes,[4,7] protein-protein interfaces,[78] protein folding,[79] molecular recognition,[4] ion selectivity in some channels,[80,81] protein-ligand interactions,[1] and neurotransmitter receptors.[8] Owing to the biological importance of cation–π interactions and the computational prohibition of QM calculations on these systems, molecular models for these interactions are crucial. Since electronic polarization represents an important "force" in cation–π interactions, polarizable potential models are required for accurate modeling of these interactions.[69]

Cation–π interactions can compete with cation-water interactions. For example the enthalpy of formation of benzene–K^+ complex is −19.2 kcal/mol, compared to −17.9 kcal/mol for K^+–H_2O.[82] Cation–π interactions become weaker in aqueous solutions compared to the gas phase,[72] yet their existence in aqueous solution has been confirmed.[83–85] While the computational and experimental literature on cation–π interactions in the gas phase is abundant, studies of these interactions in water are rare[83] and further studies are required for accurate understanding of their strength and existence.

Interplay between noncovalent interactions has been observed to affect the stabilization energy of the complex combining these interactions.[22–24,71] Interplay between cation−π and π−π interactions showed that the two interactions work in cooperative way such that the presence of one interaction strengthens the other with a net increase in the complex stabilization energy.[22,23] The excess amount in the stabilization energy, the difference between the observed stabilization energy and that expected from the simple sum of the individual stabilization energies in each interaction, is called the synergetic energy.[22,23] Though this cooperativity was measured from ab initio

calculations and confirmed by a survey of the Cambridge Structural Database (CSD),[22] no experimental or theoretical investigations on the cooperativity between the two interactions in aqueous solutions have been reported so far.

In this work, we parameterize polarizable empirical force fields for NH_4^+ and for the interactions of Li^+, Na^+, K^+, and NH_4^+ with benzene as well as the interaction of NH_4^+ with H_2O. CHARMM[86] FF is used for this purpose with polarization in the systems based on the classical Drude oscillators.[25,30,87] We then apply these models to investigate and measure the binding between cations and benzene in water and to investigate the interplay between cation–π and π–π interactions in water. We also validate the NH_4^+−H_2O model by calculating the free energy of hydration of the ion as well as its hydration structure. For this purpose, we perform ab initio QM calculation (geometry optimization and potential energy surfaces) at the MP2/6-311++G(d,p) level of theory on the interactions of the four cations with benzene monomer as well as on the NH_4^+–H_2O complex. The calculated ab initio properties of the complexes are then used for parameterization of the polarizable potential models. Molecular dynamics (MD) simulations of NH_4^+, benzene−M^+ (where M^+ is Li^+, Na^+, K^+, or NH_4^+), $(benzene)_2$, and $NH_4^+(benzene)_2$ complexes in water are then performed using the optimized potential models, in order to validate the NH_4^+–H_2O model, measure the strength of cation–π and π–π interactions, and the interplay between the two interactions in water.

2.2. Methods

2.2.1. Ab initio calculations

The geometry of Li^+, Na^+, K^+, and NH_4^+ complexes with H_2O, benzene monomer, dimer, and trimer as well as the water–benzene, benzene dimer, and benzene trimer complexes are fully optimized at the Møller−Plesset (MP2, full electron) level and the 6-311++G(d,p) basis set using Gaussian 09 program.[88] The interaction energies are corrected (E^{CP}) for basis set superposition error (BSSE) by the counterpoise method of Boys and Bernardi.[89] The optimization of Li^+, Na^+, K^+, and NH_4^+ in complex with benzene monomer and H_2O as well as the H_2O–benzene complex is performed without imposing any geometry constraints. The optimization of the alkali metal ions complexes with benzene dimer and trimer are performed imposing C_{6v} symmetry, while C_{2v} symmetry is imposed in optimization of NH_4^+ complexes. Optimization of benzene dimer and trimer are performed imposing D_{6h} symmetry. Cation−$(benzene)_2$ and cation−$(benzene)_3$ systems are considered herein to further investigate the cooperativity between cation–π and π–π interactions[22,23] and to test the performance of the optimized force field models in measuring such cooperativity.

Potential energy surfaces (PESs) of the four cations in complex with benzene monomer and of the NH_4^+–H_2O complex are calculated at MP2/6-311++G(d,p) level of theory and all interaction energies are corrected for BSSE. The curves are computed imposing the gas phase optimized geometries of interacting monomers, calculated at the same level of theory. PESs of the alkali cations in complex with benzene are calculated by scanning both the perpendicular and the parallel movement of the ion, relative to the

benzene plane. Two potential curves are calculated for ammonium ion in complex with benzene. The first curve is calculated by scanning the distance between the nitrogen atom of NH_4^+ in its bidentate conformation and the center of the benzene molecule (X). The second curve is calculated by scanning the angle X···N–H in order to investigate the interaction energy as a function of the orientation of the ion (unidentate, bidentate, or tridentate) on top of benzene surface. Two curves are calculated for NH_4^+–H_2O complex by scanning the N···O distance and the orientation of NH_4^+ (unidentate, bidentate, or tridentate) relative to O.

2.2.2. Molecular mechanical calculations

2.2.2.1. Potential energy function and parameterization strategy

Molecular mechanics (MM) calculations are all performed with the program CHARMM.[55] Polarizable force field models based on classical Drude oscillators[25,30,87] are parameterized for NH_4^+ and the interactions of the four cations (Li^+, Na^+, K^+, and NH_4^+) with benzene and for NH_4^+–H_2O complex. In the Drude oscillator model polarizability is introduced by attaching fictitious, charged particles to all nonhydrogen atoms via a harmonic spring with force constant k_D. The partial charge of the polarizable atom q is redistributed between the Drude particle and the atom core with the Drude charge q_D being determined from the atomic polarizability via the relation $\alpha = {q_D}^2/k_D$. The net charge of the atomic core is thus $q_c = q - q_D$. A separation r_D between the Drude particle and the polarizable atom results in a dipole $q_D r_D$. The electrostatic energy

term in the additive potential energy function is modified to include interactions between atomic cores and Drude particles. A term describing the self-energy of a polarizable atom ($\frac{1}{2}k_D r_D^2$) is also added to the potential energy function.[30] The resulting potential energy function can be written as following:[30,90]

$$U(R) = U_{ion,self}(R) + U_{ion,solvent}(R) + U_{solvent}(R) \quad (1)$$

Where

$$U_{ion,self}(R) = \frac{1}{2}k_D\left|\mathbf{r}_{ion} - \mathbf{r}_{D,ion}\right|^2 + \sum_{NH\ bonds} k_b(b - b_0)^2 + \sum_{HNH\ angles} k_\theta(\theta - \theta_0)^2 + \sum_{HH\ pairs} k_{UB}(s - s_0)^2 \quad (2)$$

in which the last three terms are for NH_4^+ only (b are NH bond lengths, θ are HNH angles, and s are HH distances) and

$$U_{ion,solvent}(R) = \sum_{j=1}^{N}\sum_i\sum_s\left(\frac{q_{ci}q_s}{|\mathbf{r}_i - \mathbf{r}_{js}|} + \frac{q_{D,j}\,q_s}{|\mathbf{r}_{D,j} - \mathbf{r}_{js}|}\right) + \sum_{j=1}^{N}\sum_i\sum_s Emin_{is}\left[\left(\frac{Rmin_{is}}{|\mathbf{r}_i - \mathbf{r}_{js}|}\right)^{12} - 2\left(\frac{Rmin_{is}}{|\mathbf{r}_i - \mathbf{r}_{js}|}\right)^{6}\right] \quad (3)$$

in which N is the number of solvent molecules, i is the atomic site of the ion (Li, Na, K, H, N), and s is the solvent molecule site (atom, lone pair, Drudes). The third term in equation 1, $U_{solvent}(R)$, is similarly obtained as the sum of bonded and nonbonded energy terms that correspond to interaction between atoms in the solvent molecules. Parameters in these equations and their definition can be found in references 30 and 90.

Table 2.1. Potential model for polarizable ammonium ion.

Atom	q (e)	Emin (kcal/mol)	Rmin/2 (Å)	α (Å^3)
N	–1.57652	2.38702956	1.3062713	–1.1966
H	0.64413	0.00399783	1.0870509	0.0000

Parameters for NH_4^+ potential (this work) are summarized in table 2.1. In this model, NH_4^+ is modeled by five atomic sites and an auxiliary Drude particle attached to the nitrogen atom. Urey-Bradley (UB) energy terms[90] are added to reproduce some IR frequencies of the ion and to prevent large distortions in its regular tetrahedral structure. The electrostatic parameters, atomic charges and polarizabilities (Table 2.1) are determined from ab initio calculation. The atomic charges are fitted to reproduce the gas phase quadrupole moment of the ion and the polarizability of N is calculated from the trace of the polarizability tensor. Finally the Lennard-Jones (LJ) parameters of N and H are optimized based on the interaction of the ion with benzene.

Parameters of the alkali metal ions and benzene are taken from references 91 and 92. An extra non-atomic site (X) at the center of the benzene ring is required in order to accurately model the interactions with Na^+ and NH_4^+. This site can be considered as a mimic of the electron density at the center of the benzene ring. It shows only VDW interaction with Na^+ and with N and H atoms of NH_4^+.

The general parameterization strategy of the polarizable force field based on Drude oscillators has been documented elsewhere.[78,91,92] The optimization of potential models for the interaction of the four cations with benzene and for interaction of NH_4^+

with H_2O is based on optimizing the Lennard-Jones (LJ) parameters between specific pairs of atoms in the interacting monomers. The "NBFIX" option of CHARMM allows to override the default values of the LJ 6-12 parameters ($Emin_{is}$ and $Rmin_{is}$) obtained from the Lorentz-Berthelot combination rule:

$$Emin_{is} = \sqrt{(Emin_i Emin_s)} \qquad \text{and} \qquad Rmin_{is} = (Rmin_i + Rmin_s)/2$$

and assign pair-specific LJ parameters ($Emin_{is}$ and $Rmin_{is}$).[86] It is thus the pair specific LJ parameters that are adjusted to optimize the polarizable models. Optimization of models for alkali cations-benzene interactions is based on adjusting pair-specific LJ parameters between atoms of ions (Li^+, Na^+, and K^+) and carbon atoms of benzene. LJ parameters between Na^+ and the X site of benzene are also optimized for accurate modeling of Na^+–benzene interactions. The LJ parameters of N and H atoms of NH_4^+ as well as their pair-specific parameters with the X site in benzene are adjusted to model NH_4^+–benzene interactions. The interaction of NH_4^+ with H_2O is optimized by adjusting pair-specific LJ parameters between N and H atoms of NH_4^+ and oxygen atom of H_2O.

Optimization of these parameters is performed in two steps using the ab initio properties (stabilization energy, geometry, and PESs) as the optimization targets. The first step in the optimization is to reproduce the ab initio PESs, especially around their minimum. In this step the coordinates of the complex are kept rigid (fixed to their ab initio scanned values) and optimization of the parameters is performed to minimize an error function that imposes a Boltzmann weight at the minimum of the PES. This function is defined as:

$$\chi^2 = \sum_k \exp\left(-\frac{E_k^{CP}}{k_B \mathrm{T}}\right) \times (E_k^{CP} - E_k^{CP})^2$$

Where k_B, T, E^{CP}, and E^{MM} are Boltzmann constant, temperature (298.15 K), the interaction energy from ab initio, and the interaction energy from the Drude model, respectively. Index *k* represents the points on the potential energy surface. Minimization of this function indicates the best agreement between the calculated interaction energies using the Drude model (E^{MM}) and the corresponding ab initio values (E^{CP}). The obtained parameters are subject to a second optimization step in which the complex geometry (position and orientation of the cation relative to the interacting molecule) and the "free" interaction energies (without imposing geometry constraints except fixing the bonds to H atoms using the SHAKE algorithm[93]) are fitted to the corresponding ab initio results. In this step we start with a configuration in the PES that is close to the fully optimized geometry of the ground state conformer and reoptimize the LJ parameters allowing the internal coordinates of the complex, except bonds to H-atoms, to relax. Parameters from the second step are more reliable than those from the first as they describe the geometry and the energetic of the complex under simulation conditions (bonds to H atoms are constraint to their equilibrium values). The aim of the first step is thus to get the closest estimate of the optimum parameters.

2.2.2.2. Molecular dynamics simulations

MD simulations are performed in order to investigate cation–π, cation–π–π and π–π interactions in water as well as the hydration structure of NH_4^+. All MD simulations are performed in the NTP ensemble at T =298.15 K and p =1 atm. The following systems are simulated: 1) A system of one ammonium ion solvated in 250 water molecules and 2)

Two systems composed of two benzene molecules in presence and absence of one ammonium ion solvated in 600 water molecules. All simulations are performed in cubic boxes with periodic boundary conditions with the SHAKE to constrain covalent bonds involving hydrogens.[93] The SWM4-NDP polarizable water model[26] is used for all simulations of aqueous solutions with a mass of 0.4 a.u. on the auxiliary Drude particles and a force constant k_D = 1000 kcal/mol/Å^2 for the atom-Drude coupling. 1fs is used as the integration time-step using velocity Verlet integrator. Electrostatic interactions are computed with particle-mesh Ewald summation, with κ = 0.34 for the charge screening, 1.0 Å grid spacing, and fourth-order splines for the mesh interpolation.[26] The real-space interactions (Lennard–Jones and electrostatic) are cut off at 15 Å and long range contribution is corrected with an average density-dependent term (Lennard–Jones long range correction).[26] The temperature of the system is controlled with a two-thermostat algorithm, where atoms are kept at room temperature (298.15 K), and the auxiliary Drude particles are kept at low temperature (1 K) to assure the self-consistent induction regime.[78]

2.2.2.3. Free energy calculations

The optimized potential model for the NH_4^+–H_2O complex is validated by calculating the free energy of solvation of an ammonium ion relative to H_2O, Na^+, and K^+ in bulk water $\left(\Delta\Delta G_{hyd}(NH_4^+ \rightarrow M^+)\right)$. Calculation of the relative free energy of hydration follows the thermodynamic integration (TI) simulation protocol established previously.[94,95] In particular the relative hydration free energy ($\Delta\Delta G_{hyd}$) of solutes A and

B is evaluated from the conventional thermodynamic cycle for solute transformation in water

$$\Delta\Delta G_{hyd}(A \rightarrow B) \equiv \Delta G_{hyd}(B) - \Delta G_{hyd}(A) = \Delta G_{mut}^{wat}$$

where ΔG_{mut}^{wat} is the relative free energy for the alchemical solute A→B "mutation" in water.

To maintain a constant number of interaction sites throughout the transformation, special hybrid residues are used (Figure 2.1), in which transformed solutes are linked together through their heavy atoms via a weak bond of force constant 5 kcal/mol/Å^2. These residues are made by bonding one original "real" ion with a "dummy" second ion (having no interactions with the real particles). The mutation involves thus variation of the nonbonded parameters. The TI/MD simulation protocol used in this work involves ligand transformation in 17 steps, controlled by a mapping parameter λ which takes the following values: 0, 0.002, 0.005, 0.05, 0.1, 0.2, 0.3, 0.4, 0.5, 0.6, 0.7, 0.8, 0.9, 0.95, 0.995, 0.998, 1. Each λ window is equilibrated for 150 ps followed by subsequent data collection for 350 ps.

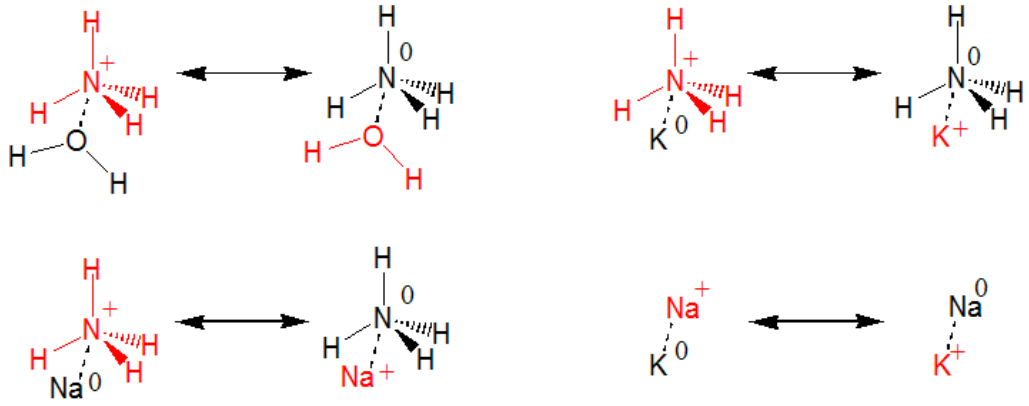

Figure 2.1. Solute transformations involved in the free energy calculations. Fragments colored in red are "real" while those colored in black are "dummy".

2.2.2.4. Potential of mean force calculations

In order to investigate the thermodynamics of cation–π and π–π association in aqueous solutions, potentials of mean force between a cation (Li^+, Na^+, K^+, or NH_4^+) and one benzene molecule and between two benzene molecules in bulk water are calculated using umbrella sampling. The distance between the centers of mass (CM) of the reactants is used as a reaction coordinate and a harmonic potential of force constant 10 kcal/mol/Å^2 is applied to bias the sampling. The reaction coordinate is separated into multiple equally separated, 0.5 Å, windows and each window is simulated for 2 ns. The unbiased PMF is reconstructed using the weighted histogram analysis method (WHAM)[96,97] and the radial variation in the entropy of the reactants pairs is taken into account by adding a $2k_BT\ln(R)$ correction term to the PMF.[98]

2.3. Results and Discussion

2.3.1. Ab initio results

2.3.1.1. Ab initio interaction energies

The optimized geometries of all studied complexes and some of their structural parameters are reported in figure 2.2. BSSE-corrected and uncorrected complexation energies (E^{CP} and E, respectively) and equilibrium distances (R_1, R_2, and R_3) obtained at the MP2/6-311++G(d,p) level of theory for Li^+, Na^+, K^+, and NH_4^+ complexes are reported in table 2.2. The complexation energies and equilibrium distances for the $(benzene)_2$, $(benzene)_3$, and benzene–H_2O complexes are also reported in table 2.2. The three equilibrium distances R_1, R_2, and R_3, in Å, represent CM separation between the cation and the benzene ring interacting with the cation, CM separation between the benzene ring interacting with the cation and the subsequent benzene ring, and the CM separation between the second and third benzene molecules, respectively. R_1 is also assigned to the CM separation between the four cations and water as well as the CM separation between water and benzene. As reported in table 2.2, the equilibrium MP2/6-311++G(d,p) interactions energies of Li^+, Na^+, K^+, and NH_4^+ with benzene monomer are –34.89, −21.08, –17.14, and –17.58 kcal/mol, respectively. Though our results are purely electronic interaction energies, neglecting thermodynamic contributions, they are comparable to the experimental gas-phase binding enthalpies of −39.3 ± 3.2, −22.5 ± 1.5, −17.7 ± 1.0, and –19.3 ± 1 kcal/mol.[49,67]

For alkali cation complexes, the interaction energy decreases (less negative) while R_1 increases on going from Li^+ to Na^+ to K^+ (see table 2.2), which is attributed to the increase of the cation size in this direction. On going from the benzene monomer to

trimer complexes with the same cation, the interaction energy increases while R_1, R_2, and R_3 decrease (see table 2.2 and figure 2.2 **a**, **b**, and **c**).

Table 2.2 also shows that: 1) the complexation energy of each cation and the benzene dimer as a whole is more negative than the sum of the complexation energy of the cation with benzene and the complexation energy in benzene dimer. 2) Both R_1 and R_2 in all cation complexes with benzene dimer are shorter than those in the cation-benzene monomer and in the benzene dimer, respectively. This indicates that cation–π and π–π interactions stabilize one another and indicates that cooperativity between both interactions contributes to the overall stabilization of the system.[22] The decrease in R_1 and R_2, which reflects the degree of cooperativity, becomes less pronounced as the number of stacked benzene rings increases, indicating that the effect of the successive addition of benzene rings will diminish on going to higher order systems.[22]

The cooperativity between the two interactions results in higher interaction energies compared to those from simple sum of the individual interactions. This extra energy gained from the interplay between the two interactions is referred to as the synergetic energy $\left(E_{syn}^{CP}\right)$. The fifth column of table 2.2 includes the synergetic energy for cation complexes with benzene dimer and trimer. This term is computed using either of the following two equations that are "almost" equivalent (equation 4 in our case).

$$E_{syn}^{CP} = E^{CP}\,(M^{+}(benz)_n) - \,(E^{CP}(M^{+}benz) + (n-1)E^{CP}(benz)_2) \quad ,n \geq 2 \qquad (4)$$

$$E_{syn}^{CP} = E^{CP}\,(M^{+}(benz)_n) - \,(E^{CP}(M^{+}benz) + E^{CP}(benz)_n) \qquad ,n \geq 2 \qquad (5)$$

where n is the number of benzene molecules, $E^{CP}(M^{+}benz)$, $E^{CP}\,(M^{+}(benzene)_n)$, $E^{CP}(benz)_2$, and $E^{CP}(benz)_n$ are BSSE corrected complexation energy of the cation

complex with benzene monomer, BSSE corrected complexation energy of the cation complex the benzene stack (dimer or trimer), BSSE corrected complexation energy of the dimer, and BSSE corrected complexation energy of the stack, respectively. The fact that the interaction energy of benzene trimer (see table 2.2) is almost twice that of the dimer confirms the approximate equivalence of the previous two equations and indicates that the complexation energy of benzene molecules arranged in a parallel stacked geometry is additive.

While the ab initio MP2/6-311++G(d,p) calculations on the complexes of Li^+ with the dimer and trimer of benzene are showing higher complexation energies compared to those calculated at MP2/6-31++G(d,p) level of theory and reported by Frontera *et al.*,[22] the calculated synergetic stabilization energy terms are almost identical (within 0.1 kcal/mol).

It should be noted that the complexes of the cations with benzene dimer or trimer arranged in a parallel stacked geometry do not correspond to the gas-phase global minimum conformers. For example the optimization of the complex in which NH_4^+ is sandwiched between two benzene molecules resulted in an optimized complex (Figure 2.2 **d**) with a BSSE-corrected interaction energy of –32.17 kcal/mol. Thus, although the stacked benzene complexes are not the global minimum, they are considered in the current work to investigate the interplay between cation–π and π–π interactions.

The data in table 2.2 show that the complexation energies of a given cation with both benzene and water are comparable. The minimum energy conformer of the benzene–H_2O complex (Figure 2.2 **e**) is one in which water is positioned on top of benzene surface and oriented close to the unidentate conformation (X···O–H angle = 16º).

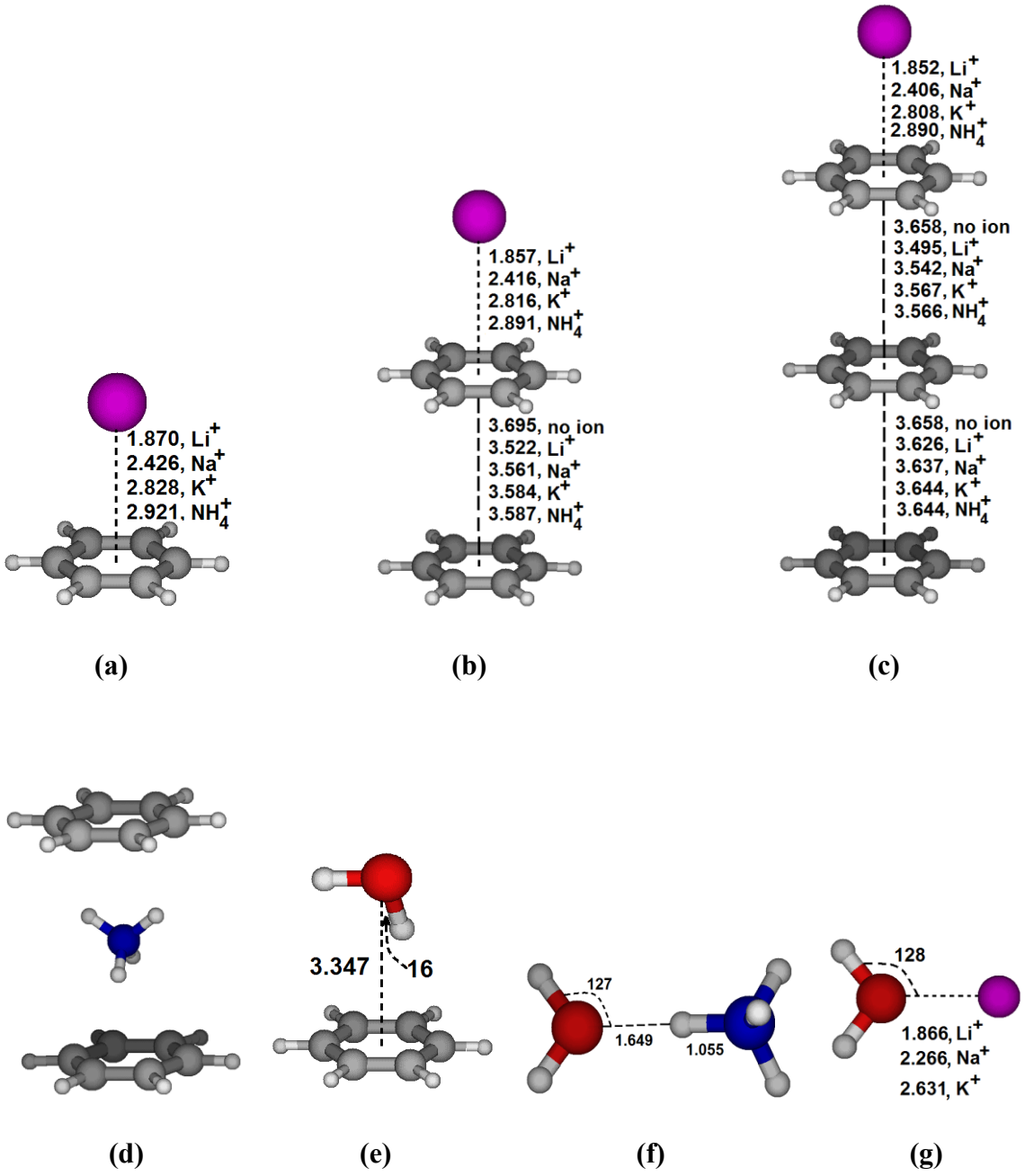

Figure 2.2. Optimized geometries at MP2/6-311++G(d,p) level of theory for Li^+, Na^+, K^+, and NH_4^+ in complex with benzene **(a)**, benzene dimer **(b)**, and benzene trimer **(c)**; sandwiched structure of $NH_4^+(benzene)_2$ complex (**d**); water-benzene complex **(e)**; ammonium-water complex **(f)**; and water complexes with Li^+, Na^+, and K^+ **(g)**.

Table 2.2. BSSE corrected and uncorrected complexation energies (E^{CP} and E, respectively), the corresponding synergetic stabilization energies (E_{syn}^{CP} and E_{syn}, respectively), the interaction energies calculated by the optimized potential models (E^{MM}) and the corresponding synergetic stabilization energies $\left(E_{syn}^{MM}\right)$, and the equilibrium distances (R_1–R_3), calculated at MP2/6-311++G(d,p) level of theory. All energies are in kcal/mol and all distances in Å.

Complex	**E**	**E^{CP}**	**E_{syn}**	$\boldsymbol{E_{syn}^{CP}}$	**R_1**	**R_2**	**R_3**	**E^{MM}**	$\boldsymbol{E_{syn}^{MM}}$
(Benzene)–Li^+	–38.84	–34.89	–	–	1.870	–	–	–35.14	–
(Benzene)–Na^+	–24.00	–21.08	–	–	2.426	–	–	–21.04	–
(Benzene)–K^+	–19.58	–17.14	–	–	2.828	–	–	–17.01	–
(Benzene)–NH_4^+	–19.78	–17.58	–	–	2.921	–	–	–17.56	–
$(Benzene)_2$–Li^+	–49.00	–41.48	5.22	4.80	1.857	3.522	–	–40.59	3.38
$(Benzene)_2$–Na^+	–32.92	–26.65	3.98	3.78	2.416	3.561	–	–25.66	2.55
$(Benzene)_2$–K^+	–28.31	–22.23	3.79	3.30	2.816	3.584	–	–21.25	2.17
$(Benzene)_2$–NH_4^+	–28.67	–22.82	3.95	3.45	2.891	3.587	–	–21.84	2.21
$(Benzene)_3$–Li^+	–56.12	–44.72	7.40	6.21	1.852	3.495	3.626	–43.62	4.34
$(Benzene)_3$–Na^+	–39.73	–29.63	5.85	4.93	2.406	3.542	3.637	–28.50	3.32
$(Benzene)_3$–K^+	–34.98	–25.10	5.52	4.34	2.808	3.567	3.644	–24.00	2.85
$(Benzene)_3$–NH_4^+	–35.37	–25.69	5.71	4.49	2.890	3.566	3.644	–24.63	2.93
$(Benzene)_2$	–4.94	–1.79	–	–	–	3.695	–	–2.07	–
$(Benzene)_3$	–10.67	–3.62	0.79	0.04	–	3.658	3.658	–4.20	0.06
(Benzene)–H_2O	–4.52	–2.43	–	–	3.347	–	–	–2.68[a]	–
H_2O–Li^+	–35.50	–33.40	–	–	1.866	–	–	–35.92[a]	–
H_2O–Na^+	–24.67	–23.09	–	–	2.266	–	–	–24.64[a]	–
H_2O–K^+	–18.93	–17.88	–	–	2.631	–	–	–17.90[a]	–
H_2O–NH_4^+	–22.16	–20.27	–	–	2.704	–	–	–20.28	–

[a] interaction energies obtained from the original models of the interacting species[26,91,92], without parameterization.

2.3.1.2. Ab initio potential energy surfaces

Potential energy curves for Li^+, Na^+, K^+, and NH_4^+ in complex with benzene monomer and for NH_4^+ in complex with H_2O are computed with rigid monomers at the MP2/6-311++G(d,p) level of theory. The ab initio computed potential curves (dashed lines) and the corresponding curves obtained from the optimized Drude models (solid lines, see section 2.3.2.1) are reported in figure 2.3.

Two curves are calculated for the interactions of the alkali cations with the benzene monomer (Figure 2.3 **(a)** and **(b)**). Curve **(a)** is calculated by positioning the cation on top of benzene center, perpendicular to its plane and scanning the distance (R) between the cation and the ring centroid (X) from 1.0 Å to 10.0 Å. This curve indicates that the depth and the extent of the potential energy well depends on the size of the cation and on its ability to approach the electron cloud of benzene.[75] Curve **(b)** is calculated by positioning the alkali cations on top of the benzene center at their equilibrium separation distances (at a site Y) and scanning the movement of the cations parallel to the benzene ring, going towards the C–C bond center. This curve shows that, though the interaction energy decreases as the cation moves away from the benzene center, some interaction energy is retained and interactions are still stabilized.[73]

Two potential curves are calculated for ammonium-benzene complex (Figure 2.3 **(c)** and **(d)**). The first curve, **(c)**, is calculated by scanning the X···N distance with ammonium in the bidentate orientation. The other curve, **(d)**, is generated by scanning the X···N–H angle. Curve **(d)** describe the interaction energy of the complex as a function of ammonium orientation in order to investigate the relative stability of the unidentate (0º,

110º), bidentate (55º), and tridentate (180º) conformers. This curve shows that the stability of the different ammonium conformers follows the order bidentate > unidentate > tridentate. The global minimum conformer however is one where the angle X···N–H is 35º or 75°, a value corresponding to an intermediate orientation of ammonium between the exact unidentate and bidentate conformations.

Two potential curves are calculated for the NH_4^+–H_2O complex (Figure 2.3 **(e)** and **(f)**). Curve **(e)** involve the scan of the N···O distance in the ammonium unidentate orientation, from 2.0 Å to 10.0 Å. Curve **(f)** involves scanning the angle O···N–H from 0º to 180º, so as to investigate the relative stability of the unidentate (0º and 110º), bidentate (55º) and tridentate conformers (180º). Curve **(f)** shows that the stability of the different conformers follows the order unidentate > bidentate > tridentate.

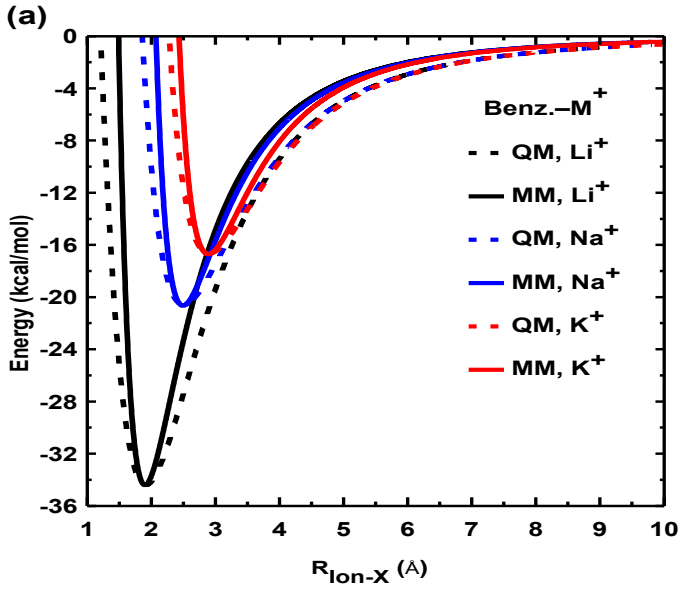

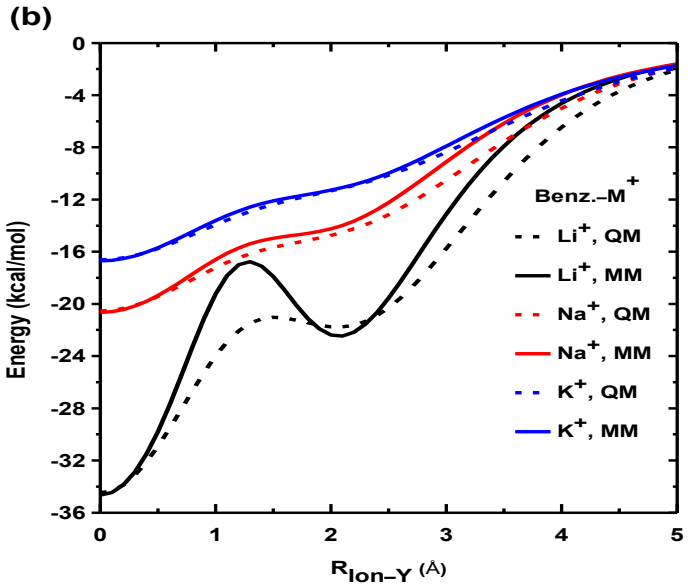
(b)
Energy (kcal/mol)
0
-4
-8
-12
-16
-20
-24
-28
-32
-36
0
1
2
3
4
5
R Ion–Y (Å)
Benz.–M+
Li+, QM
Li+, MM
Na+, QM
Na+, MM
K+, QM
K+, MM

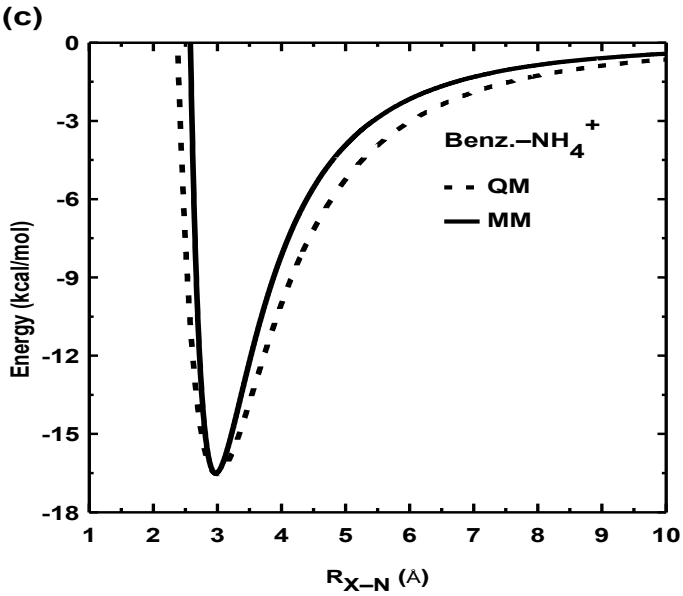
(c)
Energy (kcal/mol)
0
-3
-6
-9
-12
-15
-18
1
2
3
4
5
6
7
8
9
10
R X–N (Å)
Benz.–NH4+
QM
MM

(d)

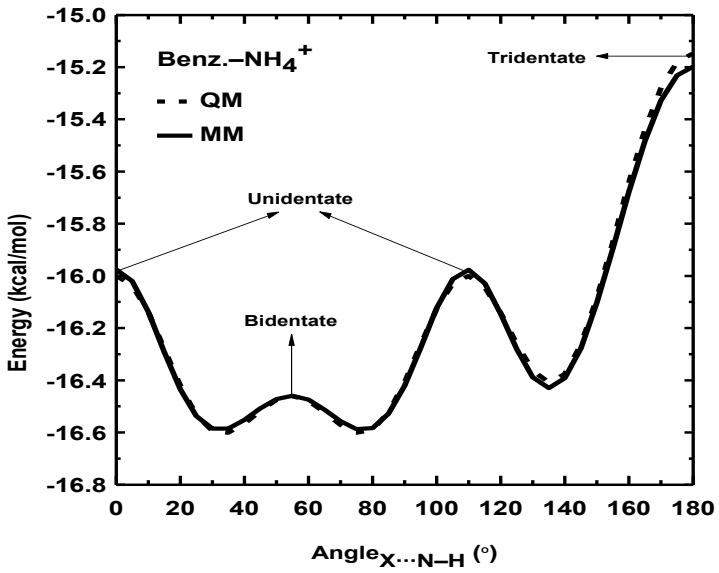
Benz.–NH4+
QM
MM
Tridentate
Unidentate
Bidentate
Energy (kcal/mol)
Angle X···N–H (°)
-15.0
-15.2
-15.4
-15.6
-15.8
-16.0
-16.2
-16.4
-16.6
-16.8
0
20
40
60
80
100
120
140
160
180

(e)

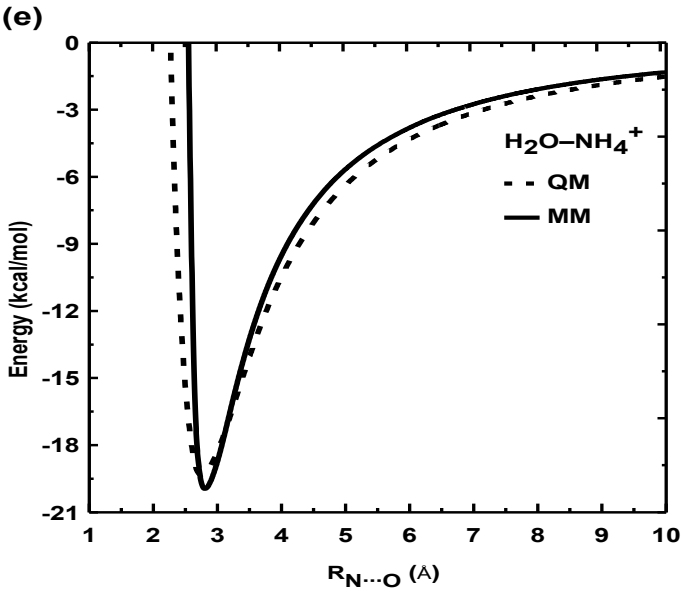
H2O–NH4+
QM
MM
Energy (kcal/mol)
R N···O (Å)
0
-3
-6
-9
-12
-15
-18
-21
1
2
3
4
5
6
7
8
9
10

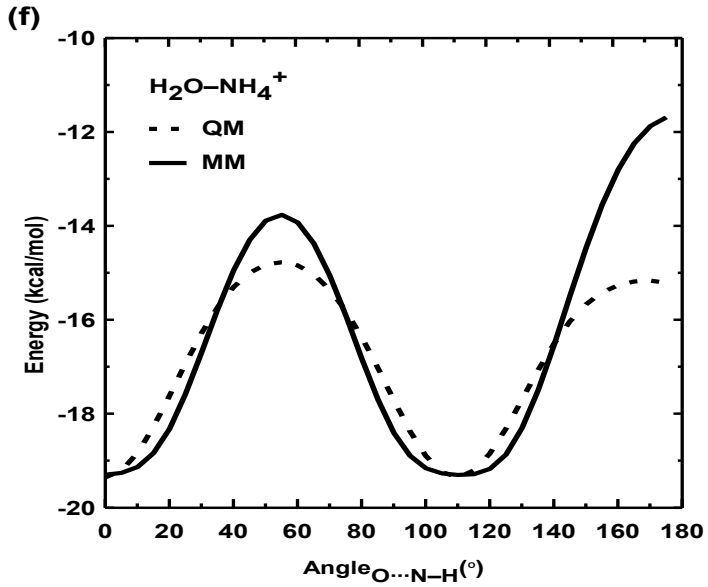

Figure 2.3. Potential energy curves for benzene–M^+ (M^+ = Li^+, Na^+, K^+, or NH_4^+) and $H_2O–NH_4^+$ complexes from ab initio MP2/6-311++G(d,p) (dashed line) and Drude (solid line): **(a)** scan of perpendicular distance between the alkali cations and benzene center; **(b)** scan of the parallel movement of alkali cations at their equilibrium distances (Y) from benzene center (1.870 Å, 2.426 Å, and 2.828 Å, for Li^+, Na^+, and K^+, respectively) toward C–C bond center; **(c)** scan of the distance between N of NH_4^+ in its bidentate conformer and benzene center; **(d)** scanning the orientation of NH_4^+ on top of benzene at X···N distance = 3.0 Å; **(e)** scan of O···N distance in $H_2O–NH_4^+$ complex; and **(f)** scan of O···N–H angle in $H_2O–NH_4^+$ complex at O···N distance = 2.7 Å.

2.3.2. Molecular mechanics results

2.3.2.1. Optimized force field

Equilibrium structural parameters for the potential model of NH_4^+ (N–H bond and H–N–H angle) are obtained from ab initio optimization of the ion in the gas phase at MP2/6-311++G(d,p) level of theory, and found to be 1.024 Å and 109.47º, respectively. Bond, Urey-Bradley, and angle force constants are fitted in CHARMM[86] based on ab initio calculated IR frequencies of gaseous NH_4^+ (ν = 3×1496, 2×1734, 3413, and 3×3547 cm^{-1}). Parameters $k_b = 470\ \text{kcal/mol/Å}^2$, $k_{UB} = 9\ \text{kcal/mol/Å}^2$, and $k_\theta = 25\ \text{kcal/mol/rad}^2$ are chosen because they yield comparable IR frequencies (ν = 3×1716, 2×1940, 3461, and 3×3546 cm^{-1}) and maintain structural stability of the ion during MD simulations. Although these frequencies are overestimating the ab initio bending vibrational frequencies of the ion (ν = 1496 cm^{-1} and 1734 cm^{-1}), they give fair agreement with the ab initio calculated PES in which the H–N–H angle is scanned (Figure 2.4), especially within 5 kcal/mol from the equilibrium.

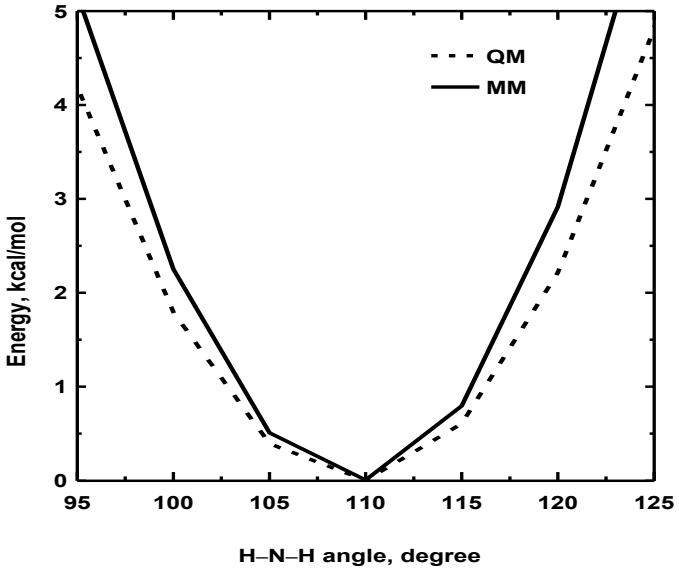

Figure 2.4. Potential energy surface for angle bending in NH_4^+, calculated from QM (dashed line) and Drude model (solid line).

Nonbonded parameters (atomic charges, polarizability and LJ parameters) of the new polarizable ammonium model are reported in table 2.1. Optimized pair-specific LJ parameters for the interaction of the four cations (Li^+, Na^+, K^+, and NH_4^+) with benzene and for NH_4^+–H_2O interaction are listed in table 2.3. These parameters are initially optimized based on the ab initio PESs and finally adjusted to reproduce the ab initio calculated geometry and interaction energy in the global minimum complex (see columns "E^{CP}" and "E^{MM}" of table 2.2). The models also reproduce the ab initio calculated PESs as shown in figure 2.2. A fair agreement is also observed for the interaction of the four cations with the dimer and trimer of benzene molecules, with a maximum deviation of ~1.1 kcal.

Table 2.3. Optimized pair-specific LJ parameters for the interactions of Li^+, Na^+, K^+, and NH_4^+ with benzene and the interaction of NH_4^+ with water.

Ion	Atom, i	Ion–Benzene interaction				Ion–water interaction	
		$Emin_{iC}$ (kcal/mol)	$Rmin_{iC}$ (Å)	$Emin_{iX}$ (kcal/mol)	$Rmin_{iX}$ (Å)	$Emin_{iO}$ (kcal/mol)	$Rmin_{iO}$ (Å)
NH_4^+	N	0.4058387	3.3962713	0.1470587	3.5005950	0.1018465	3.7592014
	H	0.0109515	2.3562713	0.0060183	3.2808392	0.0092367	2.8848120
Li^+	Li^+	0.0644005	3.1950579	0.000000	0.0000000	–	–
Na^+	Na^+	0.2004369	3.3592376	0.0099919	3.6398984	–	–
K^+	K^+	0.4266716	3.5744944	0.0000000	0.0000000	–	–

The dashes indicate that the original atomic LJ parameters of the alkali ions[92] and water[26] are used to calculate the mixed LJ parameters and no pair-specific parameters are used.

2.3.2.2. NH_4^+– H_2O potential model

The optimized model for NH_4^+–H_2O interaction reproduces the ab initio calculated complexation energy and PESs (see table 2.2 and figure 2.3 **(e)** and **(f)**). To further validate the model, the solvation structure of the ion in water and its free energy of hydration relative to H_2O, Na^+, and K^+ are calculated.

MD simulation of one ammonium ion solvated in a cubic box containing 250 SWM4-NDP water molecules is performed in the NTP ensemble for 10 ns and the solvation structure of the ion is investigated from the analysis of the last 7 ns. The atom-atom correlation functions $g_{NO}(r)$ and $g_{HO}(r)$, where N and H refer to NH_4^+ are reported in Figure 2.5. The first peak in the $g_{NO}(r)$ function shows a maximum at 2.85 Å, and a

minimum at 3.37 Å. An integration up to this minimum results in a coordination number of 5.3, in agreement with experimental[99] and ab initio MD[100] studies which report coordination numbers of 5.2 and 5.3, respectively. H–O RDF shows a first peak at 1.85 Å and a minimum at 2.36 Å. The integration up to the first minimum in the H–O RDF results in a coordination number of 1.05. The fact that the coordination number obtained from H–O RDF is less than the expected number, 5.3/4 = ~1.3, based on the calculated coordination number from N–O RDF, indicates that four water molecules are hydrogen-bonded to the four protons of NH_4^+ in a tetrahedral structure around the ion, while the remaining water molecules, ~1.3, are much more mobile, in agreement with previous results from ab initio MD simulations.[100]

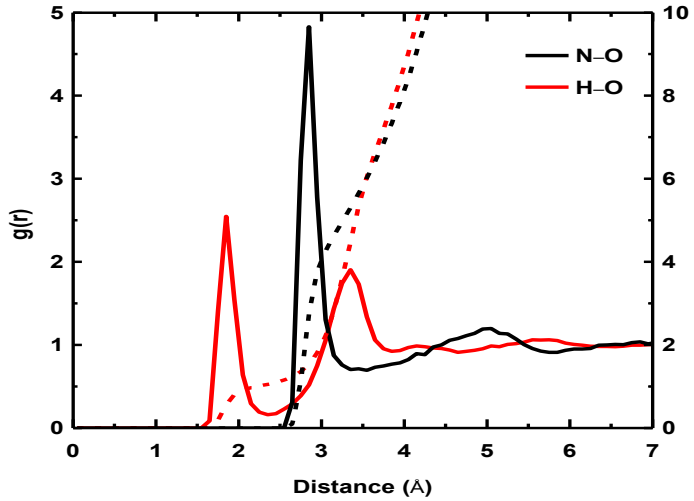

Figure 2.5. N−O (black) and H−O (red) radial distribution functions (solid lines) and running integration numbers (dashed lines) from molecular dynamics simulations of NH_4^+ in water at 298.15 K.

Hydration free energy is an important property of ions. Reliable simulations of ions in aqueous solutions require models that reproduce their free energy of hydration (ΔG_{hyd}). To further validate the NH_4^+–H_2O potential model, we calculate the change in free energy of hydration associated with mutation of NH_4^+ to H_2O, Na^+ or K^+. The change in free energy for mutating Na^+ to K^+ is also calculated. The results together with corresponding experimental data[101–105] are reported in table 2.4. On the basis of multiple runs, the overall precision of the calculated values is of the order of 0.1 kcal/mol.

Table 2.4. Relative hydration free energies (ΔG_{mut}^{wat}) in kcal/mol) as calculated from TI/MD simulations in bulk water and the corresponding experimental values.

Mutation	ΔG_{mut}^{wat}	**Experiment**
$NH_4^+ \rightarrow H_2O$	61.70	(61.80[101], 65.58[104])[a]
$NH_4^+ \rightarrow Na^+$	–18.61	–18.10[105], –19.12[101]
$NH_4^+ \rightarrow K^+$	–1.17	–0.50[105], –2.39[101]
$Na^+ \rightarrow K^+$	16.73	16.73[101], 17.16[103], 17.60[102,105]

[a] calculated using the hydration free energy of ammonium ion in references 101 and 104, and using –6.32 kcal/mol as the experimental hydration free energy of water[106].

The data in table 2.4 show good agreement between the calculated and experimental data. Taking into account the hydration free energy of the SWM4-NDP water molecule, –5.9±0.1[26], this results in a hydration free energy of NH_4^+ equal to –67.60 kcal/mol, in close agreement with the experimental value of –68.12 kcal/mol reported by Marcus[101]. It should be noted that the NH_4^+–H_2O interaction model is not optimized to reproduce the experimental results; parameterization was performed so as to reproduce the ab initio properties of the NH_4^+–H_2O complex. This further confirms the transferability of the parameterized NH_4^+–H_2O model.

2.3.2.3. Cation–π interactions in aqueous solutions

Cation–π interactions are strong in the gas phase as seen from the calculated interaction energies in table 2.2. These interactions however become much weaker in aqueous solutions.[72,83–85] The trend of the interaction energies of the three alkali cations Li^+, Na^+, and K^+ with benzene in the gas phase follows, according to table 2.2, the order $Li^+ > Na^+ > K^+$. This trend is reported[1] to show a reverse ordering when the interactions occur in water and the cation–π affinity follows the order $K^+ >> Na^+, Li^+$.

In order to measure the binding affinity and strength of the four studied cations with benzene in water, PMF calculations are performed and the results are given in figure 2.6. Our finding for the binding trend of Li^+, Na^+, and K^+ with benzene in water is in agreement with previous results.[1] Li^+ and Na^+ do not associate with benzene in presence of water as evidenced by the absence of a minimum near the gas-phase calculated equilibrium distances between the CM of the two ions and benzene. For Li^+, the weak

minimum (−0.2 kcal/mol) observed at CM separations of 5.1 Å may suggest that benzene is favored to exist in the second solvation shell of the ion. It should be noted that the interaction energies of Li^+ with benzene at this distance, as calculated from the PES, is −4.7 kcal/mol. Benzene in the second solvation shell of the ion will thus be stabilized by the interaction with ion-coordinated water molecules in addition to the long distance interaction with the cation. K^+ and NH_4^+ on the other hand bind benzene in water with energies of –1.10 and –1.36 kcal/mol at equilibrium CM separation of 3.28 and 3.37 Å, respectively. These observed CM separations are 0.45 Å longer than the gas-phase-calculated distances (see table 2.2).

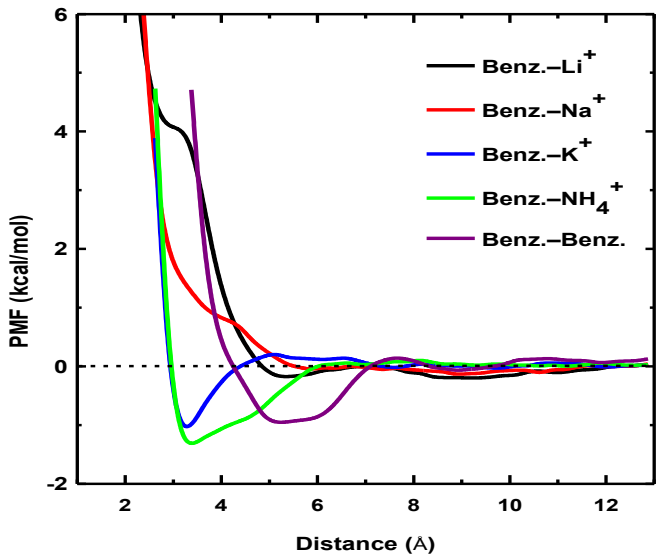

Figure 2.6. Potential of Mean Force between the centers of ions and benzene and between the centers of two benzene molecules in water.

Coordination of ions with benzene in water at or near the gas phase calculated CM separations will result in unfavored steric contacts, repulsive VDW interactions, between coordinated water molecules and benzene. Thus solvated ions move far from benzene to reduce the steric contacts and minimize the loss of coordinated water molecules. Table 2.5 shows the number of water molecules in the first solvation shell of Li^+, Na^+, K^+, and NH_4^+ with the ion being constrained at different distances from benzene center (R_{M-X}, Å). These coordination numbers are calculated by the integration of the pair distribution function, g_{MO}, where M is the alkali ion or the nitrogen atom of NH_4^+, up to the minimum after its first peak (2.56, 3.24, 3.56, and 3.37 Å for Li^+, Na^+, K^+, and NH_4^+, respectively)[92].

Table 2.5 shows that the presence of the ions at distances from benzene centers equal or close to the gas phase equilibrium values (1.87, 2.43, 2.83, and 2.92 Å for Li^+, Na^+, K^+, and NH_4^+, respectively) is expected to result in significant loss of the ion coordinated water molecules. The data for Li^+ are showing that the ion is located at average distance from benzene center higher than the value of the reaction coordinate up to a distance of 5.5 Å. The shoulder of the PMF for Li^+ corresponds to the deformation of the tetrahedral coordination followed by the loss of one of the water molecules from the first shell. Na^+ is also found at an average distance from the center of benzene higher than the value of the reaction coordinate until a distance of 6.0 Å. The shoulder for Na^+ corresponds to the loss of the sixth water molecule from the first hydration shell. K^+ and NH_4^+ on the other hand are found at larger distances compared to the reaction coordinate values up to distances of 4.5 and 4.0 Å, respectively.

Table 2.5. Average values of the R_{M-X} distances obtained from the umbrella sampling simulations and the corresponding number of water molecules in coordination with the cation.

$R_{M-X,}$ (Å)	Average of R_{M-X}, (Å)				H_2O-coordination number			
	Li^+	Na^+	K^+	NH_4^+	Li^+ (4.0)	Na^+ (5.6)	K^+ (6.9)	NH_4^+ (5.3)
1.0	2.22	–	–	–	2.96	–	–	–
1.5	2.33	–	–	–	2.99	–	–	–
2.0	2.48	2.71	–	–	3.00	3.94	–	–
2.5	2.73	2.88	3.03	3.07	3.00	4.25	5.18	4.18
3.0	3.20	3.18	3.17	3.22	3.26	4.56	5.33	4.35
3.5	3.87	3.61	3.45	3.51	3.93	4.82	5.50	4.45
4.0	4.22	4.08	3.93	3.99	3.99	4.97	5.90	4.72
4.5	4.64	4.60	4.49	4.48	4.00	5.12	6.22	4.84
5.0	5.06	5.07	5.02	4.96	4.00	5.36	6.50	4.97
5.5	5.51	5.56	5.52	5.46	4.00	5.56	6.73	5.03
6.0	6.01	6.01	6.03	5.99	4.00	5.56	6.94	5.14

Values between brackets are the coordination numbers of the ion in bulk water. Values for the alkali cations are from reference 92. The dashes indicate that the corresponding values of the reaction coordinate are not considered for the cation.

Based on the data reported in table 2.5, the number of water molecules in coordination with K^+ and NH_4^+ at the observed equilibrium distances in figure 2.6 (3.28 and 3.37 Å, respectively) will be slightly larger than 5.33 and 4.35, respectively. These values are showing that the two ions are losing ~1.6 and ~1.0 water molecules when complex with benzene at these distances.

The small Li^+ and Na^+ ions move to distances at which binding of the ion to benzene becomes energetically unfavored, compared to ion-water binding. K^+ and NH_4^+ are large in size and are located initially at larger distances from benzene. Small displacement (0.45 Å) of these ions away from benzene is thus required to relax the interactions and binding to benzene still energetically favored.

Figure 2.6 also shows the PMF between the centers of two benzene molecules in water with an equilibrium separation at 5.2 Å, and a binding free energy of −0.96 kcal/mol, in excellent agreement with the value of −1.0±0.05 kcal/mol for the heat of dimerization of benzene in water reported by Hallen *et al*.[107]

2.3.2.4. Effect of cations on π–π interactions in water

Ab initio calculations in the gas phase show that cooperativity exists between cation–π and π–π interactions. MD simulations of two benzene molecules in presence (see figure 2.7) and absence of one ammonium ion reveal how this cooperativity translates in aqueous medium.

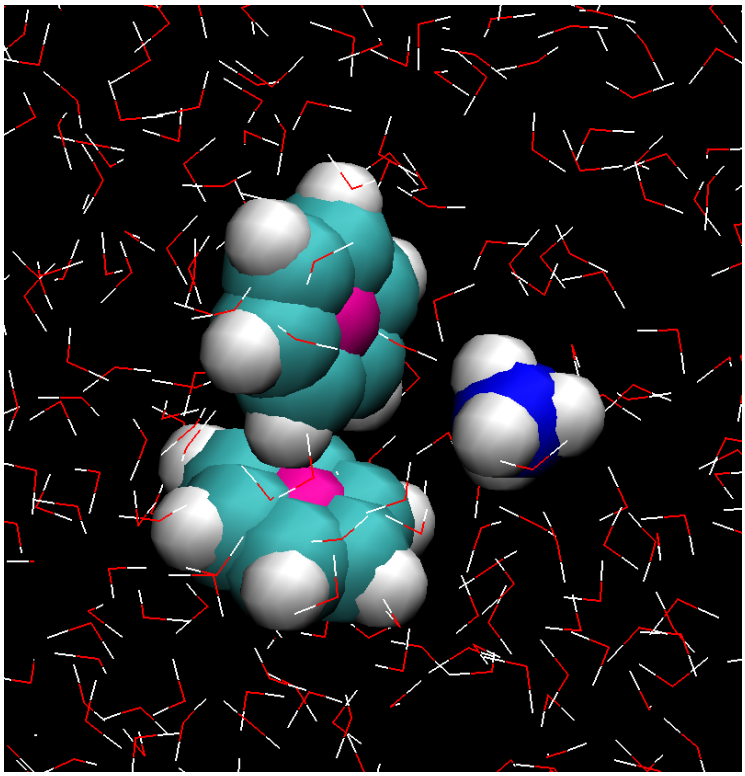

Figure 2.7. A snapshot of the simulation of $NH_4^+(benzene)_2$ complex in 600 SWM4-NDP water molecules. Atom colors are red for oxygen, blue for nitrogen, cyan for carbon, white for hydrogen, and pink for the non-atomic site in benzene center.

The effect of NH_4^+ on the association of the two benzene molecules in water can be investigated from the g_{XX} RDF, where X is benzene center, in presence and absence of the cation. Figure 2.8 **(a)** shows the X−X RDF calculated from both simulations. The two curves have similar shapes with a broad maximum in the range 5.1–5.5 Å. The function, however, possesses higher probability for $NH_4^+(benzene)_2$ system indicating that the degree of π–π association increases in presence of the cation. This indicates that cooperativity exists between cation–π and π–π interactions in aqueous solutions. The

most probable arrangement of the two benzene molecules relative to the cation can be detected from the X···N···X angular distribution (Figure 2.8 **(b)**). This distribution is characterized by a peak in the range 20–55° with a maximum probability density for an X···N···X angle at 37º. This indicates that the most stable NH_4^+(benzene)$_2$ complex is one with "cation–π–π" motif. The low probability in the angular distribution curve near 180° indicates that the sandwiched (benzene–NH_4^+–benzene) conformer is unfavored in solution. This is in contrast to gas phase ab initio calculations, which showed the sandwiched complex of NH_4^+ to be 9.35 kcal/mol more stable than the stacked complex. This can be attributed to the expected high degree of dehydration of the ion accompanying the sandwiched conformation.

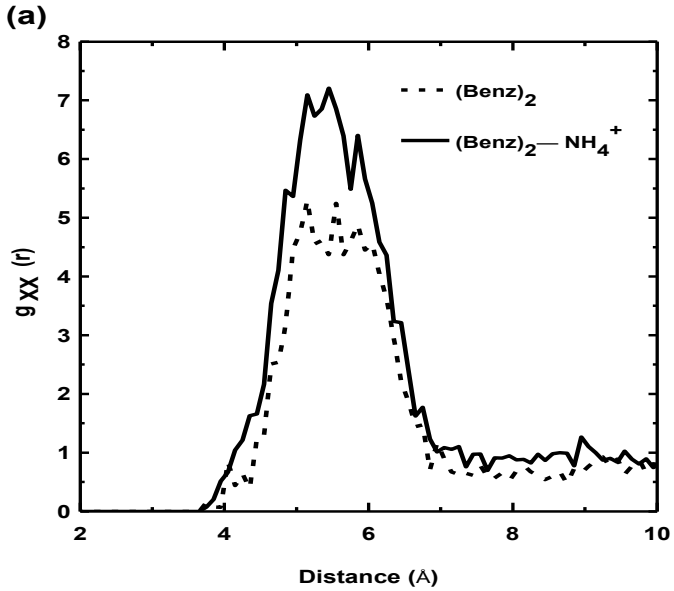

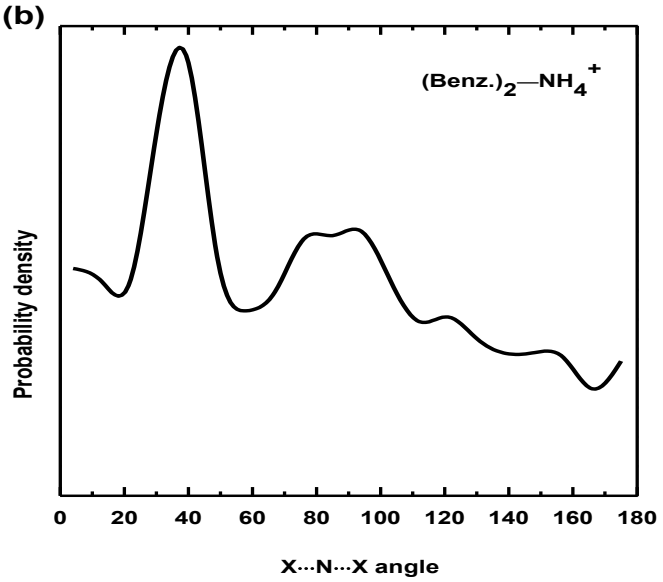

Figure 2.8. (a) CM radial distribution functions between benzene molecules, **(b)** X···N···X angular distribution.

2.4. Conclusions

In the current study, ab initio QM calculations on cation–π interactions between Li^+, Na^+, K^+, and NH_4^+ and benzene monomer, dimer, and trimer show that cation–π interactions are strong in the gas phase and become stronger as more π systems are introduced in stacked arrangements. Polarizable models for NH_4^+ and the interaction of the four cations with benzene are parameterized. An extra "non-atomic" site in benzene center is introduced to accurately model its interaction with Na^+ and NH_4^+. The optimized potential models reproduced the ab initio properties of the complexes and will serve as reliable models for studying biological systems in which cation–π interactions are thought to play important rules. A polarizable model for NH_4^+–H_2O interaction that

reproduces both the gas phase complexation energy and the experimental hydration free energy and hydration structure of the ion is also reported.

Potential of mean force on cation–benzene complexes in aqueous solutions shows that while Li^+ and Na^+ do not bind benzene in water, K^+ and NH_4^+ possess –1.0 and –1.4 kcal/mol as binding free energies. Binding of benzene to the hydrated ion at or near the gas phase equilibrium distance between the ion and benzene is observed to results in a significant loss of the water molecules in the first solvation shell of the ion. Ions move thus far from benzene to minimize the loss of coordinated water molecules. The small ions, Li^+ and Na^+ possess rigid and strong complexes with coordinated water molecules, they are thus solvated with water and do not bind benzene in aqueous solutions. Water complexes with the larger K^+ and NH_4^+ ions, on the other hand are less rigid and less strong, partial dehydration of these ions and binding to benzene is thus energetically favored in aqueous solutions. Although K^+ and NH_4^+ bind benzene at comparable center of mass separations in water (3.28 Å and 3.37 Å, respectively), NH_4^+ binds benzene more strongly than K^+. This is attributed to the larger loss of water molecules in coordination with K^+.

The observed binding trend of the four ions with benzene in water suggests possible explanations of chemical phenomena that involve effect of ions or salts on π systems in aqueous solutions. Of these, is the influence of inorganic salts on the solubility of aromatic hydrocarbons. Inorganic salts decrease the solubility "salting-out" of aromatic hydrocarbons in aqueous solutions. The degree of salting-out has been reported to depend on the type of the salt and its concentration.[108,109] The salting-out of benzene in presence of the chloride salt of the four cations Li^+, Na^+, K^+, and NH_4^+ is reported to

follow the order $Na^+ > K^+ > Li^+ > NH_4^+$. According to the calculated binding energies of the four cations with benzene in water, we may suggest the salting-out effect to occur by the following mechanism. Small ions (Li^+ and Na^+) bind water strongly and do not bind benzene in their first solvation shells. This will result in increasing the concentration of benzene in the solution spaces that are not occupied by the ions and their first solvation shells, leading to benzene association and salting-out. The larger ions (K^+ and NH_4^+) on the other hand weakly bind benzene in their first solvation shells which lead to less salting-out. According to this mechanism and taking in consideration that benzene shows a tendency to exist in the second solvation shell of Li^+, benzene salting-out by the four ions would follow the order $Na^+ > Li^+ > K^+ > NH_4^+$. Although this suggested mechanism reproduces the relative ordering of the three cations Na^+, K^+, and NH_4^+, it fails to reproduce lithium's position. The presence of the same anion in these systems might play different roles in presence of different cations and detailed investigations of the microscopic structure of benzene in different aqueous salt solutions might reveal findings that reproduce the exact experimental ordering.

While ab initio MP2/6-311++G(d,p) calculations on $NH_4^+(benzene)_2$ complex showed that the sandwiched conformer is more stable than the stacked one, MD simulation on $NH_4^+(benzene)_2$ complex in water shows that the most stable complex is one with cation–π–π motif. The instability of the sandwiched conformer in water is attributed to the significant dehydration of the cation accompanying such binding mode. Protein environment (geometrical constraints and low dielectric constant) on the other hand may results in different stable binding modes for cation–π_2 complexes. A survey of the PDB for cation–π_2 complexes will serve to elucidate the abundance of these complexes and their favored conformations.

3. Polarizable potentials for ammonia interacting with water and with amino acid model compounds

Abstract

Polarizable force field models based on classical Drude oscillators are generated for NH_3 and its interactions with H_2O and 10 compounds that model the peptide backbone and five amino acids; Ser, Phe, Tyr, Trp, and His. The studied amino acids-model compounds are N-methylacetamide, ethanol, benzene, toluene, phenol, p-methylphenol, indole, 3-methylindole, imidazole, and 4-methylimidazole. Optimization of the potential models is based on ab initio calculations on the complexes at the MP2/6-311++G(d,p) level of theory. The minimum energy conformers in all NH_3 complexes that are observed in the ab initio calculations are reported. The optimized model for NH_3–H_2O complex reproduces the experimental hydration free energy of NH_3 without further adjustments and is used to investigate the hydration structure of NH_3. The potential model for NH_3–NH_3 interaction is optimized to reproduce the density of liquid ammonia at its boiling point. The model reproduces the density, heat of vaporization, and structure of liquid ammonia at different thermodynamic conditions without further adjustments.

3.1. Introduction

Ammonia is used as a solvent in organic reactions and has a widespread use in many industrial sectors as refrigerant, fertilizer, cleaner, and as precursor to nitrogenous compounds such as fuel and explosives. In a biological context, ammonia is an important and preferred source of nitrogen for many organisms, it undergoes uptake by transmembranes proteins as part of cell nitrogen metabolism.

Different experimental[110–118] and computational[119–132] studies have been conducted to investigate the structural properties of liquid and aqueous ammonia solutions. The structure and degree of hydrogen bonding in liquid ammonia have been studied experimentally using X-rays[110–114] and neutron scattering[115–118] as well as computationally[119–130] These studies are showing that ammonia is one of the weakest hydrogen bonded liquids.[118,128] The structure of aqueous ammonia solutions has also been studied by X-ray diffraction[110] as well as by theoretical simulations.[131,132] Reliable potential models that reproduce the experimental data, however, are still required.

Ammonia is known to be involved in translocation processes in proteins[133]. An example is the transfer of ammonia in the enzyme Glutamine-dependent amidotransferases[134]. The transfer of ammonia in these enzymes occurs via the diffusion across interdomain channels.[134] An important pathway of ammonia or ammonium (Amm) transport is provided by the family of MEP/Amt/Rh proteins from archaea, bacteria, and eukarya.[135–139] The mechanism of transport and the nature of the net transported species, ammonia or ammonium, in these proteins however is not yet understood. Potential

models for ammonia interactions with amino acid side chains are thus important to investigate the mechanism of action of these proteins and enzymes.

In this work, we develop polarizable potential models for NH_3 and its interaction with 12 compounds; H_2O, NH_3, and 10 model compounds for the peptide backbone and five amino acids. The modeled amino acids are Ser, Phe, Tyr, Trp, and His which are chosen because of the polarizable nature of their side chains and the role they are thought to play in Amm transport proteins. N-methylacetamide (NMA) is chosen as a model for the peptide backbone; ethanol for Ser; Benzene, toluene for Phe; phenol, P-methyphenol for Tyr; Indole, 3-methyindole for Trp; and imidazole, 4-methyl imidazole for His. The methyl substituted compounds are considered in order to accurately model the amino acids. For this purpose, ab initio calculations on the complexes of NH_3 with the twelve compounds are performed at MP2/6-311++G(d,p) level of theory. The ab initio properties of the complexes are then used to optimize the potential models for the ammonia complexes. The NH_3–H_2O potential model is validated by calculation of the hydration free energy of NH_3. In contrast to all models, the NH_3–NH_3 potential model is optimized to reproduce the density of liquid ammonia at its boiling point is validated by calculating the density and structure at other thermodynamic conditions.

3.2. Methods

3.2.1. Ab initio calculations

Full geometry optimizations of all compounds and of different conformers in their complexes with NH_3 are performed at MP2 level with the 6-311++G(d,p) basis set using Gaussian 09 program.[88] Geometry of all complexes are optimized without imposing any symmetry constraints. The local minimum nature of the optimized structures is confirmed using a frequency calculation, which showed no imaginary frequencies in all reported complexes. The interaction energies are corrected for basis set superposition error (BSSE) using the Boys and Bernardi counterpoise technique.[89] The NH_3−NH_3 and NH_3−H_2O complexes are also optimized at the CCSD(T)/6-311++G(2d,2p) level of theory, and the results are found in agreement with the previous level of theory. All other quantum mechanical (QM) calculations are thus performed at the MP2/6-311++G(d,p) level of theory.

Various potential energy surfaces (PESs) describing the interaction of the different compounds with ammonia are computed at same level of theory and corrected for BSSE. The curves are computed with rigid monomers in their gas phase optimized geometries. In most cases, the curves are calculated by orienting NH_3 such that the geometry of the system is close to that of the global minimum conformer and the scan involves mainly the distance between the two fragments from 2.0 Å to 10.0 Å. For benzene and toluene, in addition to scanning the distance between N and the ring center (X), a scan of the X···N−H angle is performed. This scan aims to investigate the preferential orientation (unidentate, bidentate, or tridentate) of NH_3 on the ring surface.

3.2.2. Potential energy function and parameterization strategy

Molecular mechanics (MM) calculations are performed with the program CHARMM.[86] A new polarizable interaction potential is developed for ammonia based on ab initio calculations on NH_3 and its complex with H_2O. Polarizable force field models are also parameterized for the interaction of NH_3 with the other eleven studied compounds (NH_3, ethanol, NMA, benzene, toluene, phenol, p-methylphenol, indole, 3-methylindole, imidazole, 4-methylimidazole). All the polarizable interaction models are adjusted to reproduce the ab initio properties of the complexes, except for the NH_3−NH_3 interaction model which is optimized to reproduce the density of liquid ammonia at its boiling point (239.65 K).

Polarization in these models is based on the classical Drude oscillators.[25,87] Polarizability is introduced in the classical Drude oscillator model by attaching mass-charged particles to polarizable atoms via a harmonic spring with force constant k_D. The partial charge of the polarizable atom q is redistributed between the Drude particle and the atom core with the Drude charge q_D being determined from the atomic polarizability via the relation $\alpha = {q_D}^2/k_D$. A separation r_D between the Drude particle and the polarizable atom results in a dipole $q_D r_D$. Thus electronic polarization is mimicked by relative displacement of both charges due to an external electrostatic field.

Table 3.1. Potential model for polarizable ammonia.

Atom	q (e)	Emin (kcal/mol)	$R_{min}/2$ (Å)	α (Å^3)
N	–0.99576	0.1043429	2.0780073	–1.6905
H	0.33192	0.0699455	0.555818	0.0000

Parameters for NH_3 potential model (current study) are summarized in table 3.1. In this model, NH_3 is modeled by four atomic sites in addition to an auxiliary Drude particle attached to the nitrogen atom. The electrostatic parameters, atomic charges and polarizabilities, are determined from ab initio calculation. The atomic charges are fitted to reproduce the gas phase dipole moment and the polarizability of N is calculated from the trace of the polarizability tensor. Finally the Lennard-Jones (LJ) parameters of N and H are treated as adjustable parameters to reproduce the ab initio calculations of NH_3–H_2O complex.

The optimized model of NH_3 did not reproduce the density of liquid ammonia at its boiling point and the model for NH_3–NH_3 interaction is thus optimized for this purpose. Interaction between the original models of NH_3 and NMA reproduces the ab initio calculations on their complex and no optimization is performed for the NH_3–NMA model. Optimization of ammonia interactions with other compounds, on the other hand is found necessary to reproduce their ab initio results. The parameterization of polarizable force fields for NH_3 interactions is performed following our previous strategy.[I] In particular the currently introduced ammonia model and the previously reported polarizable models for interacting compounds[26,91,140–142] are used and optimization is based on adjustment of the LJ parameters between specific pairs of atoms from NH_3 and the interacting ligand. By default, the parameters of the LJ 6-12 interaction $Emin_{ij}$ and $Rmin_{ij}$ for atoms *i* and *j* are generated using the Lorentz-Berthelot combination rule:

$$Emin_{ij} = \sqrt{\left(Emin_i Emin_j\right)} \qquad \text{and} \qquad Rmin_{ij} = \left(Rmin_i + Rmin_j\right)/2$$

The "NBFIX" option of CHARMM parameter file allow to override the default values from the combination rules and assign pair-specific LJ parameters.[34] Optimization of the potential models is thus based on adjustment of the pair-specific LJ parameters between N of NH_3 and one specific atom type in the interacting compound. These atoms are N of ammonia, indole, and 3-methylindole, aromatic carbon atoms of benzene and toluene, O of ethanol, phenol, and p-methylphenol, and N3 of imidazole and 4-methyl imidazole. Adjustment of the LJ pair-specific parameters in ammonia dimer utilizes the density of liquid ammonia at 239.65 K as optimization target, while for other ammonia interactions, optimization is performed using the ab initio properties of the complexes as target values.

Adjustment of the LJ parameters of N and H in NH_3 and the pair-specific LJ parameters is performed in two steps following our previously reported strategy.[I] In the first, the ab initio PESs are considered the target and an iterated optimization of the parameters is performed until the best fit between the PESs calculated by the potential model and from ab initio calculations is achieved. The LJ parameters are adjusted to optimize the following error function:

$$\chi^2 = \sum_k \exp\left(-\frac{E_k^{CP}}{k_B \mathrm{T}}\right) \times (E_k^{CP} - E_k^{CP})^2$$

where k_B, T, E^{CP}, and E^{MM} are the number of points in the potential energy surface, Boltzmann constant, temperature (298.15 K), BSSE-corrected interaction energy, and force field-calculated interaction energy of the complex, respectively. Index k represents the points on the potential energy surface. The obtained parameters are subject to a second optimization in which the geometry of the complex (position and orientation of the NH_3 relative to the interacting molecule) and the "free" interaction energies (without

imposing geometry constraints except fixing the bonds to H atoms using the SHAKE algorithm[93]) are the optimization targets.

We start by optimizing the interaction between the simple "unmethylated" compounds (benzene, phenol, indole, and imidazole) and test the transferability of the optimized parameters to the methylated "complex" models (toluene, p-methylphenol, 3-methylindole, and 4-methylimidazole). The optimized parameters for the simple compounds are considered transferable to the complex ones if they give good agreement with ab initio calculations on the later complexes, otherwise the parameters are subject to further adjustments.

3.2.3. Molecular dynamics

Previous computational studies on liquid ammonia have artificially imposed its experimental density by performing simulations using the canonical[120,124,128,131] (NVT) or the microcanonical[127,130] (NVE) ensembles, in which the volume of the system corresponds to the experimental density of the liquid at the studied thermodynamic conditions. Structural properties obtained from such simulations are thus artifact of the volume constraint and do not provide an accurate description of the performance of the theoretical model. The model we are developing aims at reproducing the density of liquid ammonia by performing the simulations in the isothermal–isobaric ensemble (NPT). In the NPT ensemble, the volume changes and attains certain equilibrium at which, the density of the solution and its structural properties can describe the quality of the model.

Two different systems are simulated by MD in the NTP ensemble. The first system is composed of 250 polarizable ammonia molecules, simulated at the boiling

point of ammonia (T = 239.65 K) and pressure P= 1 atm, in order to optimize the NH_3–NH_3 potential model through reproducing the density of the neat liquid at these thermodynamic conditions. The same system is simulated at the experimental conditions of the neutron diffraction experiment[118] (T = 213 K and P= 1.2 atm) in order to validate the model and compare the calculated structure of liquid ammonia with the experiment. The second is a system of one ammonia molecule solvated in 250 water molecules, simulated in order to investigate the hydration structure of NH_3 at T = 298.15 K and P= 1.0 atm. All systems are simulated in cubic boxes with periodic boundary conditions. Long-range electrostatic interactions are computed with particle-mesh Ewald summation. A smooth real-space cutoff is applied between 14 and 15 Å with an Ewald splitting parameter of $0.34 Å^{-1}$, a grid spacing of 1.0 Å, and a fourth-order interpolation of the charge to the grid. The temperature of the system is controlled with a two-thermostat algorithm, where atoms are kept at previously mentioned temperatures whereas auxiliary Drude particles are kept at low temperature (1 K) to assure the self-consistent induction regime.[87] The NTP ensemble is simulated using Nose–Hoover thermostat[143,144] and the modified Andersen-Hoover barostat of Martyna et al.[145] along with 1 fs time step. The SWM4-NDP polarizable water model[87] is used for simulation of the aqueous solution. The internal geometry of water molecules as well as the N–H bond lengths in ammonia are fixed using the SHAKE algorithm.[93] All systems are simulated for 10ns and the last 7 ns are used for data analysis.

3.2.4. Free energy calculation

Optimization of LJ parameters of N and H atoms in NH_3 are based on ab initio calculations on NH_3–H_2O complex. The final parameters are validated by calculating the hydration free energy of NH_3. The free energy of hydration of NH_3 relative to H_2O $\left(\Delta\Delta G_{hyd}(NH_3 \rightarrow H_2O)\right)$ is calculated following thermodynamic integration (TI) simulation protocol established previously.[I,94,95] In particular the relative hydration free energy ($\Delta\Delta G_{hyd}$) of solutes NH_3 and H_2O is evaluated from the conventional thermodynamic cycle for solute transformation in water

$$\Delta\Delta G_{hyd}(H_2O \rightarrow NH_3) \equiv \Delta G_{hyd}(NH_3) - \Delta G_{hyd}(H_2O) = \Delta G_{mut}^{wat}$$

where ΔG_{mut}^{wat} is the relative free energy for the alchemical solute $H_2O \rightarrow NH_3$ "mutation" in water.

To maintain a constant number of interaction sites throughout the transformation, special hybrid residues are used (Figure 3.1).[I] These residues are made by bonding one original "real" molecule with a dummy second molecule in a cubic box of 250 SWM4-NDP water molecules. Force constant of 5 kcal/mol/Å^2 is assigned to the intermolecular bonded atoms. The TI/MD simulation protocol used in this work involves ligand transformation in 17 steps, controlled by the mapping parameter λ which takes on of the following values: 0, 0.005, 0.02, 0.04, 0.1, 0.2, 0.3, 0.4, 0.5, 0.6, 0.7, 0.8, 0.9, 0.96, 0.98, 0.995, 1. The calculation of the free energy increments at each value of λ includes equilibration for 150 ps and subsequent data collection for 350 ps.

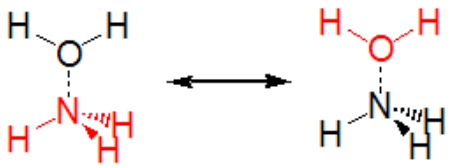

Figure 3.1. Solute transformation involved in free energy calculation. Solutes colored red are "real" while those colored black are "dummy".

3.3. Results and Discussion

3.3.1. Minimum energy conformers

The labeling diagram of the twelve studied compounds used in this work is displayed in figure 3.2. Geometry optimization of NH_3 in the gas phase gives 1.013 Å for N–H bonds and 107.29º for the H–N–H angle, in close agreement with the experimental values, 1.012 Å and 107.67º, respectively.[146] Ab initio geometry optimizations at MP2/6-311++G(d,p) level of theory show that most ligands form more than one stable, minimum energy complex with NH_3. Table 3.2 lists the BSSE-corrected and uncorrected interaction energies in all minimum energy conformers of all NH_3 complexes. Of the different stable conformers, the H-bonded conformer is found more stable than other possible conformers. The most stable conformers for NH_3 complexes with benzene and toluene on the other hand are characterized by NH_3–π interactions, in which NH_3 is positioned on top of the aromatic ring and interact with π electrons. For the same ligand complex, the O−H···N(NH_3) conformer is found more stable than the O···H−N(NH_3) conformer. The presence of the electron donating methyl group in the studied aromatic compounds results in increasing the electron density of the moiety. While this results in a decrease in the

interaction energy of most H-bonded conformers in which NH_3 is the H acceptor, it increases the interaction energy of NH_3–π bonded complexes, in comparison with the corresponding conformers in the simple, unmethylated, aromatics.

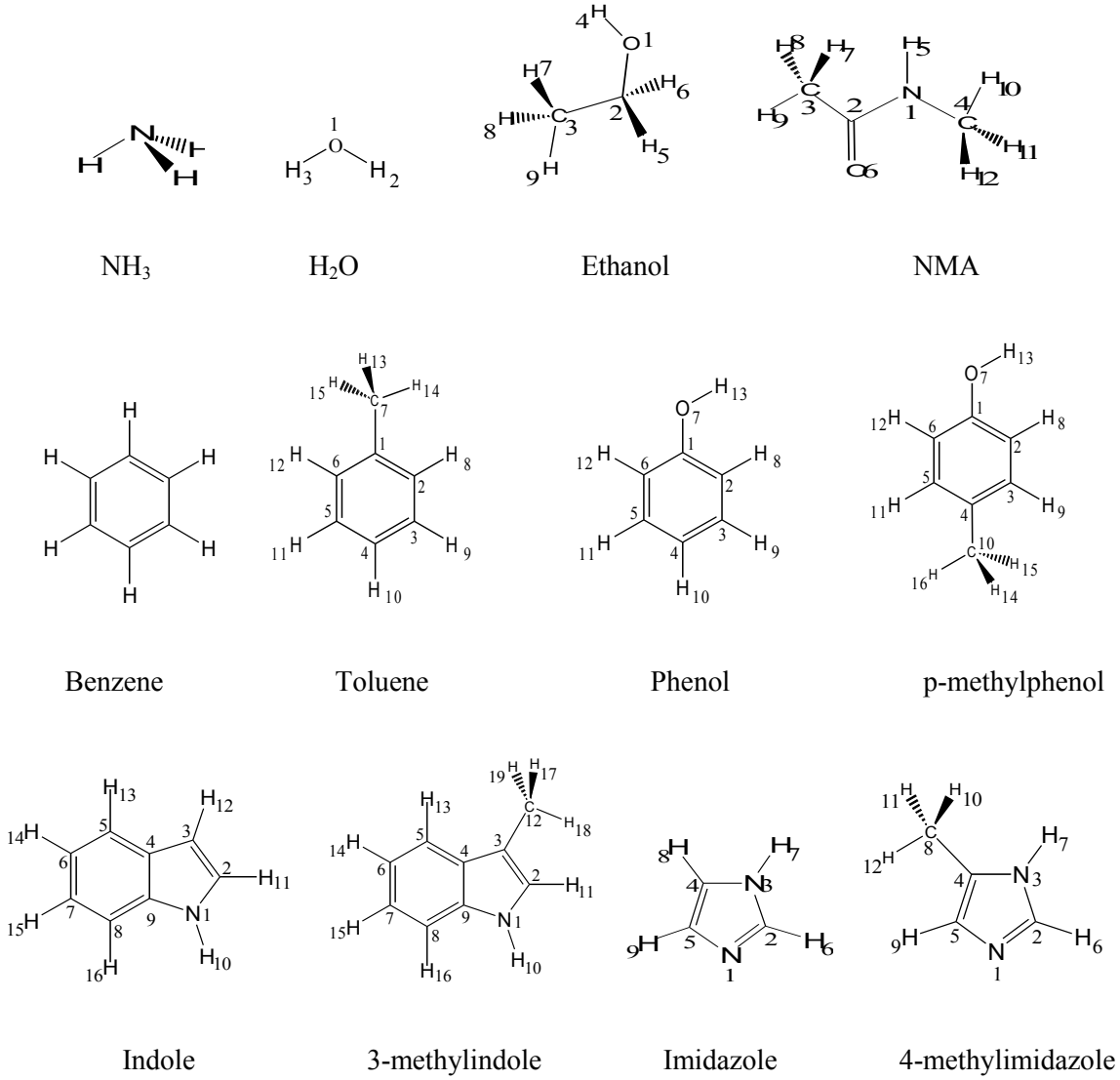

Figure 3.2. Labeling diagram of 12 studied compound interacting with NH_3.

Table 3.2. Interaction energies, in kcal/mol, without and with BSSE correction (E and E^{CP}, respectively) for the different minimum energy conformers of NH_3 complexes at the MP2/6-311++G(d,p) level of theory.

complex	conformer	E	E^{CP}	complex	conformer	E	E^{CP}
	a	–3.80	–2.73	NH_3–H_2O	–	–7.46	–5.89
$(NH_3)_2$		(–3.08)	(–2.57)			(–6.63)	(–5.79)
	b	–3.80	–2.68				
		(–3.21)	(–2.70)				
NH_3–Ethanol	a	–7.73	–5.86	NH_3–NMA	a	–7.59	–5.76
	b	–4.38	–3.07		b	–5.33	–3.88
	a	–3.53	–1.75		a	–4.57	–2.47
NH_3–benzene	b	–2.62	–1.30	NH_3–toluene	b	–2.64	–1.32
					c	–2.49	–1.20
					d	–2.42	–1.20
	a	–10.61	–8.28		a	–10.43	–8.10
	b	–4.21	–2.68		b	–4.13	–2.69
NH_3–phenol	c	–3.76	–1.70	NH_3–p-methylphenol	c	–4.52	–2.41
	d	–2.74	–1.42		d	–2.75	–1.43
	e	–2.76	–1.34		e	–2.69	–1.36
	f	–2.59	–1.28				
	a	–8.94	–6.94		a	–8.76	–6.73
	b	–6.23	–3.72		b	–6.41	–3.80
	c	–4.85	–2.47		c	–5.46	–2.86
NH_3–indole	d	–3.48	–2.23	NH_3–3-methylindole	d	–3.54	–2.11
	e	–2.50	–1.25		e	–2.69	–1.15
	f	–2.24	–1.04		f	–2.25	–0.96
	g	–2.28	–1.00		g	–2.18	–0.88
	h	–2.21	–0.92				
	a	–9.57	–7.58		a	–9.38	–7.30
	b	–5.51	–4.37		b	–5.55	–4.38
NH_3–imidazole	c	–4.77	–3.69	NH_3–4-methylimidazole	c	–4.92	–3.82
	d	–4.64	–2.96		d	–5.25	–3.37
	e	–3.68	–2.42				

Values in brackets are CCSD(T)/6-311++G(2d,2p) results.

3.3.1.1. Ammonia dimer

Geometry optimization on ammonia dimer shows two stable conformers, the eclipsed (**a**) and staggered (**b**) conformers (Figure 3.3). The interaction energy of the dimer is comparable in both conformers (Table 3.2), with conformer **a** being 0.05 kcal/mol more stable than **b**. CCSD(T)/6-311++G(2d,2p) results on the dimer show slight larger inter molecular separation with **b** being 0.12 kcal/mol more stable than **a**.

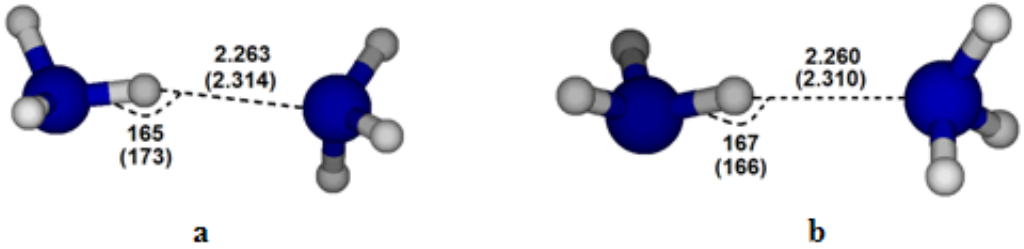

Figure 3.3. Optimized geometries of ammonia dimer in (**a**) eclipsed and (**b**) staggered conformations. Distances in Å and angles in degrees. Values in brackets are CCSD(T)/6-311++G(2d,2p) results.

3.3.1.2. Ammonia-water complex

Geometry optimization of ammonia-water complex shows only one stable complex with O–H···N type of hydrogen bond. Optimization of the O···H–N hydrogen bonded conformer did not result in a stable local minimum, instead the O–H···N bonded conformer is obtained, in agreement with microvave and radio frequency spectral experimental results.[147] As shown in figure 3.4, CCSD(T)/6-311++G(2d,2p) predicts slight larger intermolecular separations, however the interaction energy of the complex (Table 3.2) is in close agreement with MP2/6-311++G(d,p) result.

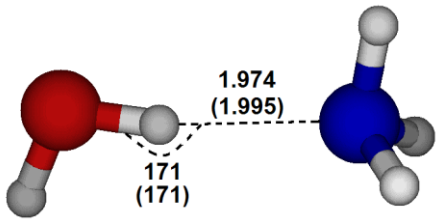

Figure 3.4. Optimized geometry of NH_3–H_2O complex. Values in brackets are CCSD(T)/6-311++G(2d,2p) results.

3.3.1.3. Ammonia-ethanol complex

Geometry optimizations on ammonia-ethanol complex are performed on the O−H···N and O···H–N hydrogen bonded complexes. Two optimum minimum energy geometries are obtained (Figure 3.5). The interaction energy in **a**, –5.86 kcal/mol, is about twice the interaction energy of **b**, –3.07 kcal/mol, indicating that O–H···N type of hydrogen bonding is more favored than the O···H–N type. The stability of the type of hydrogen bonding in **b** which is not observed in ammonia–water complex is attributed to the interaction of the lone pair of electrons of the nitrogen atom with one H atom of the C3 atom as evidenced be structural data in figure 3.5 **b**.

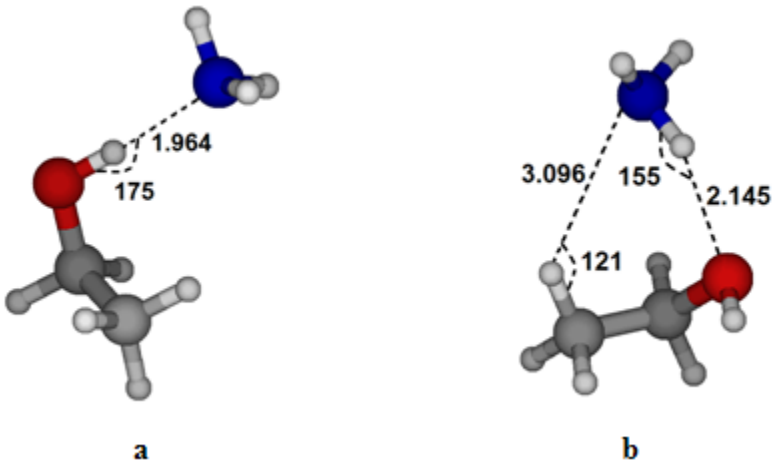

Figure 3.5. Optimized geometries of different minimum energy conformers in NH_3-ethanol complex.

3.3.1.4. Ammonia-N-methylacetamide complex

Two stable conformers are found in the interaction of NH_3 with NMA (Figure 3.6). Conformer **a** is the global minimum with NH_3 H-bonded to NMA and acts as H-acceptor. Figure 3.6 **b** suggests that the complex is stabilized by interaction of N-lone pair of electrons with one H atom of C3. While ammonia-ammonia and conformer **a** in ammonia-NMA complexes are characterized by N–H···N(NH_3) type of H-bonding, the interaction energy in the later complex is ~2.1 times that in the first. This is attributed to the presence of the electron withdrawal carbonyl group in NMA.

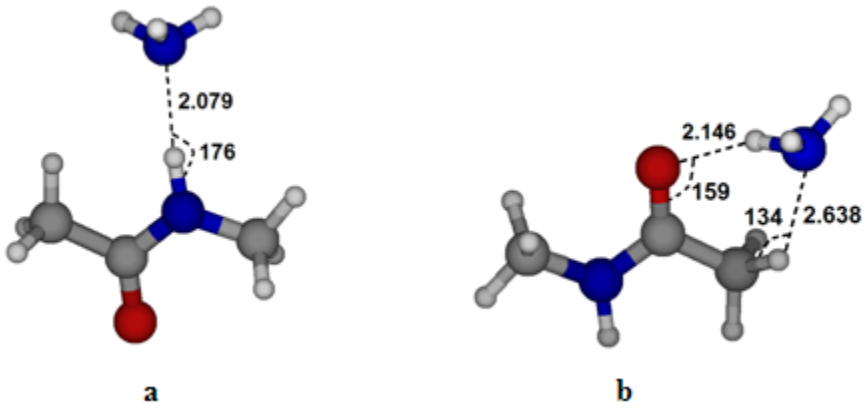

Figure 3.6. Optimized geometries of different minimum energy conformers in NH_3-NMA complex.

3.3.1.5. Ammonia-benzene complex

Geometry optimization on various initial conformers of the NH_3-benzene complex shows only two minimum energy structures (Figure 3.7). The global minimum conformer, **a**, is one in which ammonia resides above the benzene plane in agreement with the optical and microwave spectral results reported by Rodham *et al.*[148] In this conformer, NH_3 is oriented toward benzene surface so that only one proton is interacting with the π–cloude "unidentate conformation"[148]. It should be noted that optimization of the zero, bi, and tridentate conformers resulted in less stable complexes that correspond to 2nd order saddle points. Conformer **b** is a H-bonded complex that is 0.45 kcal/mol less stable than conformer **a**.

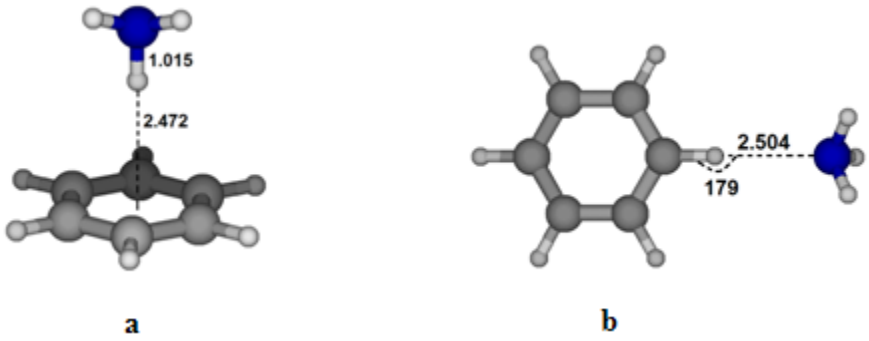

Figure 3.7. Stable, minimum energy conformers in NH_3-benzene complex.

3.3.1.6. Ammonia-toluene complex

Optimized minimum energy conformers of the NH_3–toluene complex and some structural data are reported in figure 3.8. Similar to benzene, the global minimum conformer, **a**, is an NH_3–π complex. In this conformer, NH_3 is displaced from the ring center toward C1 and is oriented such that two protons are interacting with the π cloud and its lone pair is interacting with one H of C7. The higher interaction energy of this conformer, compared to benzene is the result of the increased electron density of the aromatic ring due to the methyl group. The other conformers, **b**, **c**, and **d**, are complexes with NH_3 being H-bonded to the three different aromatic Hydrogens (ortho, meta, and para). Table 3.2 indicates that the interaction energy in these complexes follow the trend ortho (**b**) > meta (**c**) = para (**d**).

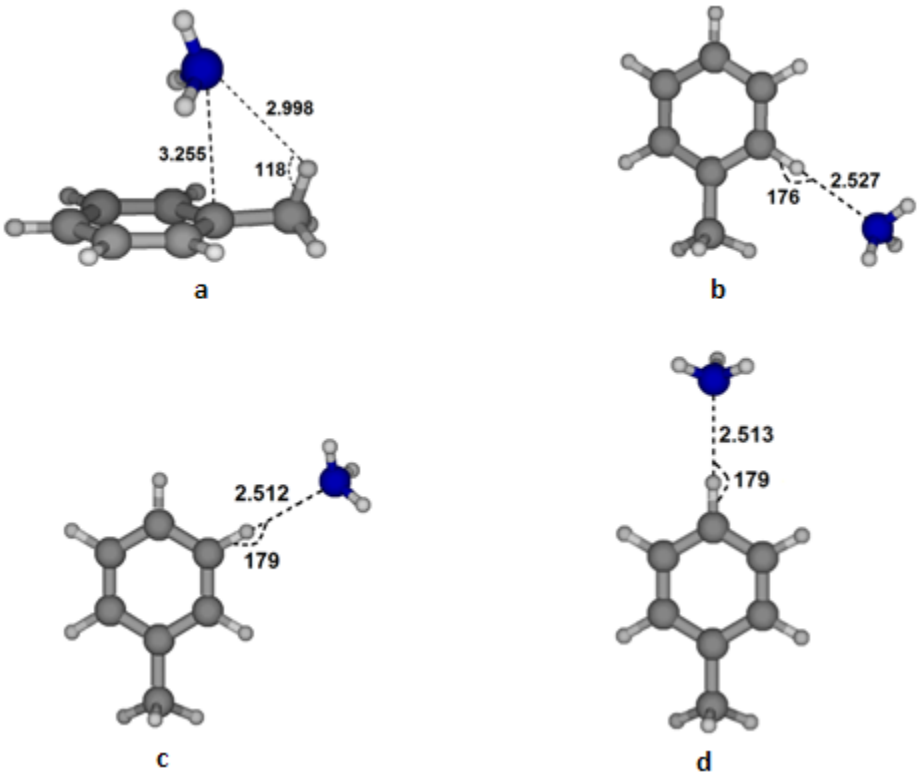

Figure 3.8. Optimized geometries of different minimum energy conformers in NH_3-toluene complexes.

3.3.1.7. Ammonia-phenol complex

The different stable, minimum energy conformers of the NH_3-phenol complex and their characteristic intermolecular parameters are shown in figure 3.9. The global minimum conformer, **a**, is O–H···N hydrogen-bonded complex and its higher interaction energy compared to the corresponding NH_3 complexes with H_2O and ethanol is the consequence of the electron withdrawing nature of the phenyl ring. O···H–N type of hydrogen bonding resulted in the second highest energy conformer, **b**. Conformer **c** is an NH_3–π complex in which NH_3 is slightly displaced from the ring center toward C1. Conformers **d**, **e**, and **f** correspond to hydrogen bonding of NH_3 with the aromatic hydrogens H9, H10, and H11. Table 3.2 indicates that the presence of NH_3 cis relative to the hydroxyl group, **d**, is energetically favored than the trans, **e**, position.

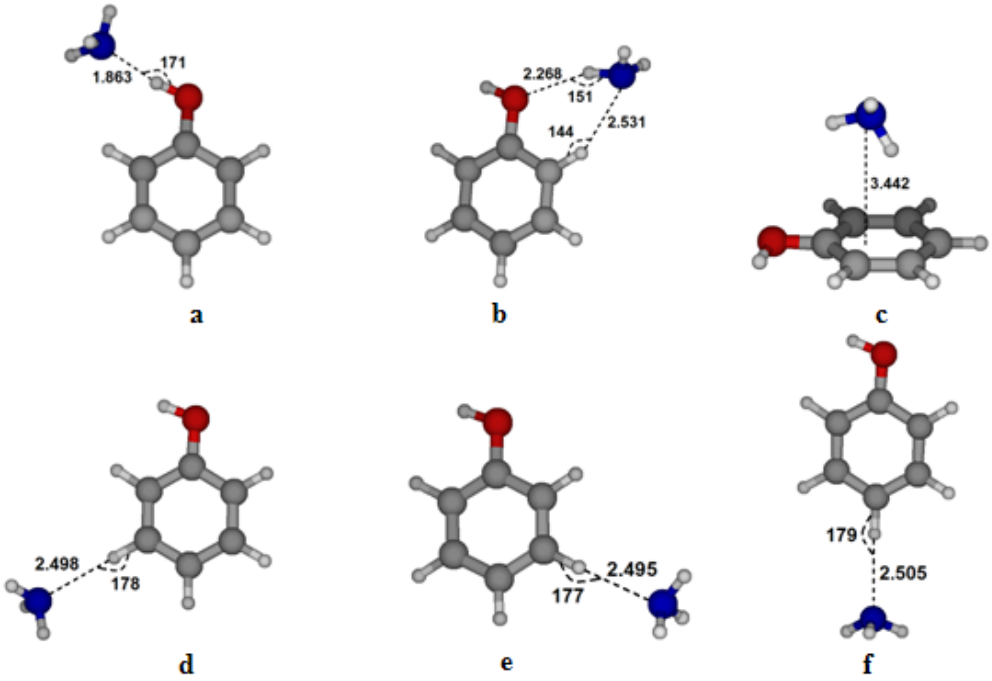

Figure 3.9. Optimized geometries of different minimum energy conformers in the NH_3-phenol complex.

3.3.1.8. Ammonia-p-methylphenol complex

The geometry of the optimized conformers for ammonia in complex with p-methylphenol and some of their structural data are reported in figure 3.10. These conformers are structurally similar to the corresponding NH_3-phenol complex with the exception of conformer **c** in which NH_3 is displaced from the center of the ring toward C4 instead of C1. The electron donating nature of the methyl group results in a decrease in the interaction energy of the N···H–O hydrogen bonded complex (**a**) and increase in the NH_3–π complex (**c**), in comparison with the corresponding phenol complexes.

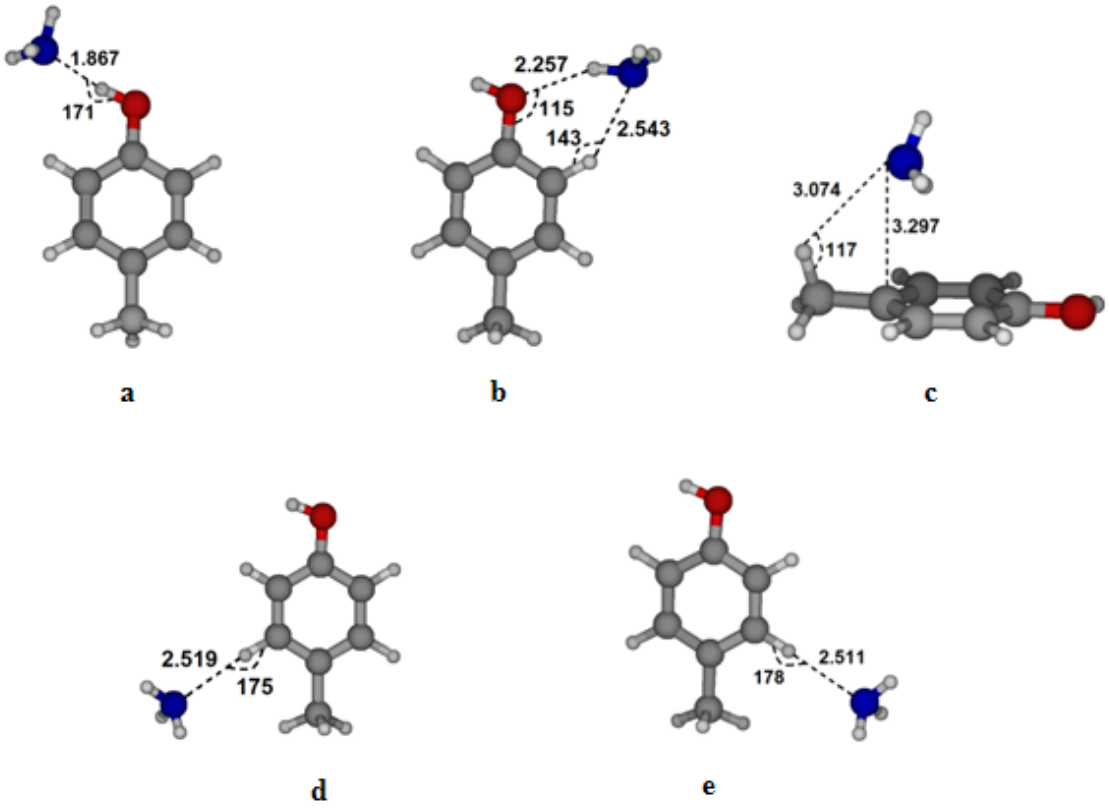

Figure 3.10. Optimized geometries of different minimum energy conformers in the NH_3-p-methylphenol complex.

3.3.1.9. Ammonia-indole complex

Geometry optimizations of different possible NH_3–indole complexes showed eight minimum energy conformers (Figure 3.11). The global minimum conformer, **a**, is (indole)N–H···N(NH_3) hydrogen bonded complex. The high interaction energy in this conformer compared to similar H-bonded complexes in ammonia dimer and ammonia-NMA complexes is attributed to the electron withdrawing nature of the aromatic moiety. Conformers **b** and **c** are NH_3–π type of complexes in which NH_3 is oriented in a bidentate conformation with one proton interacting with the π cloud of the five-membered ring and another interacting with the π cloud of six-membered ring. N is positioned on top of C9 in **b**, while it is located on top of C4 in **c**. The other conformers **(d–h)** involve H-bonding of NH_3 with the aromatic hydrogens H11, H12, H13, H15, and H14, with an increase in the interaction energy as the donor carbon atom becomes close to N1.

3.3.1.10. Ammonia-3-methylindole complex

Figure 3.12 shows the optimized geometries of the minimum energy conformers in the NH_3-3-methylindole complex. These conformers are structurally similar to the corresponding NH_3-indole conformers. Substitution of H12 in indole by the methyl group results in increasing the electron density of the π cloud and N1H10 group, which in turns results in an increase in the interaction energies in the NH_3–π complexes, **b** and **c**, and decrease of the interaction energy in the (3-methylindole)N–H···N(NH_3) H-bonded complex, **g**, compared to the corresponding NH_3 complexes with indole.

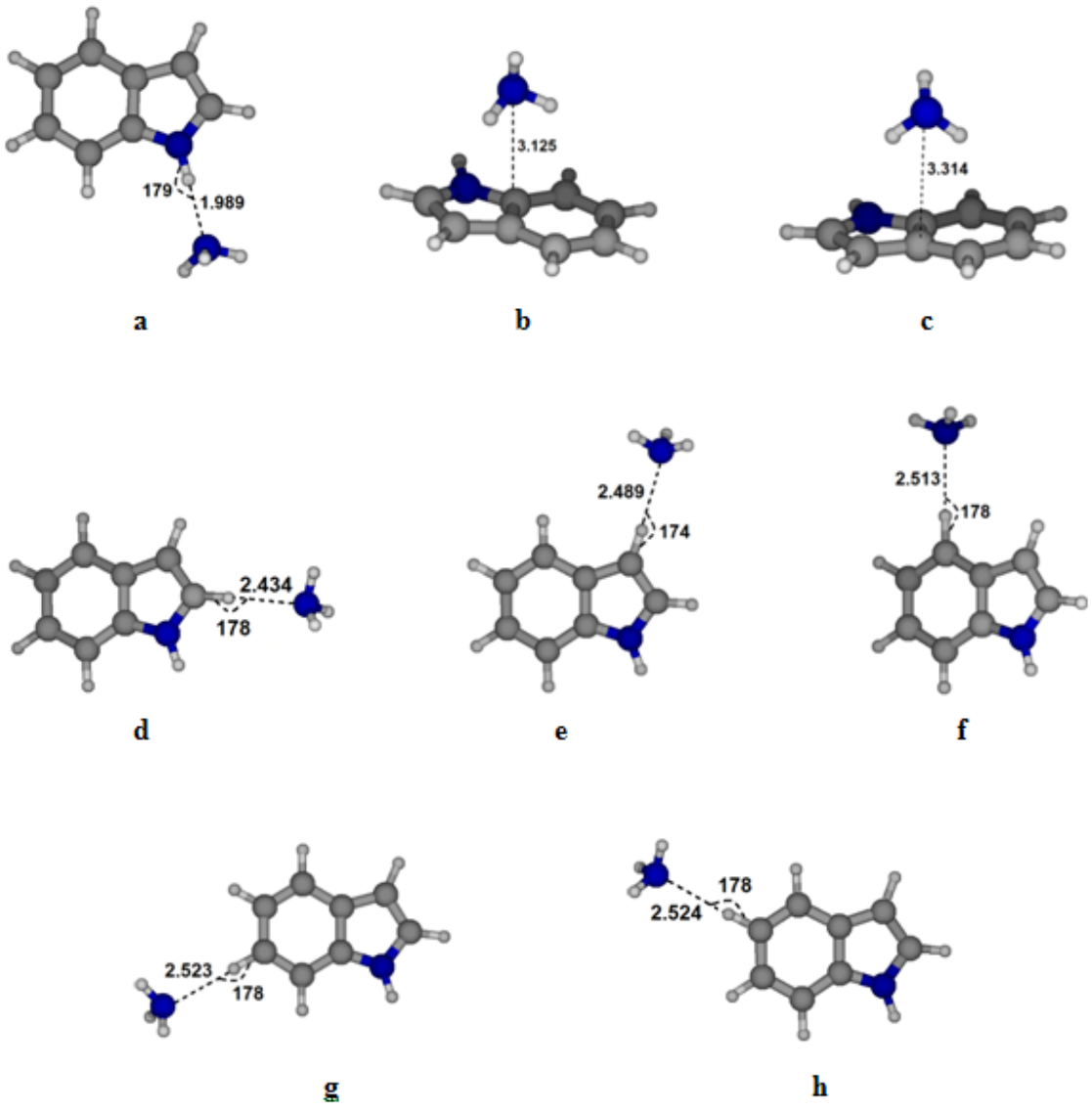

Figure 3.11. Optimized geometries of different minimum energy conformers in NH_3-indole complex.

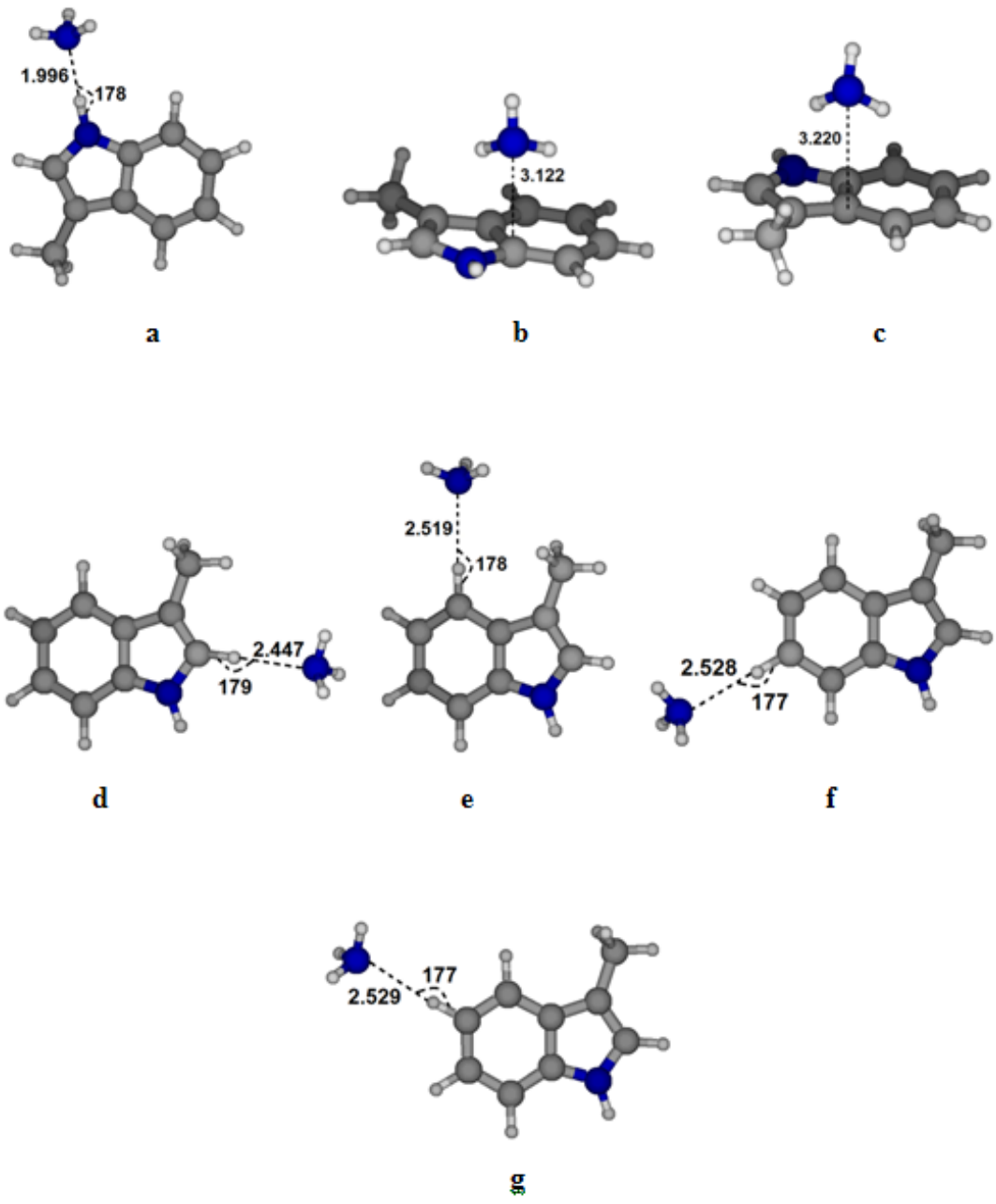

Figure 3.12. Optimized geometries of different minimum energy conformers in NH_3-3-methylindole complex.

3.3.1.11. Ammonia-imidazole complex

The five minimum energy conformers in NH_3-imidazole complex are reported in figure 3.13. In the global minimum conformer, **a**, NH_3 act as H-acceptor and is hydrogen bonded to imidazole via (imidazole)N3–H7···N(NH_3) type of hydrogen bonding. NH_3 form two other hydrogen bonded complexes, **b** and **c**, in which NH_3 act both as H-donor and acceptor. Conformer **d** involves NH_3–π interaction with N of NH_3 positioned on top of N3 and pointing one of its hydrogen atoms toward the π cloud of the five-membered ring. Conformer **e** is characterized by (imidazole)C4–H8···N(NH_3) hydrogen bonding.

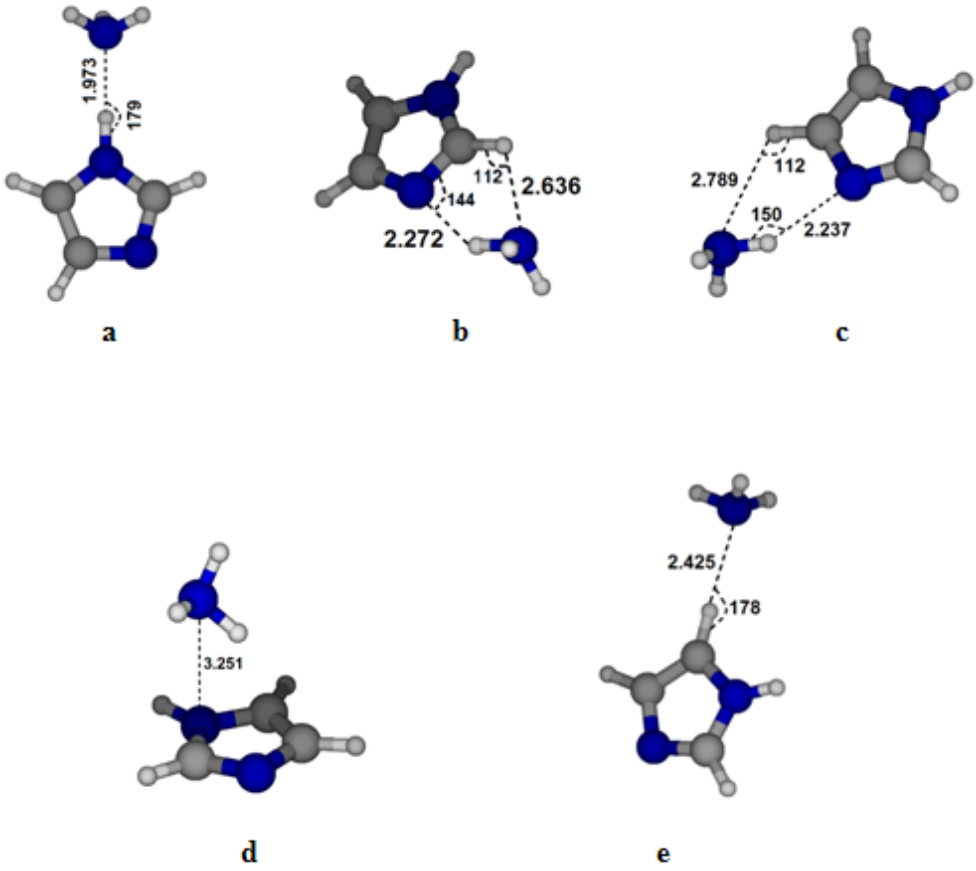

Figure 3.13. Optimized geometries of different minimum energy conformers in NH_3-imidazole complexes

3.3.1.12. Ammonia-4-methylimidazole complex

Four energy minima conformers are obtained in the NH_3-4-methylimidazole interactions (Figure 3.14), which are structurally similar to conformers **a**–**d** found in NH_3-imidazole interactions. The decrease in the interaction energy of conformer **a** and increase in the interaction energy of **d**, in comparison with the corresponding NH_3-imidazole conformers is attributed to the methyl group.

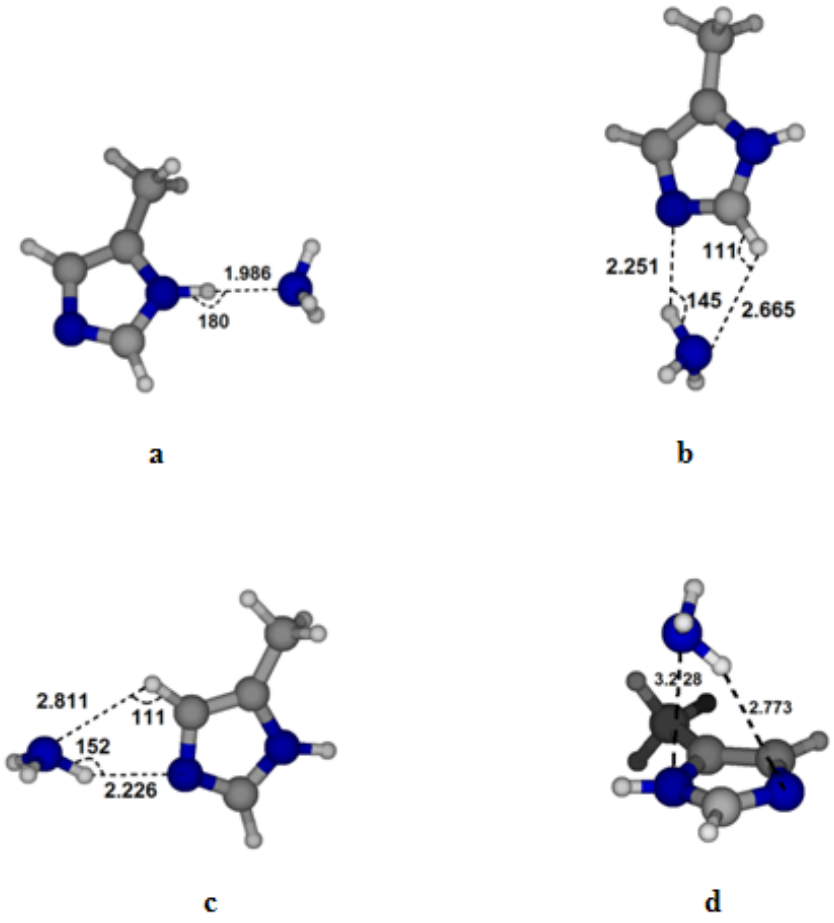

Figure 3.14. Optimized geometries of different minimum energy conformers in NH_3-4-methylimidazole complexes.

3.3.2. Potential energy surfaces

Ab initio calculated PESs for NH_3 complexes are reported as dashed lines in figure 3.15 together with the curves calculated from the optimized Drude models (solid lines, see section 3.3.3). Three potential energy curves are calculated for NH_3–H_2O complex. In the first two curves (Figure 3.15 **(a)**) the N···O distance is scanned with water acting as the H-donor or H-acceptor. Curve **(b)**, shows the scan of the N···O–H angle at O···N distance = 3.0 Å. A scan of the N···N distance in the NH_3 dimer is shown in curve **(c)**. Two PESs are calculated for the complex of NH_3 with ethanol (Figure 3.15 **(d)**) by the scan of the N···O distance, with NH_3 acting as H-acceptor in one and H-donor in the second. Two potential energy curves are calculated for NH_3–NMA complex with NH_3 similarly being the H-acceptor or H-donor (Figure 3.15 **(e)**). In case of benzene, two curves (Figure 3.15 **(f)** and **(g)**) are computed by scanning the distance between N and the ring centroid (X) as well as the angle X···N−H, respectively. In case of toluene, NH_3 is positioned on top of benzene such that N is on top of the ring center with its lone pair oriented toward the methyl group and similar to benzene a scan involved both the distance between N and the center of the ring (Figure 3.15 **(f)**) and the angle X···N−H (Figure 3.15 **(h)**). A scan of the O7···N distance is performed for the complexes of phenol and p-methylphenol with NH_3 and the results are shown in curve **(i)**. The N1···N distance is scanned in the complexes of NH_3 with indole and 3-methylindole and the corresponding results are shown in curve **(j)**. A scan of the N3···N distance is generated for the imidazole and 4-methylimidazole complexes with NH_3, as shown in curve **(k)**.

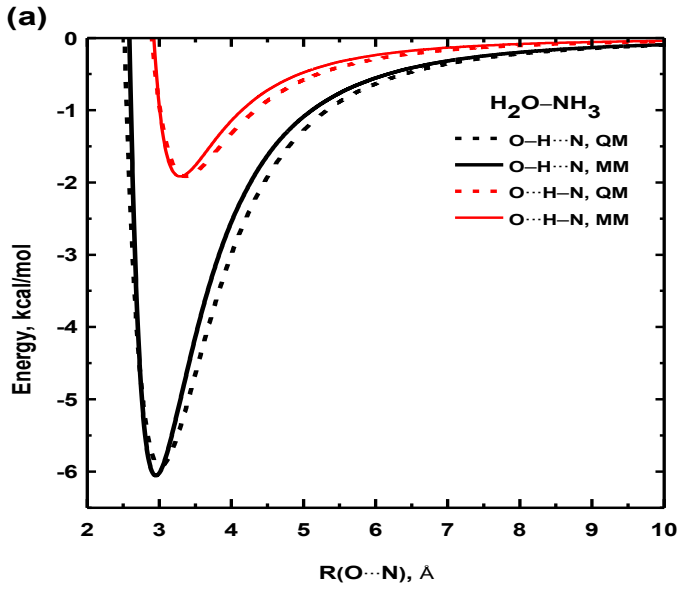
(a)
H2O–NH3
O–H···N, QM
O–H···N, MM
O···H–N, QM
O···H–N, MM
Energy, kcal/mol
R(O···N), Å

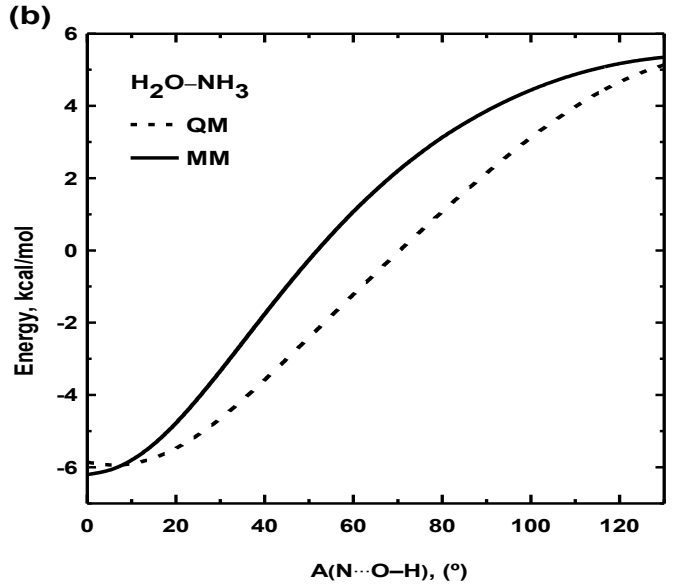
(b)
H2O–NH3
QM
MM
Energy, kcal/mol
A(N···O–H), (°)

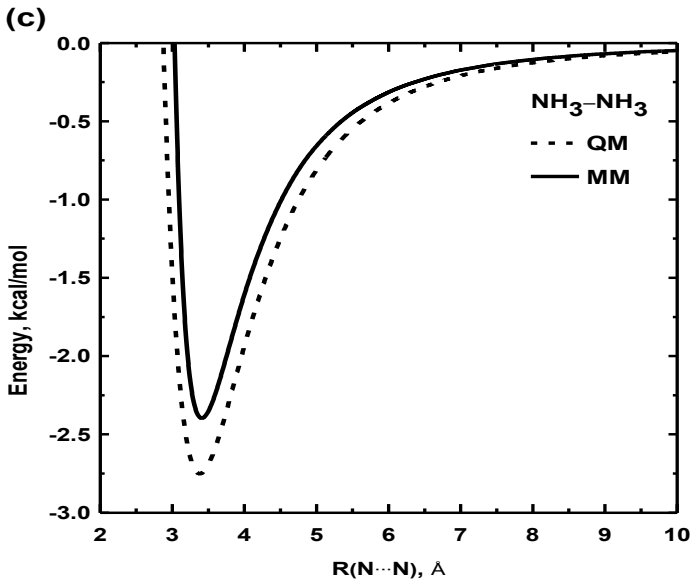
(c)
0.0
-0.5
-1.0
-1.5
-2.0
-2.5
-3.0
Energy, kcal/mol
2
3
4
5
6
7
8
9
10
R(N···N), Å
NH3–NH3
QM
MM

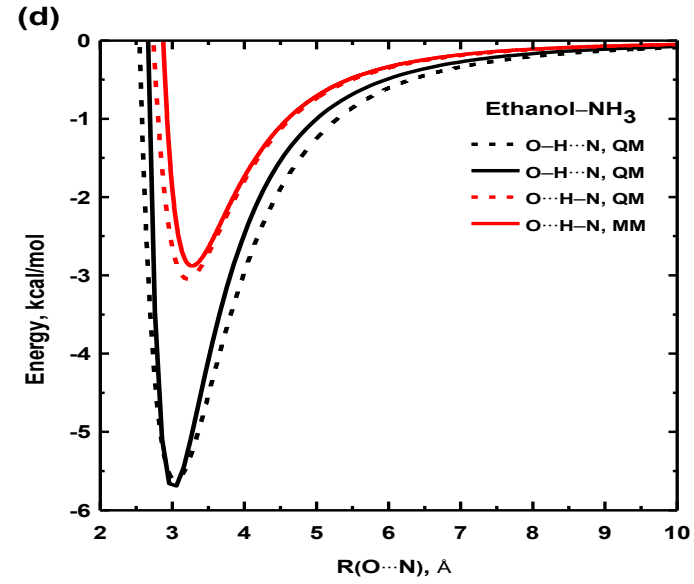
(d)
0
-1
-2
-3
-4
-5
-6
Energy, kcal/mol
2
3
4
5
6
7
8
9
10
R(O···N), Å
Ethanol–NH3
O–H···N, QM
O–H···N, QM
O···H–N, QM
O···H–N, MM

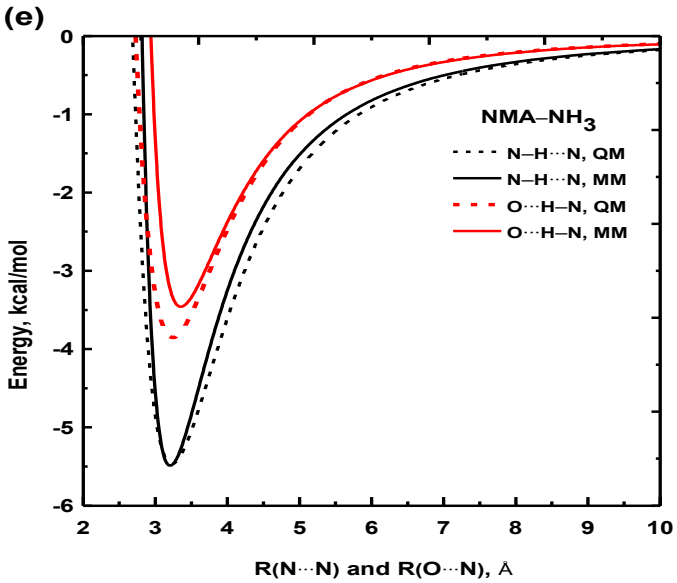
(e)
NMA–NH3
N–H···N, QM
N–H···N, MM
O···H–N, QM
O···H–N, MM
Energy, kcal/mol
R(N···N) and R(O···N), Å

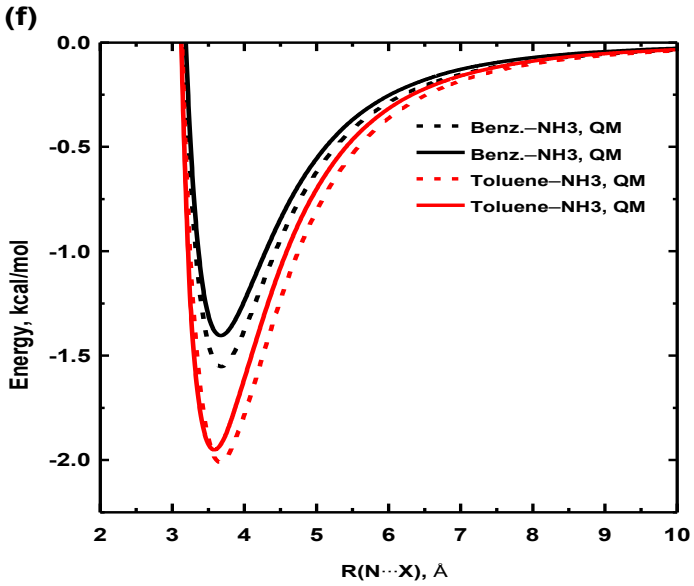
(f)
Benz.–NH3, QM
Benz.–NH3, QM
Toluene–NH3, QM
Toluene–NH3, QM
Energy, kcal/mol
R(N···X), Å

(g)

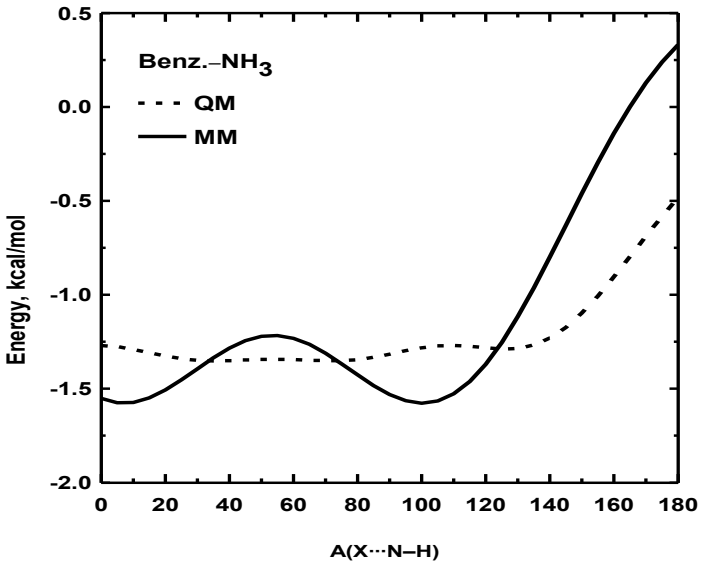
Benz.–NH3
QM
MM
Energy, kcal/mol
0.5
0.0
-0.5
-1.0
-1.5
-2.0
0
20
40
60
80
100
120
140
160
180
A(X···N–H)

(h)

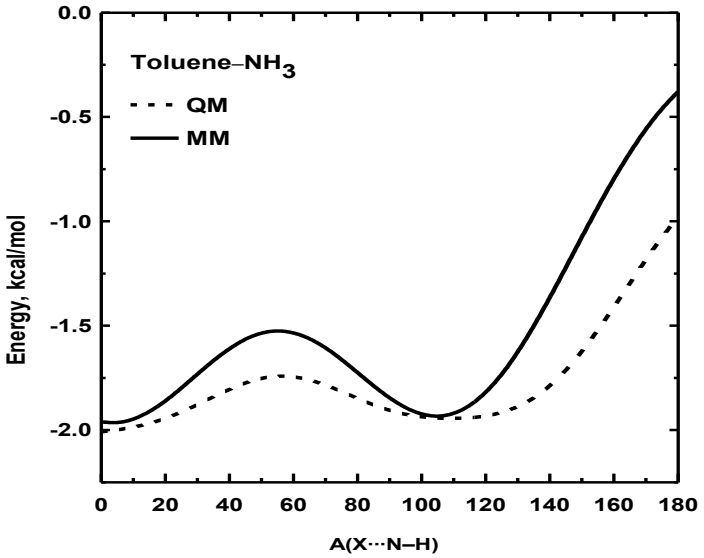
Toluene–NH3
QM
MM
Energy, kcal/mol
0.0
-0.5
-1.0
-1.5
-2.0
0
20
40
60
80
100
120
140
160
180
A(X···N–H)

(i)

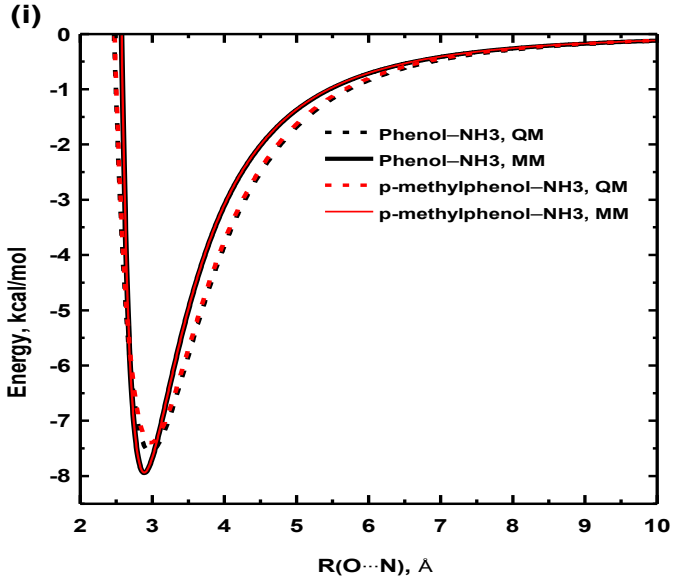
Phenol–NH3, QM
Phenol–NH3, MM
p-methylphenol–NH3, QM
p-methylphenol–NH3, MM
Energy, kcal/mol
R(O···N), Å

(j)

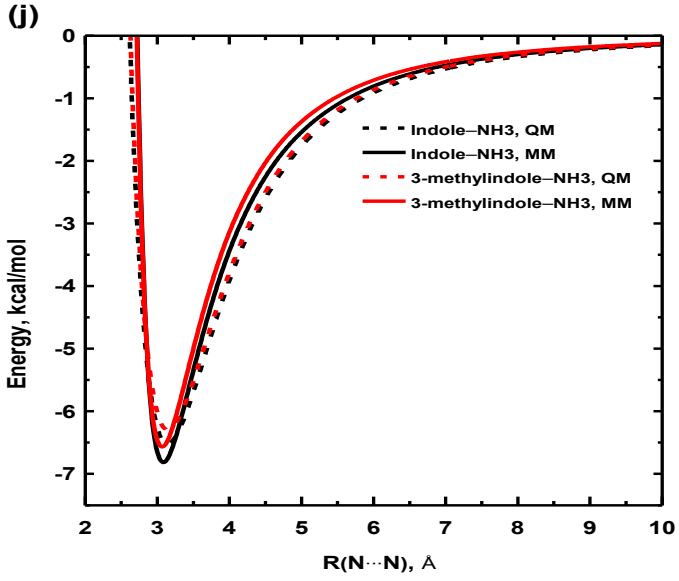
Indole–NH3, QM
Indole–NH3, MM
3-methylindole–NH3, QM
3-methylindole–NH3, MM
Energy, kcal/mol
R(N···N), Å

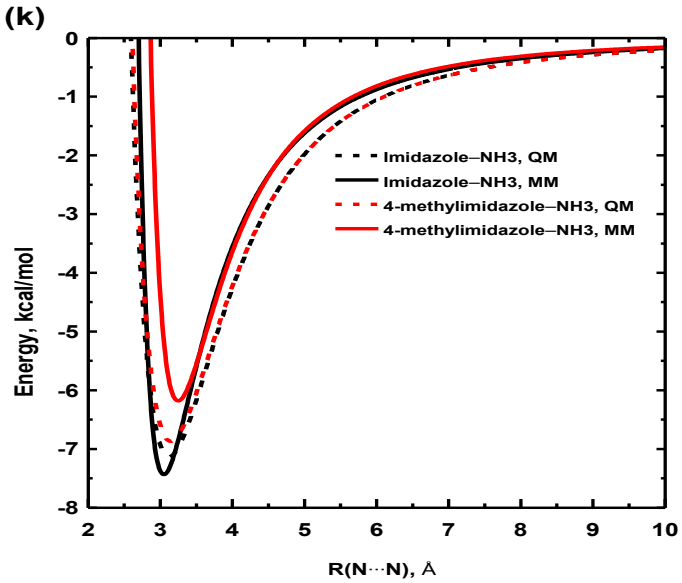

Figure 3.15. Potential energy curves for NH_3 complexes with all studied compounds. **(a)**, Complexation energy of NH_3 with H_2O as a function of N···O distance with H_2O being the H-donor (black) and H-acceptor (red); (**b)**, Complexation energy in NH_3–H_2O complex as a function of N···O–H angle at N···O distance of 3.0 Å; (**c**), Complexation energy in NH_3 dimer as a function of N···N distance; (**d)**, Complexation energy as function of N···O distance in NH_3-ethanol complex with ethanol acting as H-donor (black) and H-acceptor (red); (**e**), Complexation energy in NH_3-NMA complex as a function of N···N distance with NMA being H-donor (black) and H-acceptor (red); (**f**), Complexation energy in NH_3–benzene (black) and NH_3–toluene (red) complexes as function of X···N distance; (**g**), Scan of X···H–N angle in NH_3–benzene complex at X···N = 3.4 Å; (**h**), Scan of X···H−N angle in NH_3–toluene complex at X···N = 3.6 Å; (**i**), Scan of N···O distance in the NH_3-phenol (black) and NH_3-p-methylphenol (red); (**j**), Scan of N···N distance in the NH_3-indole (black) and NH_3-3-methylindole (red); (**k**), Scan of N···N distance in the NH_3-imidazole (black) and NH_3-4-methylimidazole (red). Dashed curves are MP2/6-311++G(d,p) results and solid lines are Drude models results.

3.3.3. Optimized force field

The structural parameters (N–H bond length = 1.013 Å and H–N–H angle = 107.29º) of NH_3 potential model are determined from geometry optimization of NH_3 at MP2/6-311++G(d,p) level of theory. The corresponding bond and angle force constants (k_b and k_θ, respectively) are set based on ab initio IR frequencies of gaseous NH_3 (ν = 1069, 2×1665, 3530, and 2×3681 cm^{-1}). The values, k_b = 525.0 kcal/mol/Å^2, and k_θ = 42.0 kcal/mol/rad^2 are chosen since they give comparable high frequencies (ν = 1614, 2×2218, 3556, and 2×3666 cm^{-1}) and maintain the structural geometry of NH_3 in MD simulations. While these parameters are overestimating the lower frequencies (bending vibrational frequencies), they give a fair agreement with the ab initio calculated angle bending PES, especially near the equilibrium value (Figure 3.16).

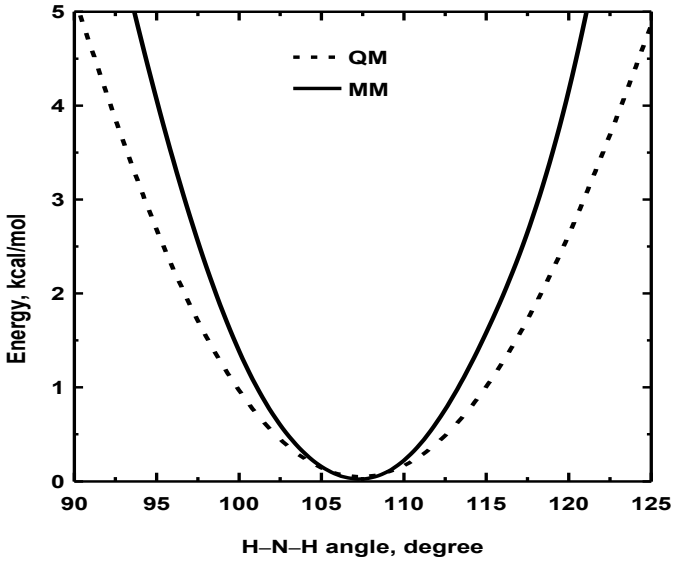

Figure 3.16. Potential energy surface for angle bending in NH_3, calculated from QM (dashed line) and Drude model (solid line).

Parameters for NH_3 potential model are reported in table 3.1. Table 3.3 summarizes the adjusted pair-specific LJ parameters between N of NH_3 and selected atoms in the interacting compounds. The optimized parameters for ammonia interactions with benzene and phenol reproduced the ab initio results for toluene and p-methylphenol, respectively. No further optimization is thus required for ammonia interactions with the later two compounds (toluene and p-methylphenol). Although parameters for ammonia complexes with indole and imidazole give fair agreement with the ab initio results on ammonia complexes with the corresponding methyl substituted compounds, we further optimized the parameters for better agreement. In figure 3.15, we plot the PESs calculated by the optimized models (solid lines) and those from ab initio calculations at MP2/6-311++G(d,p) level of theory (dashed lines). A good agreement between the two curves is observed. The slight deviation in ammonia dimer potential energy curve (Figure 3.15 **(c)**) is based on the fact that the parameters for the ammonia dimer model is adjusted based on the density of liquid ammonia and not based on the ab initio calculations. Ammonia-benzene potential model does not reproduce the angle scanned curve (Figure 3.15 **(g)**), however fair agreement between the two calculated curves is observed. Parameters in table 3.3 are those that reproduce the ab initio calculated geometries and interaction energies in the global minimum conformers of NH_3 complexes. We thus list the BSSE corrected (E^{CP}) complexation energies of the global minimum conformer and the corresponding complexation energies obtained by the optimized Drude models (E^{MM}) in table 3.3 for the purpose of comparison.

Table 3.3. Molecules interacting with NH_3 and their atoms together with the corresponding atom types that are selected to optimize the pair-specific LJ parameters with N of NH_3. The interaction energies (E^{MM}, kcal/mol) of the global minimum conformers obtained from the optimized models and the corresponding ab initio interaction energies (E^{CP}, kcal/mol) are reported in the last two columns, respectively.

Molecule[a]	Atom, j	Atom type	Pair-specific LJ parameters		E^{MM}	E^{CP}
			$Emin_{Nj}$ (kcal/mol)	$Rmin_{Nj}$ (Å)		
H_2O	–	–	–	–	–5.68	–5.89
NH_3	N	NNH3	0.21357610	3.960168890	–2.66	–2.73
Ethanol	O1	OD31A	0.61679281	3.44897910	–6.01	–5.86
NMA	–	–	–	–	–5.99	–5.76
Benzene	C1–6	CD2R6A	0.07034828	4.22565622	–1.806	–1.75
Toluene	C1–6	CD2R6A	0.07034828	4.22565622	–2.15	–2.47
Phenol	O7	OD31C	0.52870554	3.27473540	–8.28	–8.28
p-methylphenol	O7	OD31C	0.52870554	3.27473540	–8.10	–8.10
Indole	N1	ND2R5A	0.15256536	3.93073764	–6.94	–6.94
3-methylindole	N1	ND2R5A	0.54843186	3.52226841	–6.71	–6.73
Imidazole	N3	ND2R5A	0.83596139	3.40420408	–7.57	–7.58
4-methylimidazole	N3	ND2R5A	1.15876106	3.54234710	–7.42	–7.30

[a] Original models, except for NH_3, are taken from references,26, 91, and 140–142. The dash in the table indicate that no NBFIX parameters are required for these complexes, instead original atomic LJ parameters are used to calculate the mixed LJ parameters between all nonbonded atoms.

3.4. Hydration free energy of NH_3

The free energy of hydration of NH_3 relative to that of H_2O is calculated to validate the NH_3–H_2O potential model. The calculation follows the TI/MD simulation protocol in which NH_3 is mutated into H_2O in bulk water ($\Delta\Delta G_{hyd}$ ($NH_3 \rightarrow H_2O$)). On the base of multiple runs, the calculated value is –2.0±0.1 kcal/mol. The fact that the free energy of hydration of SWM4-NDP water molecule is –5.9±0.1 kcal/mol[87] results in a hydration free energy of NH_3 of –3.9±0.1 kcal/mol, in agreement with the experimental reported value of –4.3 kcal/mol.[106] It should be noted that no fitting was performed to reproduce the experimental value; the atomic LJ parameters of NH_3 were parameterized to reproduce the structure and energy of the NH_3–H_2O complex. By comparison, the NH_3 polarizable model of Dang and Garrett[132] yields –5.6±0.5 kcal/mol as the free energy of hydration of ammonia in water, which is considerably overestimating the experimental value.

3.3.5. Hydration structure of NH_3

The fact that our model of NH_3 is reproducing the H_2O–NH_3 complexation energy and geometry and the experimental hydration free energy of NH_3, suggests that it would provide a reliable solvation structure of ammonia in water. MD simulation on one ammonia molecule dissolved in 250 water molecules is thus performed to investigate the hydration structure of NH_3. The atom–atom radial distribution functions (RDF) $g_{NO}(r)$, $g_{NH}(r)$, $g_{HO}(r)$, and $g_{HH}(r)$ are reported in figure 3.17 **(a)–(d)**.

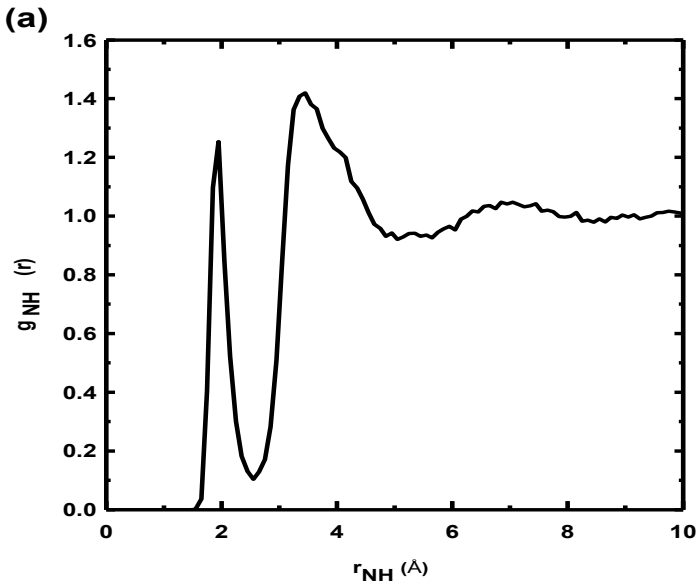
(a)
1.6
1.4
1.2
1.0
0.8
0.6
0.4
0.2
0.0
g NH (r)
0
2
4
6
8
10
r NH (Å)

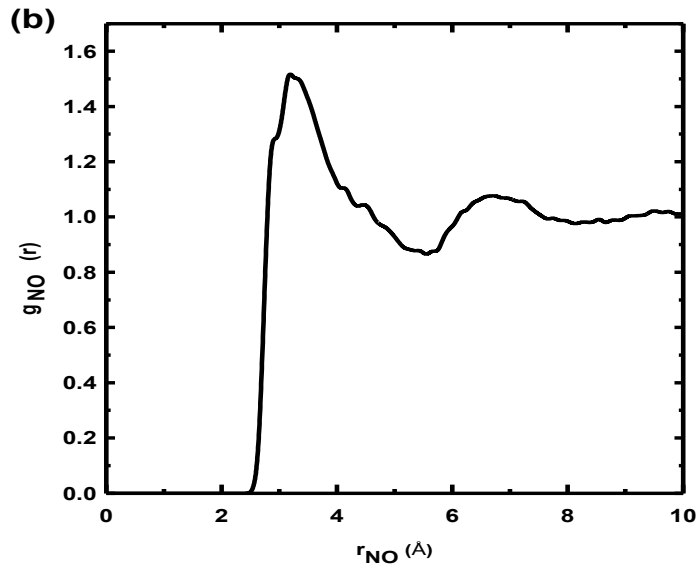
(b)
1.6
1.4
1.2
1.0
0.8
0.6
0.4
0.2
0.0
g NO (r)
0
2
4
6
8
10
r NO (Å)

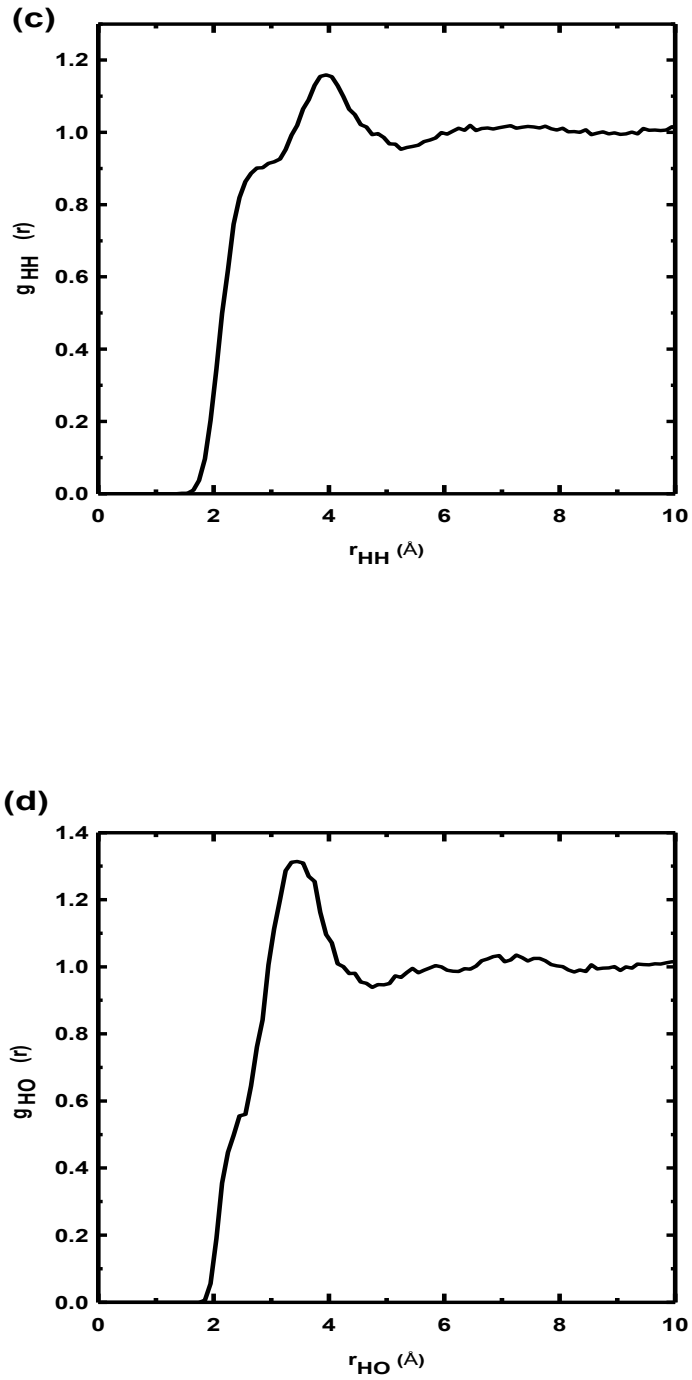

Figure 3.17. Nitrogen-hydrogen **(a)**, nitrogen-oxygen **(b)**, hydrogen-hydrogen **(c)**, and hydrogen-oxygen **(d)** radial distribution functions between ammonia molecule and water obtained from MD simulation results.

The N–H(H_2O) RDF exhibits a sharp, narrow, and well separated peak at 1.9 Å that corresponds to O–H···N hydrogen bonding interactions. The integration up to its minimum at 2.55 Å yields a coordination number of 1.7. A second peak centered at 3.4 is due to hydrogen atoms of water molecules interacting with NH_3 through O···H–N hydrogen bonding. In contrast to the first peak, the second peak depicts a less rigid solvation structure, as evidenced by the broader and less symmetric peak, indicating that O–H···N interactions are stronger and more stable than the O···H–N.

The N–O RDF exhibits a shoulder at 2.95 Å followed by a peak at 3.25 Å. Based on the calculated PESs for NH_3–H_2O complex (see figure 3.15 **(a)**), these two peaks can be assigned to O–H···N and O···H–N hydrogen bonded interaction, respectively. The week interaction in the O···H–N bonded complexes is the reason for the broad and asymmetric second peak. The peak at ~6.7 Å indicates a weak second hydration shell.

The (NH_3)H–H(H_2O) RDF displays a shoulder at 2.73 Å and a weak peak at 3.95, due to hydrogen atoms from water molecules bonded to NH_3 in the O–H···N and O···H–N hydrogen bonded modes, respectively.

The (NH_3)H–O RDF possesses a shoulder at ~2.3 Å that corresponds to O···H–N bonded complexes and a peak at 3.45 Å, due to O–H···N bonded complexes.

3.3.6. Liquid ammonia

Optimization of potential model for NH_3–NH_3 interaction is performed by fitting the N-N pair-specific LJ parameters so as to reproduce the experimental density of liquid ammonia at T = 239.65 K and p = 1 atm. MD simulation of 250 NH_3 molecules at 239.65 K and 1 atm is performed for 10 ns time period using the optimized parameters for ammonia dimer (Table 3.3). The last 7ns simulation results show 21.78 Å for the box length, which correspond to a density 0.684 g/cm^3, closely matching the experimental value of 0.682 g/cm^3.[149]

The enthalpy of vaporization, ΔH_{vap}, is an important property of liquids. In MD simulations, ΔH_{vap} can be calculated from the following equation.[150]

$$\Delta H_{vap} = -\frac{\langle E_l \rangle}{N} + RT$$

where $\langle E_l \rangle$ corresponds to the average of the potential energy of the liquid. The average potential energy of the system, in the last 7 ns, is found to be –1271.3 kcal/mol which corresponds to ΔH_{vap}= 5.561 kcal/mol, in close agreement with the experimental value, 5.577 kcal/mol.[151] It should be noted that the ammonia dimer model has not been further adjusted to reproduce the experimental enthalpy of vaporization.

Ricci *et al.*[118] conducted a neutron diffraction experiment to investigate the microscopic structure of liquid ammonia at two sets of thermodynamic conditions, one of which being T = 213 K, p = 1.2 atm. We simulated the system of 250 ammonia molecules at these thermodynamic conditions with the NTP ensemble. Similarly to the previous system, 10 ns of MD simulation are performed and the analysis is based on the last 7 ns.

The results show an average box length of 21.44 Å, which corresponds to a density of 0.717 g/cm^3, in excellent agreement with the experimental value, 0.715 g/cm^3.[118] It should also be noted that the ammonia dimer model has not been further optimized to reproduce this density. Figure 3.18 shows the atom–atom RDFs $g_{NN}(r)$, $g_{NH}(r)$, and $g_{HH}(r)$ of liquid ammonia along with the experimental RDFs of Ricci *et al*.[118] Compared to previous computational models used to simulate liquid ammonia using classical MD simulations[124,127,128] and ab initio/MD simulations,[120,123,124,128,130] our model presents the best agreement with the experimental structure of the liquid. It should be noted that the shoulder in the $g_{NN}(r)$ at 2.7 Å and the peak in the $g_{NH}(r)$ at 1.6 Å, observed experimentally are not reproduced by any literature model.

The $g_{NN}(r)$ function presented in figure 3.18 **(a)** shows three peaks centered at 3.4, 6.6, and 9.6 Å, indicating three well defined shells of neighboring molecules. The coordination number at the position of the first minimum in the $g_{NN}(r)$ curve, 5.1 Å, is found to be 13.7, in close agreement with the experimentally observed value of 14.[118]

The $g_{NH}(r)$ function reported in figure 3.18 **(b)** is similarly characterized by three peaks located at 3.6, 6.6, and 9.6 Å. The shoulder at 2.5 Å corresponds to the intermolecular N–H bonds.[118]

The $g_{HH}(r)$ function in figure 3.18 **(c)** has the same characteristic features of the experimental function. The higher intensity and sharpness of the first peak in our model compared to the experimental one is due to the applied constraints on the N–H bonds.

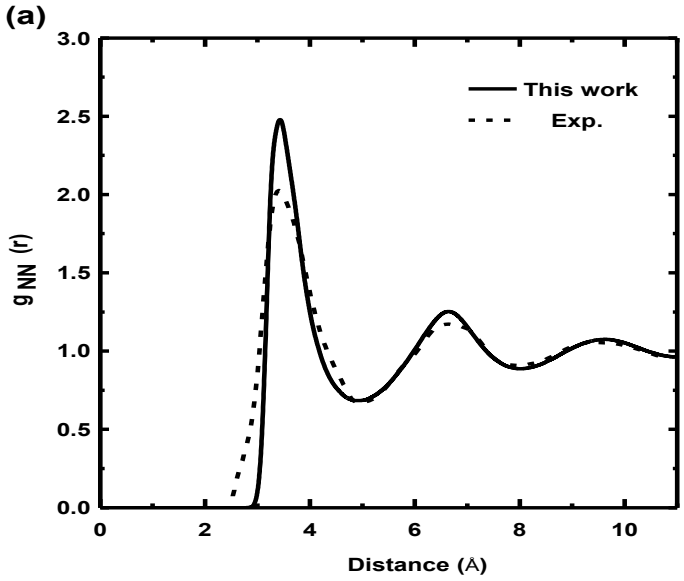
(a)
This work
Exp.
g_{NN} (r)
Distance (Å)

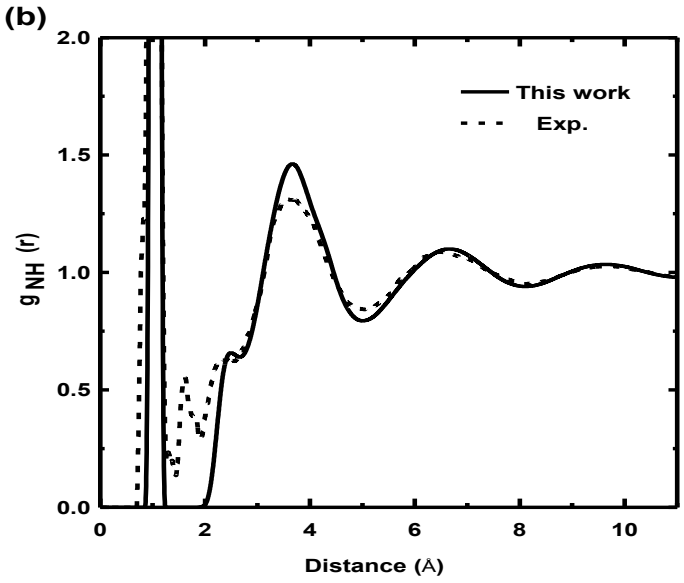
(b)
This work
Exp.
g_{NH} (r)
Distance (Å)

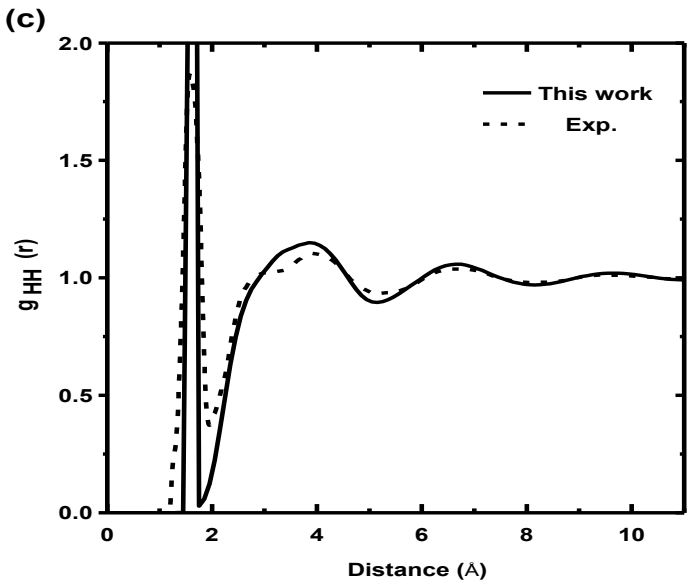

Figure 3.18. (a) N–N, **(b)** N–H, **(c)** H–H RDFs for atoms in liquid ammonia in comparison with NDIS experiment[118].

3.4. Summary

Ab initio QM calculations on NH_3, H_2O, and model compounds for the peptide backbone (NMA) and for amino acids side chains (ethanol, benzene, toluene, phenol, p-methylphenol, indole, 3-methylindole, imidazole, and 4-methylimidazole), and on their complexes with NH_3 have been performed in the gas phase at the MP2/6-311++G(d,p) level of theory. Minimum energy conformers in these complexes are reported. PESs of all NH_3 complexes are generated with respect to the global minimum conformers imposing the gas phase optimized geometries of the interacting monomers. Novel polarizable potential model for NH_3 is optimized based on the ab initio properties of NH_3 and its complex with water. The model reproduced the experimental free energy of hydration of NH_3 without further adjustments and used to investigate the hydration structure of NH_3. Optimization of the potential model for NH_3–NH_3 interaction was based on the density of liquid ammonia at its boiling point. Surprisingly however, the model reproduced the enthalpy of vaporization of the liquid at the boiling point and the density as well as the structure of liquid ammonia at other thermodynamic conditions without further adjustment. Polarizable potential models for the interaction of NH_3 with the other studied compounds are also optimized based on the ab initio calculations on the complexes. It should be noted that potential models for NH_3 interactions with the studied amino acid model compounds have not been reported in literature to date and the models will serve as reliable molecular models in studying biological processes involving NH_3.

4. Ammonium affinity and ion selectivity of the bacterial transporter AmtB studied using a polarizable force field for cation–π interactions

Abstract

The *Escherichia coli* AmtB protein is a member of the ubiquitous Amt family of ammonium transporters. AmtB proteins are homotrimers with one channel at the center of each monomer. Four binding sites (S1 to S4) have been identified crystallographically in the channel, with S1 located on the periplasmic surface of the protein and the other sites located in the pore lumen. While S1 is known to be selective for NH_4^+, over NH_3 and other monovalent ions, the nature of the species, NH_4^+ or NH_3, that binds the other sites, especially S2, has not been confirmed so far. Although free energy calculations have shown that permeation of the ionic species is prohibitive and NH_4^+ has to deprotonate at some point along the permeation pathway, the position where deprotonation occurs and the identity of the proton acceptor have not been identified. The present computational study addresses the issue of selectivity of the periplasmic binding site (S1) of AmtB toward Na^+, K^+, and NH_4^+ as well as the relative binding affinity of NH_4^+ to S1 and S2. Polarizable force fields based on classical Drude oscillators are developed for the interactions of Na^+, K^+, and NH_4^+ with model compounds of the amino acids side chains that exist in S1 and S2 (Ser, Phe, Trp, and His). These force field models are optimized based on ab initio quantum mechanical calculations on the interactions of the ions with the model compounds, at the MP2/6-311++G(d,p) level of theory. The optimized models are used in hybrid polarizable/conventional molecular

dynamics simulations. Our calculations show that of all three ions, only NH_4^+ can reach S1 site confirming that S1 selects NH_4^+ over Na^+ and K^+. We also find that S2 has higher affinity to NH_4^+ compared to S1, suggesting that deprotonation does not occurs in S1 and the ion is stable enough to reach S2.

4.1. Introduction

Ammonia/ammonium (Amm) is the preferred source of nitrogen for many bacteria, fungi, and plants[36,152], while for other organisms such as mammals it is a toxic metabolic waste product.[135,136] To facilitate the transport of Amm and/or methylammonium (MA), plants, bacteria, yeast, and mammals express transmembrane proteins of the Amt/MEP/Rh family.[36,135,136,152] AmtB is an ammonium transporter protein present in the bacterial inner membrane which provides a source of nitrogen for amino acid synthesis in bacteria. The structure of AmtB from *Escherichia coli* has been determined by X-ray crystallography.[32,33] These structures show that AmtB is a homotrimer (Figure 1.5 **a**) with one pore at the center of each monomer. The 20 Å-long pore is narrow and highly hydrophobic with two almost totally conserved histidine residues (His168 and His318).

Under physiological pH, Amm exists predominantly in its ionic form (NH_4^+). Thus it is NH_4^+ that binds the periplasmic entry (S1) of the AmtB channel.[32,33] The crystal structure of AmtB is showing at that site what is likely an NH_4^+ ion in coordination with three aromatic amino acids Phe115, Phe103, and Trp148 through cation–π interactions. In addition, the ion is H-bonded to Ser219.[32]

Experimental studies on AmtB[37] and other Amm transport proteins[36,38] have shown that S1 is selective for NH_4^+ over other monovalent cations. The results show that while Cs^+ and Tl^+ inhibit the protein activity[37], Na^+ and K^+ do not inhibit the functionality of these proteins.[36,37,38] The inhibition of the protein activity might by the result of binding ions (other than ammonium) to S1 which prevent ammonium from binding and inhibit its transport. The experimental results clearly suggesting that S1 is selective for NH_4^+ over the biologically abundant monovalent ions, Na^+ and K^+.

So far, computational studies[39,40] on the selectivity of the S1 have not shown good agreement with the previous experimental results. A combined QM/MM investigation on the binding selectivity of AmtB toward Na^+, K^+, NH_3, and NH_4^+ performed by Nygaard *et al*.[39] showed that K^+ can reach S1 of AmtB. Luzhkov *et al*.[40] have reported that S1 is selective for NH_4^+ against Li^+, Na^+, K^+, Rb^+, and Cs^+ by 3.3, 4.4, 2.6, 2.5, and 2.4 kcal/mol, respectively. Though this indicates that NH_4^+ is selected over all alkali cations, the observed relative binding trend is not very reliable, for example K^+ and Cs^+ seem to have the same relative binding energies (~2.5kcal/mol) with respect to NH_4^+, in apparent contradiction with the experiment of Javelle *et al*.[37]

The structure of Khademi *et al.* crystallized in presence of ammonium salts[5] shows electronic density in three sites (S2, S3, S4) of the pore lumen of AmtB (see figure 1.5**b** for locations of S1 to S4). Based on the hydrophobic character of the pore, it was suggested that these sites are occupied by ammonia molecules.[32] Electronic density in the pore lumen has also been observed by Zheng *et al.*[33] for crystals grown in absence of ammonium salts, suggesting that water molecules exist in the pore lumen. Using detailed free energy calculations, Lamoureux *et al.* showed that the "hydrophobic" pore actually

stabilizes a file of water molecules that penetrate the pore from the cytoplasmic side and adopt similar positions to the crystallographic sites.[35]

Although NH_4^+ is known to be the species that binds S1, the identity of the transported species and the mechanism of transport have not been confirmed so far. Based on experimental evidences, three permeation mechanisms have been suggested namely, the electroneutral NH_3 transport,[32,33,37,153–155] NH_3/H^+ symport,[37] and NH_4^+ transport.[36,152,41,156]

Computational investigations on the transport mechanism and nature of the transported species in AmtB proteins have also been conducted and several mechanisms were reported.[31,39,40,43,157–161] To the best of our knowledge, none of the force fields employed in studying Amm transport proteins so far have been calibrated to reproduce the interactions of Amm with amino acid side chains lining the permeation pathway. Binding energies calculated using these force fields are thus expected to be unreliable and more accurate force fields are required for understanding of the binding affinity and selectivity of S1 and the transport mechanism in these families of proteins.

The focus of the present study is to provide a reliable estimate of the selectivity of S1 toward NH_4^+ against the more biologically abundant monovalent ions Na^+ and K^+. We aim also to measure the binding free energy of NH_4^+ in S2 relative to S1 in order to investigate the favored permeable species. For this purpose we calibrate polarizable force field models based on ab initio calculations on the interactions of Na^+, K^+, and NH_4^+ with nine organic compounds that model the side chains of amino acids that near S1 and S2 (ethanol, N-methylacetamide, toluene, phenol, p-methylphenol, indole, 3-methylindole, imidazole, and 4-methylimidazole). In these compounds, ethanol models Ser, N-

methylacetamide (NMA) models the peptide backbone, toluene models Phe, phenol and p-methylphenol model Tyr, indole and 3-methylindole model Trp, and imidazole and 4-methylimidazole model His. We describe amino acids side chains that are close to S1 (Ser219, Phe103, Phe107, Phe215, and Trp148) and S2 (Phe107, Phe215, Trp212, His168, and His318) by the polarizable models and use non polarizable force field for other amino acids. The hybrid polarizable/conventional force field is then applied to calculate the binding free energy of NH_4^+ in S1 relative to that of Na^+ and K^+. The binding free energy of NH_4^+ to S2 is also calculated and compared to that of S1 in order to investigate the thermodynamically favored permeable species from S1 to S2 and to suggests deprotonation position and proton acceptor along the permeation pathway.

4.2. Methods

4.2.1. Potential energy function and parameterization strategy

NH_4^+ in S1 of AmtB is stabilized by cation–π interactions with Phe103, Phe107, Trp148, and Phe215, and H-bonding to Ser219.[32] In addition, the ion interacts with water molecules in the periplasmic side of the protein. The nearest neighbors to the ion in S2 on the other hand are: Phe107, His168, Trp212, Phe215, and His318. In addition, the ion interacts with the underlying molecule occupying S3 in the pore lumen (water in our case).[35] Reliable estimation of ions binding free energy to S1 or S2 will thus require a force field for ions calibrated to reproduce their interactions with the nearest neighbors. For this purpose, we parameterize polarizable potential models based on the classical Drude oscillator[25,87,162] for the interactions of Na^+, K^+, and NH_4^+ with model compounds of these amino acid side chains.

To account for induced polarization in the region of the binding sites, a Drude particle carrying a negative charge is bound to heavy, non-hydrogen atoms via a harmonic spring.[25,87,162] The atom-Drude spring constant k_D is set to 1000 kcal/mol/Å^2 for all Drude oscillators in the system. The magnitude of the charge that the Drude particle must carry (q_D) to produce the correct polarizability α, is determined from the relation $q_D = \sqrt{\alpha K_D}$.[25,87] The methodology on the Drude polarizable models has been documented elsewhere.[87,162] Polarizable models based on the classical Drude oscillators have been developed for water,[26,163] aromatic compounds,[91] amides,[141] alcohols,[140] ammonia,[II] and ions.[I,92] We are extending these models to describe the interaction of some of these compounds with Na^+, K^+, and NH_4^+. The general strategy for parameterizing the polarizable force field has been documented elsewhere.[26,87,91,140,141,163]

Potential models for the interactions of Na^+, K^+, and NH_4^+ with water have been reported previously.[I,92] We only describe the details for optimizing potential models for the interaction of the ions and the amino acid-model compounds (ethanol, N-methylacetamide, toluene, phenol, p-methyphenol, indole, 3-methylindole, imidazole, and 4-methylimidazole). Optimization of the force field follows the procedures reported previously.[I,II] Optimization is based on adjusting the Lennard-Jones (LJ) parameters between atoms of ions (Na^+, K^+, and NH_4^+) and specific atoms in the interacting compounds. By default, the parameters of the LJ 6-12 interaction $Emin_{ij}$ and $Rmin_{ij}$ for atoms *i* and *j* are generated using the Lorentz-Berthelot combination rule:

$$Emin_{ij} = \sqrt{\left(Emin_i Emin_j\right)} \qquad \text{and} \qquad Rmin_{ij} = \left(Rmin_i + Rmin_j\right)/2$$

The "NBFIX" option of CHARMM allows to override the default values from the combination rules and assign pair-specific LJ parameters.[I,II,86,164] It is thus the pair

specific LJ parameters that are adjusted to optimize our potential models. The target values are the ab initio gas phase properties of the ions complexes with interacting compounds.

Atoms selected for parameterization are those that are most relevant to the complexation. A non-atomic site (X), described in our previous study[I] is found necessary to model the interactions of Na^+, and NH_4^+ with toluene. Similar sites are also required to model the interaction of the three ions with phenol and to model the interaction of NH_4^+ with indole and 3-methylindole. The non-atomic sites X are massless particles at the center of the six-membered ring with no electric charge and with no LJ parameters. These sites show VDW interactions with specific atoms of the ions through pair-specific LJ parameters. LJ pair-specific parameters between the ions and more than one atom in the interacting ligand are used to reproduce the ab initio results. For the purpose of simplifying the optimization process, the LJ pair-specific parameters between different pairs of interacting atoms in some complexes are set equal. Optimization is first performed on the interactions of the ions with the simple model compounds "unmethylated compounds", and the transferability of the optimized parameters to methylated compounds is then tested. In general a good performance is observed, however, the parameters are further adjusted to closely model ab initio results.

Optimization of the pair-specific LJ parameters is performed in two steps, following our previously reported strategy.[I, II] The first step in the optimization of the pair-specific LJ parameters is to reproduce the ab initio PESs. In this step the parameters are adjusted in an iterated procedure so as to reproduces the ab initio curves. The obtained parameters are the subject of a second optimization step in which the complex

geometry (position and orientation of the cation relative to the interacting molecule) and the "free" interaction energies (without imposing geometry constraints except fixing the bonds to H atoms using the SHAKE algorithm[93]) are fitted to the ab initio results.

It should be noted that while the interaction of the ions with neighboring amino acid side chains are described by the optimized polarizable force fields, nonpolarizable additive CHARMM force field PARAM27,[90] with the TIP3P water model[165] will be used for other interactions in the simulated AmtB systems. Because the Drude model is based on point charges and not point dipoles, the electrostatic interactions between the additive potential and the polarizable potential are described in a "transparent" way as charge-charge interactions.

4.2.2. Ab initio calculations

Optimized geometries of NH_4^+ and the considered nine interacting ligands were obtained by us in previous studies.[I,II] Full geometry optimizations of the complexes between these ligands and the three cations Na^+, K^+, and NH_4^+ are performed at MP2 level with the 6-311++G(d,p) basis set using Gaussian 09 program.[88] Geometry optimization is performed without imposing any symmetry constraints, except for complexes of NH_4^+ with imidazole and 4-methylimidazole, which are optimized constraining the ammonium N–H bonds at their gas phase values. This constraint is applied in order to avoid the transfer of the proton from NH_4^+ to N1 in imidazole or 4-methylimidazole. The interaction energies are corrected for basis set superposition error (BSSE) by using the Boys and Bernardi counterpoise technique.[89] Potential energy surfaces (PESs) are computed at the same level of theory and all interaction energies are

corrected for BSSE. The curves are computed with rigid monomers employing their gas phase optimized geometries by scanning the intermolecular distances between the ions and ligands.

4.2.3. AmtB simulation model

The simulation system (Figure 4.1) is built using the CHARMM-GUI web interface.[166] The high-resolution X-ray structure of AmtB determined by Khademi *et al.* is used in this work (PDB code 1U7G).[32] The three mutated residues (F68S, S126P, and K255L) in 1U7G are modified back to their native states. The protonated states of histidine residues are determined based on their individual microenvironments with the proton being attached to N_δ in the imidazole ring for His168 and to N_ε for His318. For simulations of Na^+, K^+, or NH_4^+ in the periplasmic binding site S1 (Figure 4.2), the side chains of amino acids Phe103, Phe107, Trp148, Phe215, and Ser219 are constructed to be polarizable. For simulations of NH_4^+ in site S2 (Figure 4.3), the side chains of amino acids Phe107, His168, Trp212, Phe215, His318 are made polarizable. These residues are selected because they are the nearest neighbors to the ions in the binding sites. Phe215 is considered polarizable in simulations involving ions in S1 and Phe107 is considered polarizable when NH_4^+ is simulated in S2 because their side chains are in parallel displaced arrangement which will result in additional stabilization of the ion in both sites due to the strength added to cation–π interaction by the second π system.[I,22]

A single AmtB monomer from the trimeric crystal structure is embedded in a phospholipid bilayer constructed with a total of 185 DMPC (1,2-dimyristoyl-sn-glycero-3-phosphocholine) molecules: 94 DMPC molecules on the periplasmic side and 91 on the

cytoplamic side. Water is added to both the top and bottom of the phospholipid bilayer. The systems are placed in a rectangular box of 92 Å × 90 Å × 77 Å immersed in explicit liquid water containing 33 potassium (K^+) and 36 chloride (Cl^-) ions, corresponding to a salt concentration of ~0.1 M. The final model (Figure 4.1) consists of about 66990 atoms, including the AmtB protein, 185 DMPC molecules, 13111 water molecules, 33 K^+ ions, and 36 chloride ions.

In order to accurately describe the interaction of the ion with its surroundings, two water molecules near the ion at S1 are described using the polarizable SWM4-NDP water model[26,163] and are kept in place using a weak harmonic potential. Four water molecules that have entered the pore from the cytoplasmic site and are interacting with the ion in S2 and with the polarizable side chains in S2 are also described by SWM4-NDP water model. Parameters of the polarizable amino acids side chains are taken from the studied model compound,[91,140,141] being $–CH_2$-OH from ethanol for Ser219, $–CH_2$-C_6H_5 from toluene for Phe103, Phe107, and Phe215, $–CH_2$-C_8H_6N from 3-methylindole for Trp148 and Trp212, and $–CH_2$-$C_3H_3N_2$ from 4-methylimidazole for His168 and His318. Those polarizable fragments are linked to the α carbons of the corresponding residues. To keep the fragment electrically neutral, the charge on the H atom removed is transferred to the carbon atom. All bonded parameters between polarizable and nonpolarizable atoms are taken from CHARMM27 parameters.[90]

MD simulations are performed with the program CHARMM[167] (version c34b2). The all-atom empirical potential energy function for proteins[90] and phospholipids[168] used in conjunction with the TIP3P water model.[165] All MD simulations are performed using the velocity Verlet integrator with 1fs as the integration time-step and the SHAKE algorithm to constrain covalent bonds involving hydrogens.[93] Electrostatic interactions

were computed with particle-mesh summation,[169] with $\kappa = 0.34$ for the charge screening, 1.0 Å grid spacing, and fourth-order splines for the mesh interpolation. The Lennard-Jones interactions are cut off at 12 Å. The temperature of the system is controlled with a two-thermostat algorithm, where atoms are kept at room temperature (298.15 K), and the auxiliary Drude particles are kept at low temperature (1 K) to assure the self-consistent induction regime.[87]

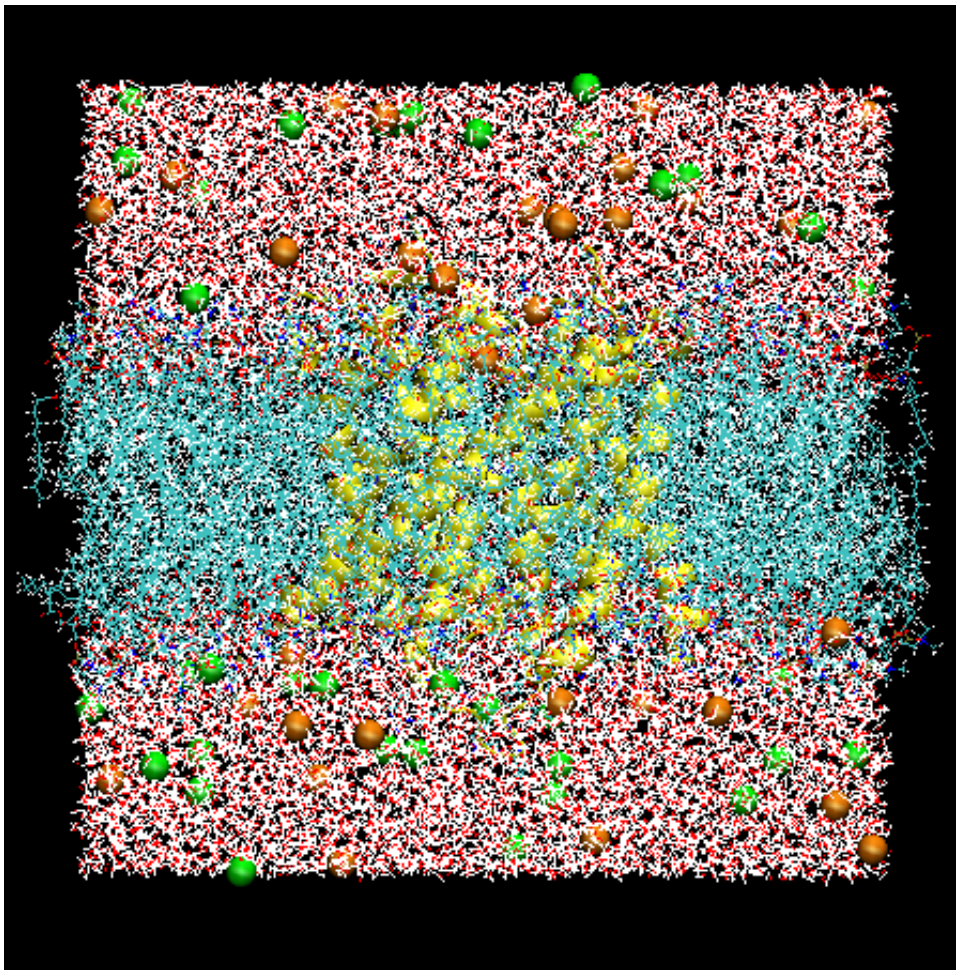

Figure 4.1. AmtB membrane protein model (unitary cell) for free energy calculations simulations. The cartoon structure of AmtB is shown in yellow. Atom colors are red for oxygen, blue for nitrogen, cyan for carbon, white for hydrogen, orange for potassium, and green for chloride.

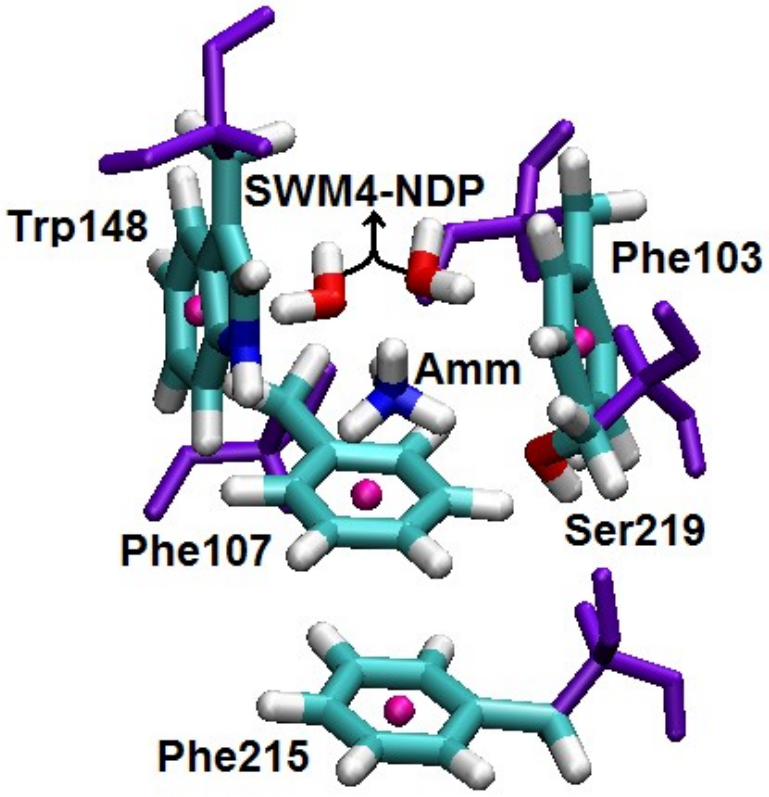

Figure 4.2. A snapshot from MD simulations showing ammonium ion in S1 and surrounding residues. Atom colors are as mentioned in figure 4.1. Non-atomic sites in Phe and Trp side chains are presented as pink spheres and nonpolarizable segments of the amino acids are colored in violet.

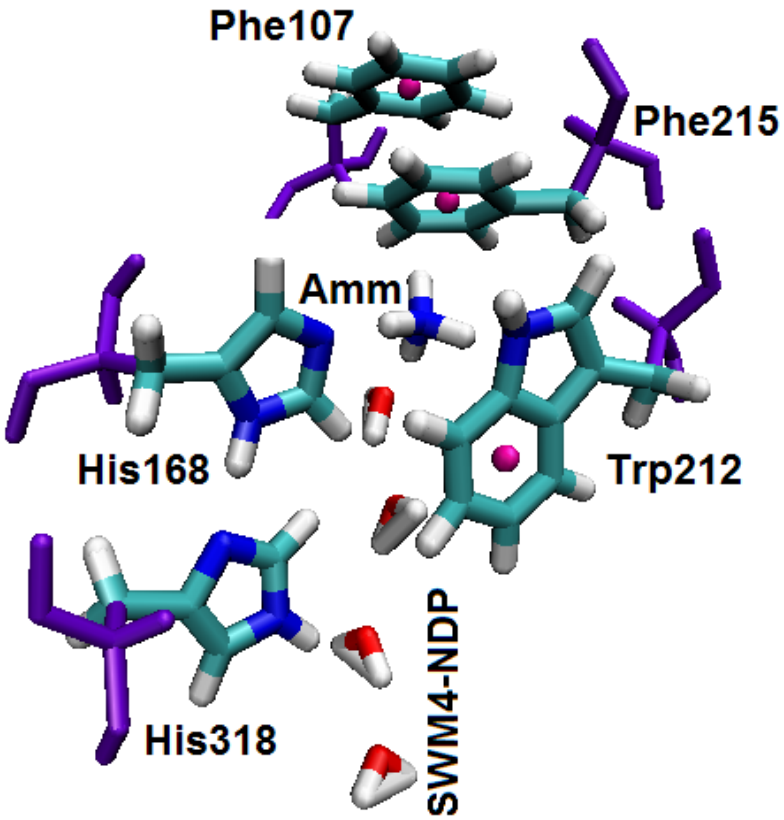

Figure 4.3. A snapshot from MD simulations showing ammonium ion in S2 and surrounding residues. Colors are as in figure 4.2.

4.2.4. Free energy calculations

Calculations of the relative free energies follow a standard protocol described elsewhere.[I,II,40,94,95] Relative binding free energies ($\Delta\Delta G_{\text{bind}}$) are evaluated from the conventional thermodynamic cycle involving the transformation of one ligand (A) into another (B).[40]

$$\Delta\Delta G_{bind}(A \rightarrow B) = \Delta G_{bind}(B) - \Delta G_{bind}(A) \equiv \Delta G_{mut}^{prot} - \Delta G_{mut}^{wat} \qquad (1)$$

where ΔG_{mut}^{prot} and ΔG_{mut}^{wat} are the relative free energies for the $A \rightarrow B$ alchemical ligand "mutation" in the binding sites and in water.[40]

To maintain a constant number of interaction sites throughout the transformation, special hybrid residues are used (Figure 4.4). As stated in our previous studies,[I,II] these residues are made by bonding one fragment representing an original ion with a second "dummy" fragment representing the second ion. Force constant of 5 kcal/mol/Å^2 is assigned to the tether between the two fragments. The ligand mutation involves thus variation of the nonbonded as well as the bond lengths and valence angles that are considered. The MD simulation protocol used in this work involves ligand transformation in 12 steps, controlled by the mapping parameter λ, which takes the following values: 0, 0.05, 0.15, 0.25, 0.35, 0.45, 0.55, 0.65, 0.75, 0.85, 0.95, and 1. The calculation of the free energy increments at each value of λ includes equilibration for 100 ps and subsequent data collection for 200 ps.

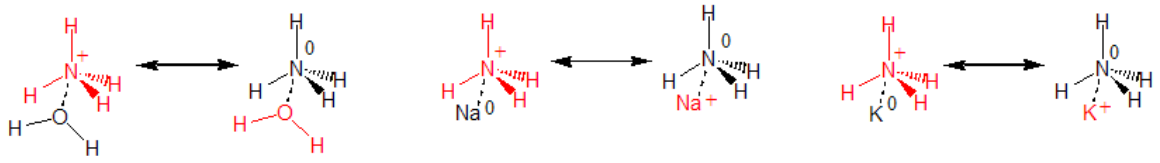

Figure 4.4. Ligand transformation involved in the free energy calculations. Ligands colored in red are "real" while those in black are "dummy".

The mutated ligands in S1, H_2O, Na^+, K^+, and NH_4^+ do not have the same stability in this binding site with NH_4^+ being more stable. Similarly NH_4^+ is more stable than H_2O in S2. A weak restraint potential is thus imposed on the ligands to prevent large drifts from S1 and S2, in order to allow for reliable measurements of relative binding free energies. The 1U7G crystal structure[5] of AmtB is showing the center of mass (CM) of NH_4^+ in S1 at distances of 2.50 and 2.84 Å from oxygen atoms of the nearest two water molecules, at distance 3.46 Å from atom CE2 of Phe107, and at distance 3.82 Å from atom CE2 of Trp148. We thus apply a potential of 5 kcal/mol/Å^2 at distances higher than 3.0 Å between the CM of the ion (Na^+, K^+, or NH_4^+) and the oxygen atoms of the two constructed polarizable water molecules. A similar potential is applied at distances larger than 4.5 Å between the CM of the ion and atom CE2 of Phe107 or Trp148. Ammonium in S2 of the 1U7G structure is 3.44 Å away from atom NE2 of His168 and 4.17 Å away from atom NE1 of Trp212. A similar potential is thus applied at distances larger than 4.0 and 5.0 Å between the CM of NH_4^+ and atoms NE2 of His168 and NE1 of Trp212, respectively.

4.3. Results and Discussion

4.3.1. Geometry optimization

The labeling diagram of all compounds used in this work is reported in figure 4.5. Table 4.1 lists the BSSE-corrected and uncorrected interaction energies in all optimized complexes as well as the interaction energies obtained from the optimized polarizable potential models (see section 4.3.3).

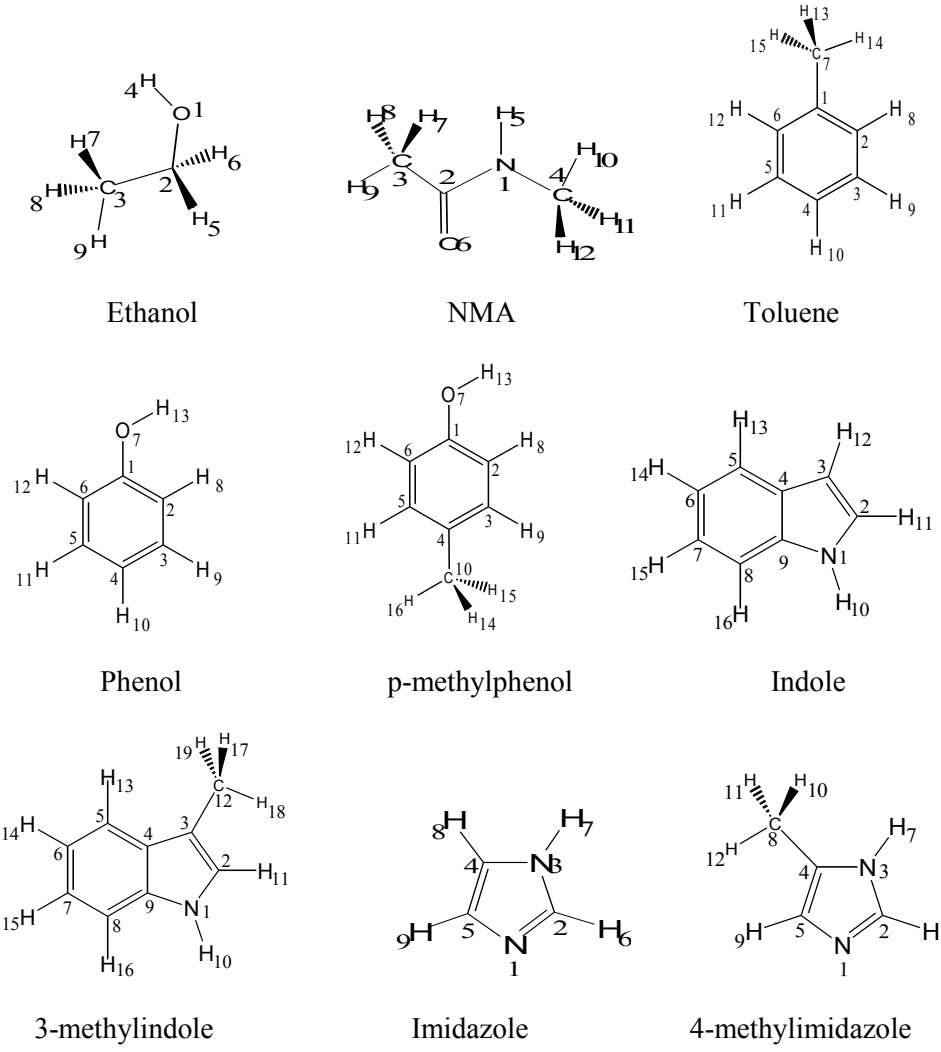

Figure 4.5. Labeling diagram of 9 studied compounds interacting with Na^+, K^+, and NH_4^+.

Table 4.1. BSSE corrected and uncorrected complexation energies (E^{CP} and E, respectively, in kcal/mol) and the interaction energies calculated by the optimized potential models (E^{MM}, in kcal/mol).

Molecule		Na^+			K^+			NH_4^+		
		E	**E^{CP}**	**E^{MM}**	**E**	**E^{CP}**	**E^{MM}**	**E**	**E^{CP}**	**E^{MM}**
Ethanol		–27.64	–26.48	–26.48	–21.31	–20.21	–20.21	–27.00	–25.02	–24.94
NMA		–39.15	–38.25	–38.25	–31.48	–30.36	–30.40	–39.10	–36.92	–36.95
Toluene		–25.77	–22.96	–22.98	–21.25	–18.79	–18.80	–21.45	–18.92	–19.06
Phenol	**1**	–26.16	–24.46	–22.25	–21.52	–19.59	–17.42	–24.90	–22.41	–19.30
	2	–24.49	–21.75	–22.30	–20.37	–18.01	–18.14	–20.67	–18.08	–18.64
p-methylphenol	**1**	–27.60	–25.97	–24.98	–22.89	–21.04	–19.02	–26.24	–23.82	–21.52
	2	–26.05	–23.37	–23.85	–21.96	–19.45	–20.26	–22.35	–19.71	–20.24
Indole		–30.45	–27.48	–27.40	–25.75	–23.22	–23.24	–26.80	–24.06	–24.06
3-methylindole		–31.48	–28.51	–28.55	–26.83	–24.08	–24.10	–27.45	–24.60	–24.60
Imidazole		–36.33	–35.28	–35.29	–28.28	–27.09	–27.10	–34.14	–32.61	–32.62
4-methylimidazole		–38.42	–37.37	–37.40	–30.08	–28.86	–28.90	–36.19	–34.62	–34.65

Geometry optimization of Na^+, K^+, and NH_4^+ complexes with the 9 studied compounds is done starting from different plausible initial conformations. The optimized minimum energy conformers of Na^+ and K^+ in complex with all ligands possess the same features. The optimized geometries of the complexes of both ions are thus reported together in figure 4.6 with parameters for K^+ in brackets.

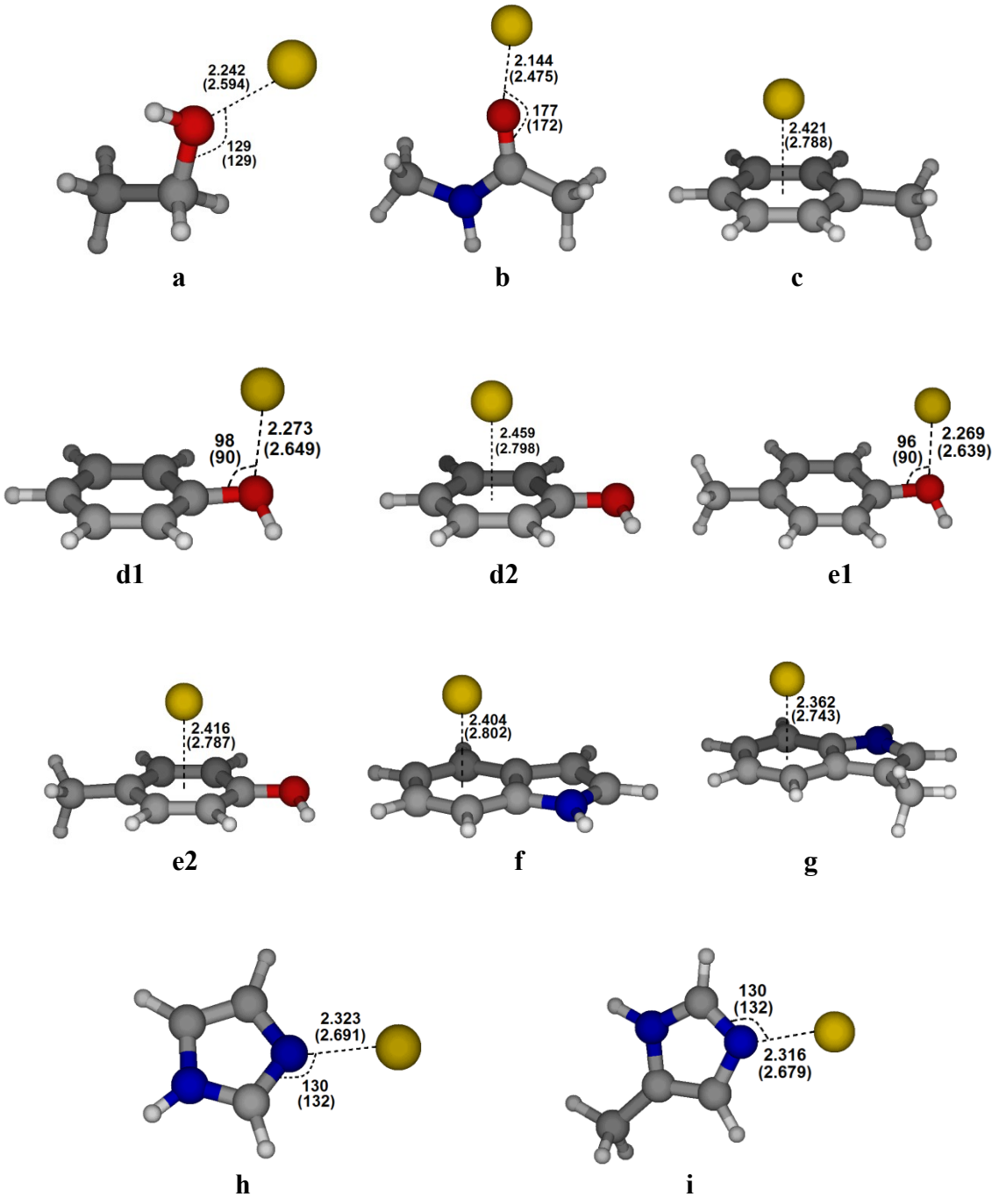

Figure 4.6. Optimized geometries for the complexes of Na^+ and K^+ (values in parentheses) with **a**, ethanol; **b** NMA; **c**, toluene; **d**, phenol; **e**, p-methylphenol; **f**, indole; **g**, 3-methylindole; **h**, imidazole; and **i**, 4-methylimidazole.

Na^+ and K^+ ions bind preferably to electronegative oxygen and nitrogen atoms, but are involved in strong cation–π interactions as well (see figures 4.6 **c**, **d2**, **e2**, **f**, and **g**). Table 4.1 shows that the interaction energies of K^+ complexes are less than the corresponding Na^+ complexes. This is due to the increase in intermolecular distance between the ion and the interacting ligand as the size of the ion increases.

Optimized geometries of NH_4^+ complexes are given in figure 4.7. These complexes are characterized by intermolecular bond distances between N of NH_4^+ and the center of the six-membered ring or the interacting hetero atom being similar to those in the corresponding K^+ complexes. The similarity in the intermolecular distances of the two ions is due to the similar sizes of the two cations. Complexes of NH_4^+ with ethanol, NMA, imidazole, 4-methylimidazole, and the global minimum complexes in phenol and p-methylphenol (Figure 4.7 **a**, **b**, **h**, **i**, **d1**, and **e1**, respectively) however are more stable than the corresponding K^+ complexes. The extra stability of these complexes is attributed to the hydrogen bonding between NH_4^+, as H-donor, and the hetero atom in the interacting ligand.

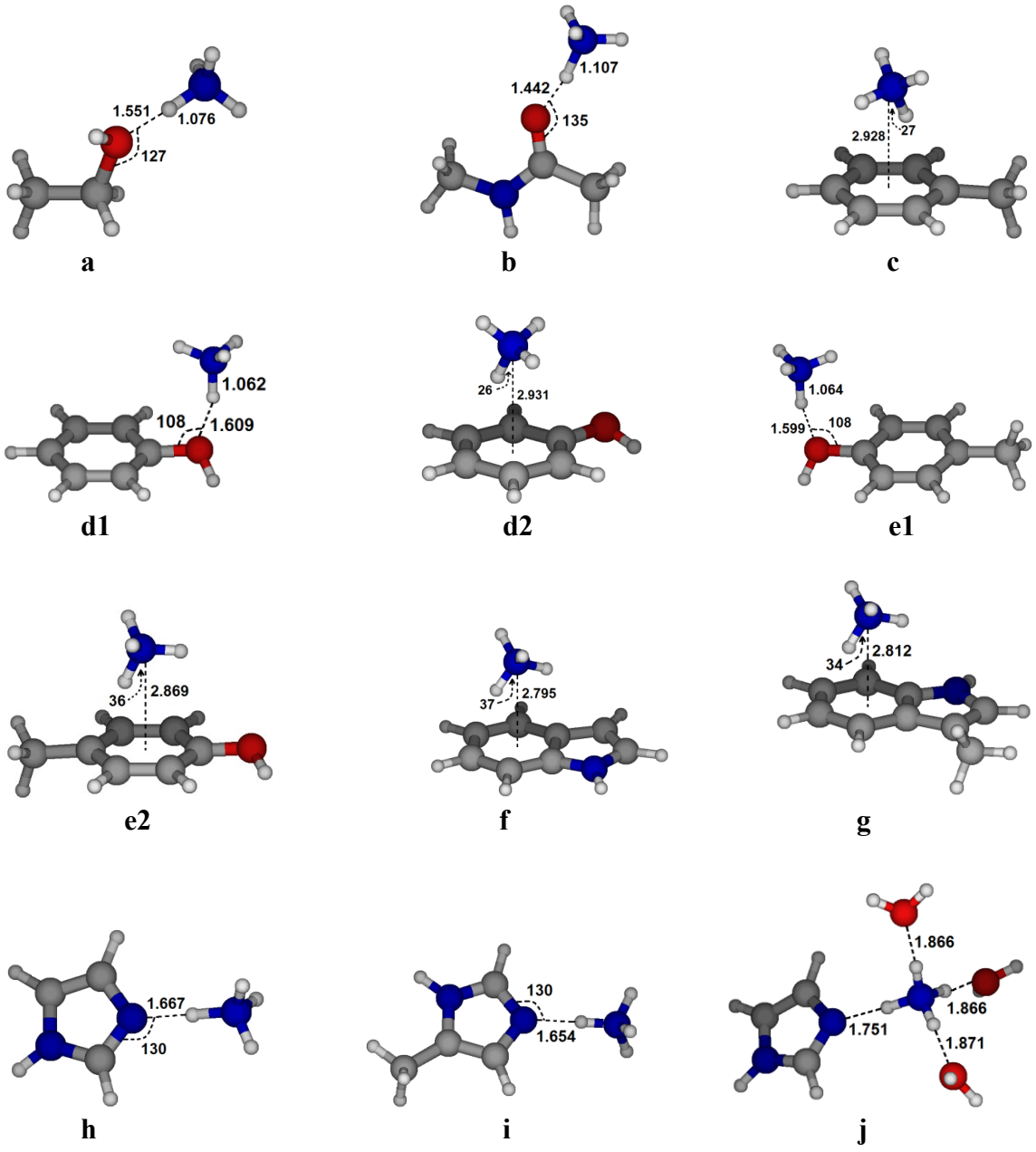

Figure 4.7. Optimized geometries for the complexes of NH_4^+ with **a**, ethanol; **b**, NMA; **c**, toluene; **d**, phenol; **e**, p-methylphenol; **f**, indole; **g**, 3-methylindole; **h**, imidazole; and **i**, 4-methylimidazole. Optimized geometry of the imidazole–$NH_4^+(H_2O)_3$ complex is given in structure **j**.

Only one minimum energy conformer is observed for ethanol, NMA, and toluene complexes with the three cations (see figures 4.6 **a**, **b**, **c** and 4.7 **a**, **b**, **c**). Two minimum energy conformers are found in the interaction of the three cations with phenol and p-methylphenol, with cations interact with O atom in the first (Figure 4.6 **d1**, **e1** and 4.7 **d1**, **e1**) and with the π cloud of the second (Figure 4.6 **d2**, **e2** and 4.7 **d2**, **e2**). As seen in conformers **d1** and **e1** in both figures, the interaction of the ions with O results in bending of the phenolic hydrogen out of the ring plane in the opposite direction of the cation. Table 4.1 shows that interaction of the ions with O results in a more stable conformer compared to interaction with the π cloud, in agreement with previous computational study.[47] Only one minimum energy conformer is found in the interaction of the three cations with indole (Figures 4.6 **f** and 4.7 **f**) and 3-methylindole (Figures 4.6 **g** and 4.7 **g**) with the cation centered on top of the six membered rings and not the five-membered one, in agreement with reported ab initio results.[46] The interaction of the cations with imidazole (Figures 4.6 **h** and 4.7 **h**) and 4-methylimidazole (Figures 4.6 **i** and 4.7 **i**) gives one stable conformer in which the cation interacts with N1 rather than the π-cloud, in accords with previous calculations.[46]

Free optimization of NH_4^+ in complex with imidazole or 4-methylimidazole results in proton transfer from the ion to the interacting ligand. Complexes **h** and **i** in figure 4.7 are therefore obtained by constraining the N−H bonds of NH_4^+ to the gas phase optimized lengths (1.024Å). Though proton transfer occurs readily in the gas phase, such transfer may not occur in aqueous solutions. For example no proton transfer is observed in a free optimization of the complex in which NH_4^+ is hydrogen bonded to imidazole and three water molecules (Figure 4.7 **j**). The constrained optimizations aim to optimize

potential models for NH_4^+ interactions with the two ligands. Interestingly, in all NH_4^+–π complexes (Figure 4.7 **c**, **d2**, **e2**, **f**, and **g**), NH_4^+ is oriented such that N is on top of the center of the six-membered ring (X) with an X···N–H angle in the range 26–37º. This is in agreement with our previous results for the NH_4^+–benzene complex[I], where the global minimum conformer is found between the unidentate and bidentate conformers.

4.3.2. Potential energy surfaces

Ab initio calculated PESs for Na^+, K^+, and NH_4^+ in complex with all studied compounds are reported in figure 4.8 (dashed lines). All curves are calculated by scanning the intermolecular distance between the interacting species between 1.0 Å and 10.0 Å. Curves **(a)** and **(b)** are calculated by scanning the distance between the CM of the ions and O of ethanol and NMA, respectively. Curves **(c)**, **(d)**, **(f)**, **(h)**, and **(i)** are calculated by scanning the distance between the CM of the ion and the center of the six-membered ring in toluene, phenol, p-methylphenol, indole, and 3-methylindole, respectively, with NH_4^+ being oriented in a unidentate conformation. Two other curves (**(e)** and **(g)**) are calculated for the complexes of the three ions with phenol and p-methylphenol, in which the geometry of the complex corresponds to the global minimum conformers and the scan involved the distance between CM of the ion and the O atom. PESs for the cations in complex with imidazole, **(j)**, and 4-methylimidazole, **(k)**, are calculated by the scan of the distance between the CM of the ion and N1 in the interacting ligand.

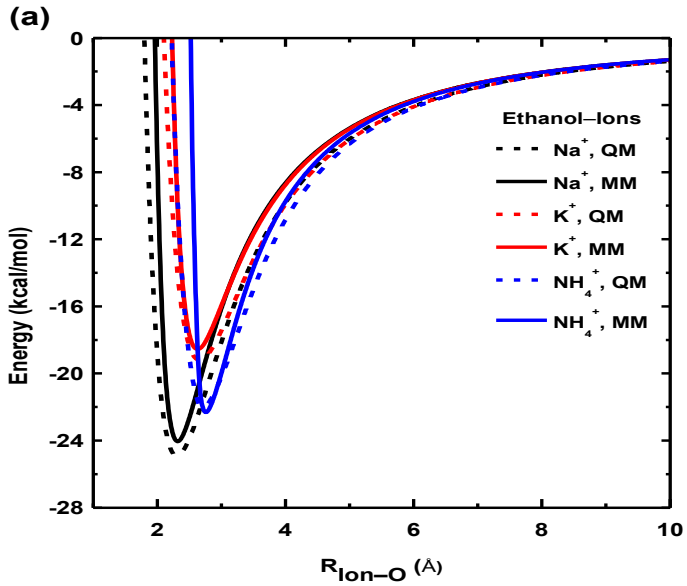
(a)
Energy (kcal/mol)
0
-4
-8
-12
-16
-20
-24
-28
2
4
6
8
10
R Ion–O (Å)
Ethanol–Ions
Na+, QM
Na+, MM
K+, QM
K+, MM
NH4+, QM
NH4+, MM

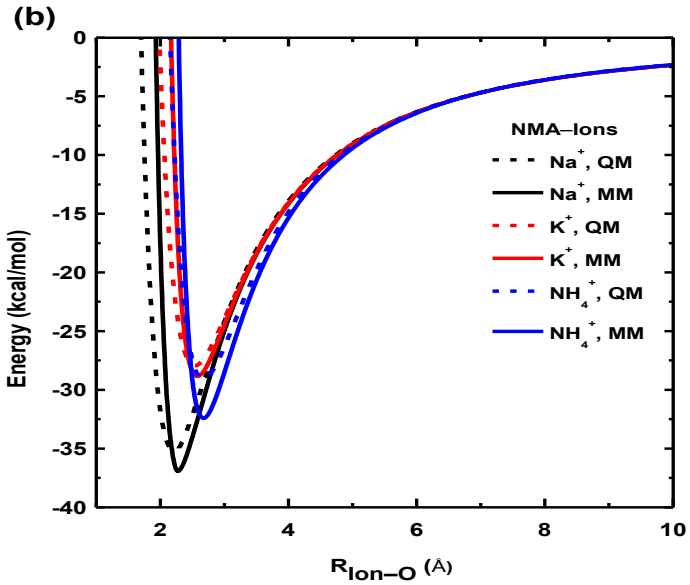
(b)
Energy (kcal/mol)
0
-5
-10
-15
-20
-25
-30
-35
-40
2
4
6
8
10
R Ion–O (Å)
NMA–Ions
Na+, QM
Na+, MM
K+, QM
K+, MM
NH4+, QM
NH4+, MM

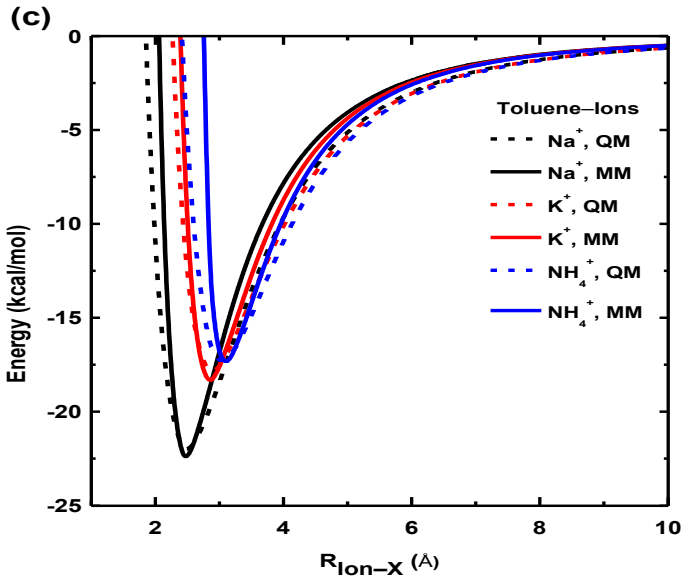
(c)
Energy (kcal/mol)
0
-5
-10
-15
-20
-25
2
4
6
8
10
R Ion–X (Å)
Toluene–Ions
Na+, QM
Na+, MM
K+, QM
K+, MM
NH4+, QM
NH4+, MM

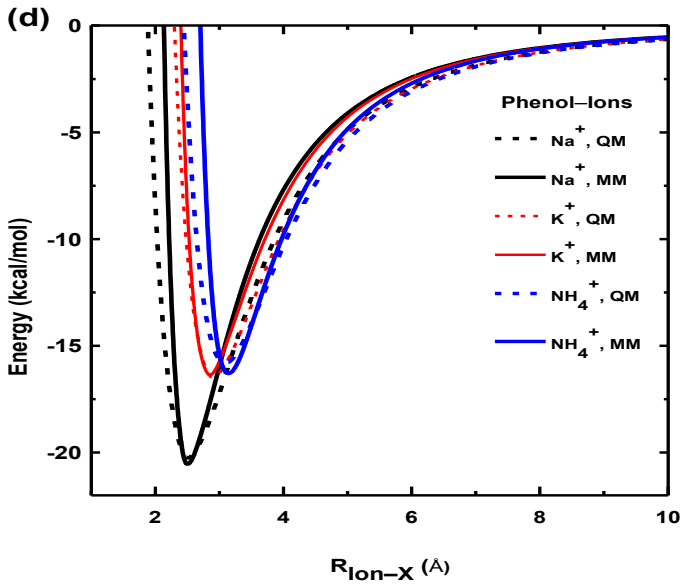
(d)
Energy (kcal/mol)
0
-5
-10
-15
-20
2
4
6
8
10
R Ion–X (Å)
Phenol–Ions
Na+, QM
Na+, MM
K+, QM
K+, MM
NH4+, QM
NH4+, MM

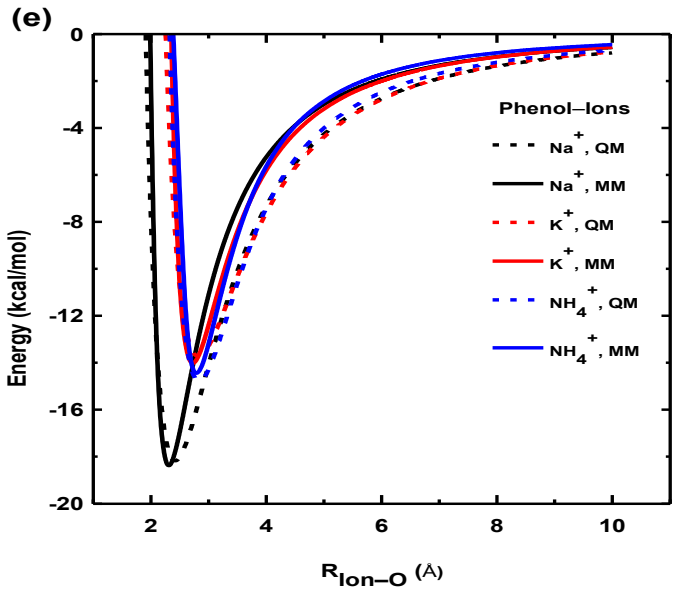
(e)
Energy (kcal/mol)
0
-4
-8
-12
-16
-20
2
4
6
8
10
R Ion–O (Å)
Phenol–Ions
Na+, QM
Na+, MM
K+, QM
K+, MM
NH4+, QM
NH4+, MM

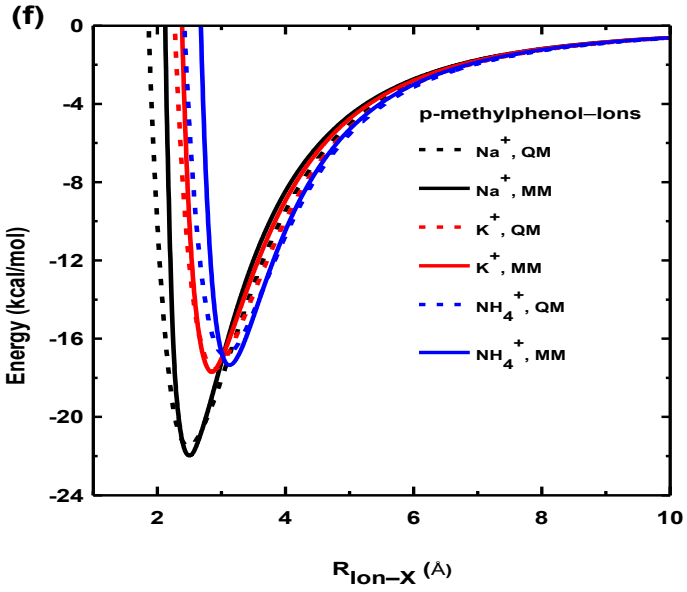
(f)
Energy (kcal/mol)
0
-4
-8
-12
-16
-20
-24
2
4
6
8
10
R Ion–X (Å)
p-methylphenol–Ions
Na+, QM
Na+, MM
K+, QM
K+, MM
NH4+, QM
NH4+, MM

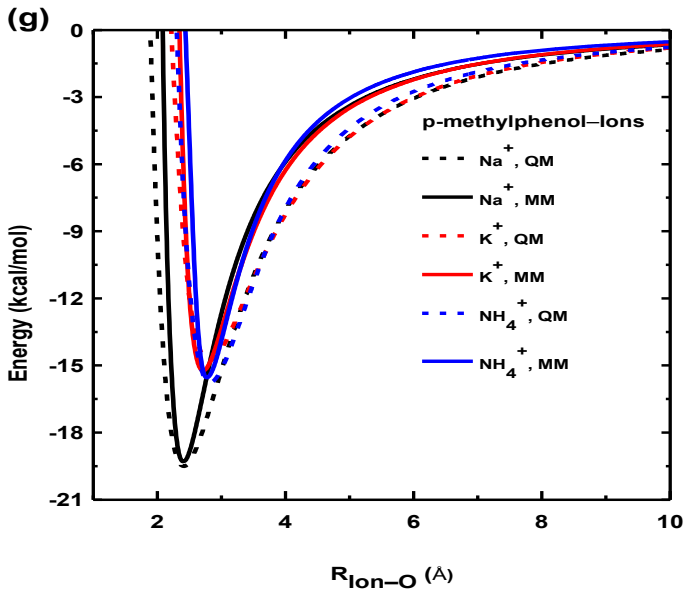
(g)
Energy (kcal/mol)
0
-3
-6
-9
-12
-15
-18
-21
2
4
6
8
10
R Ion–O (Å)
p-methylphenol–Ions
Na+, QM
Na+, MM
K+, QM
K+, MM
NH4+, QM
NH4+, MM

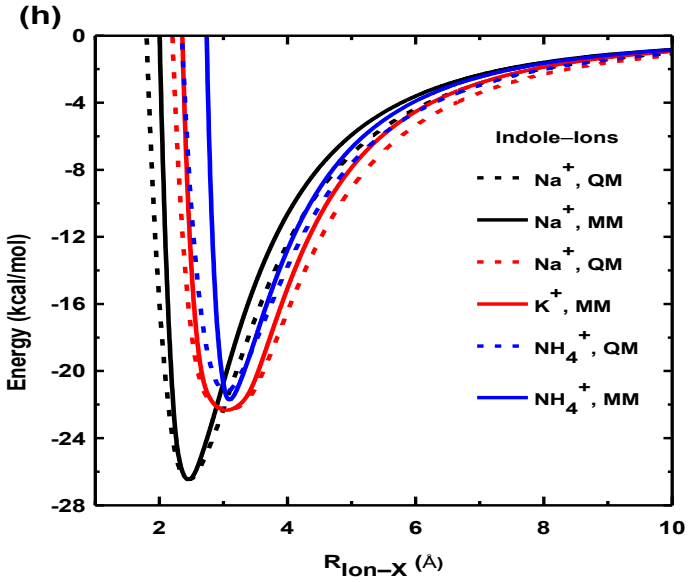
(h)
Energy (kcal/mol)
0
-4
-8
-12
-16
-20
-24
-28
2
4
6
8
10
R Ion–X (Å)
Indole–Ions
Na+, QM
Na+, MM
Na+, QM
K+, MM
NH4+, QM
NH4+, MM

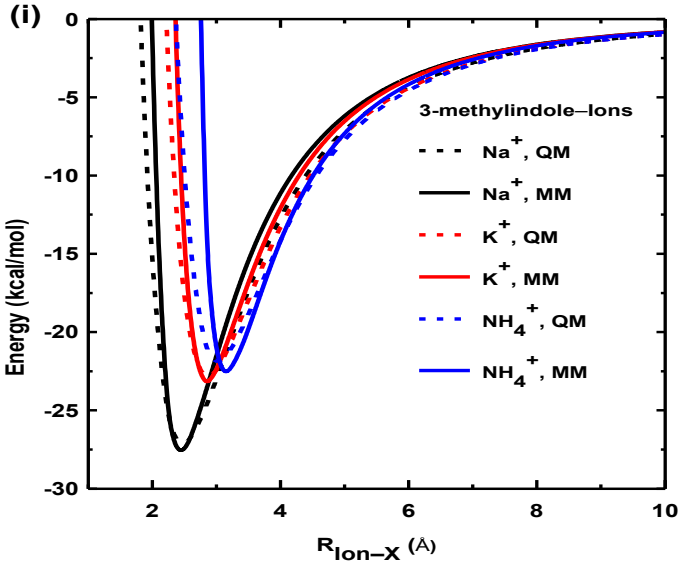
(i)
0
-5
-10
-15
-20
-25
-30
Energy (kcal/mol)
2
4
6
8
10
R Ion–X (Å)
3-methylindole–Ions
Na+, QM
Na+, MM
K+, QM
K+, MM
NH4+, QM
NH4+, MM

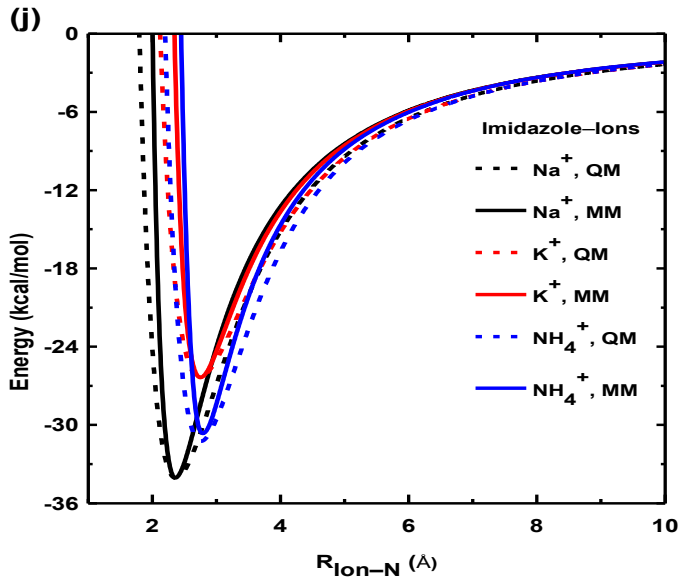
(j)
0
-6
-12
-18
-24
-30
-36
Energy (kcal/mol)
2
4
6
8
10
R Ion–N (Å)
Imidazole–Ions
Na+, QM
Na+, MM
K+, QM
K+, MM
NH4+, QM
NH4+, MM

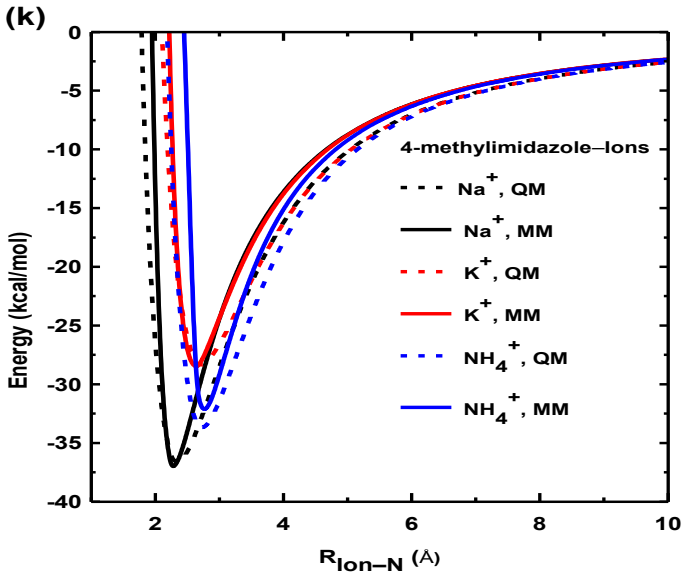

Figure 4.8. Potential energy curves calculated using ab initio MP2/6-311++G(d,p) (dashed lines) and Drude models (solid lines) for: **(a)**, ethanol–M^+; **(b)**, NMA–M^+; **(c)**, toluene–M^+; **(d)** and **(e)**, phenol–M^+; **(f)** and **(g)**, p-methylphenol–M^+, **(h)**, indole–M^+; **(i)**, 3-methylindole–M^+; **(j)**, imidazole–M^+; and **(k)**, 4-methylimidazole–M^+, where M^+ is Na^+, K^+, and NH_4^+.

4.3.3. Optimized force field

Tables 4.2 and 4.3 summarize the optimized pair-specific LJ parameters of the polarizable models. Parameters for NH_4^+–toluene complex are those previously optimized for benzene–NH_4^+ interaction.[I] The optimized parameters for NH_4^+–benzene interaction[I] are found transferable to NH_4^+–toluene complex and no further adjustment is required. Figure 4.8 shows the agreement between the PESs calculated using the optimized models (solid lines) and those from ab initio calculations at MP2/6-311++G(d,p) level of theory (dashed lines), especially near the equilibrium intermolecular distances. Table 4.1 lists the complexation energies of the global minimum conformers obtained using the optimized models (E^{MM}) which are in close agreement with the ab initio BSSE-corrected (E^{CP}) complexation energies. The optimized models for cations interacting with phenol and p-methylphenol however, slightly underestimated the complexation energy of the global minimum conformer (see Table 4.1). The fact that the force field does not reproduce the bending of the phenolic hydrogen observed in ab initio optimization of the cations in complex with O atoms of phenol and p-methylphenol, results in less stable complexes due to electrostatic repulsion between the cations and the phenolic hydrogens.

We also examined the performance of the transferability of the optimized model for NH_4^+–imidazole to the complex of the ion with imidazole and three water molecules. The model gave –23.64 kcal/mol for the complexation energy of $NH_4^+(H_2O)_3$ with imidazole in fair agreement with –21.89 kcal/mol from the ab initio calculations at MP2/6-311++G(d,p).

Table 4.2. Atoms and their types from the 9 interacting ligands and their pair-specific LJ parameters with Na^+ and K^+.

Molecule	Atom, i	Atom type	Pair-specific LJ parameters			
			Na^+		K^+	
			$Emin_{iNa+}$ (kcal/mol)	$Rmin_{iNa+}$ (Å)	$Emin_{iK+}$ (kcal/mol)	$Rmin_{iK+}$ (Å)
Ethanol	O1	OD31A	0.0646602	3.3039910	0.1243324	3.5079747
	C2	CD32A	0.1821140	4.1241884	0.1107728	4.4162018
NMA	O6	OD2C1A	0.1265593	3.1410382	0.1175736	3.5155648
	C2	CD2O1A	0.3200516	4.2791542	0.0927968	4.8724768
Toluene	C1–7	CD2R6A	0.2099100	3.3338282	0.3967730	4.3026690
	X	LP	0.0087380	3.5086672	0.0000000	0.0000000
Phenol	O7	OD31C	0.5611584	2.7723496	1.9813187	2.9146000
	X	LP	0.0088122	4.0595579	0.0054752	4.4594059
p-methylphenol	O7	OD31C	1.9972693	2.6512629	2.6417092	2.8654004
	X	LP	0.0025728	4.4983402	0.0038311	4.5960484
Indole	C5–8	CD2R6A	0.0334734	3.8759811	0.2198221	3.7019494
	C4,9	CD2R6D	0.0334734	3.8759811	0.2198221	3.7019494
3-methylindole	C5–8	CD2R6A	0.0043736	4.5302101	0.1757715	3.7481552
	C4,9	CD2R6D	0.0043736	4.5302101	0.1757715	3.7481552
Imidazole	N1	ND2R5B	0.1802843	3.1905921	0.8180299	3.2755577
	C4,5	CD2R5A	0.1935770	3.6796462	–	–
	C2	CD2R5B	0.1935770	3.6796462	–	–
4-methylimidazole	N1	ND2R5B	0.1937232	3.0987322	0.2187421	3.4183194
	C2	CD2R5B	0.2048993	3.9754195	0.2902294	4.3026690

The dashes indicate that no pair-specific LJ parameters are used; instead the standard mixing rule is applied.

Table 4.3. Atoms and their types from the 9 interacting ligands and their pair-specific LJ parameters with N and H of NH_4^+.

Molecule	Atom, i	Atom type	Pair-specific LJ parameters			
			N		H	
			$Emin_{iN}$ (kcal/mol)	$Rmin_{iN}$ (Å)	$Emin_{iH}$ (kcal/mol)	$Rmin_{iH}$ (Å)
Ethanol	O1	OD31A	0.2387032	4.4784472	0.0056963	2.9830579
	C2	CD32A	0.2485402	4.4784472	–	–
NMA	O6	OD2C1A	0.0268833	4.3252218	0.0004449	2.7216686
	C2	CD2O1A	0.5612547	4.4757974	0.00518658	3.2710700
Toluene[a]	X	LP	0.1470587	3.5000595	0.0060183	3.2808392
Phenol	O7	OD31C	0.4299035	3.4721698	0.0024378	2.7034540
	X	LP	0.0286866	4.5811533	0.0000000	0.0000000
p-methylphenol	O7	OD31C	0.3975307	3.3358123	0.0184439	2.5637375
	X	LP	0.0187195	4.6998372	0.0000000	0.0000000
Indole	C5–8	CD2R6A	0.3072126	3.6967341	0.0122287	3.3760382
	C4,9	CD2R6D	0.3072126	3.6967341	0.0122287	3.3760382
	X	LP	0.6602695	3.1297834	0.0270212	2.9105631
3-methylindole	C5–8	CD2R6A	0.3105234	3.7323063	0.0083613	3.4949277
	C4,9	CD2R6D	0.3105234	3.7323063	0.0083613	3.4949277
	X	LP	0.6632312	2.9908044	0.0271424	2.7715841
Imidazole	N1	ND2R5B	0.1159641	3.9018492	0.0104965	2.7094400
4-methylimidazole	N1	ND2R5B	0.1135793	3.8854367	0.0131107	2.7372252

[a] parameters are taken from interaction with benzene.[I] The dashes in the table indicates that no pair-specific LJ parameters are used; instead the standard mixing rule is applied.

4.3.4. Binding affinity and selectivity of AmtB external site

Amm exists and binds S1 in its ionic form (NH_4^+) under physiological pH conditions.[32,33] In a previous study,[I] we reported the hydration free energy of NH_4^+ relative to H_2O, Na^+, and K^+ which were obtained from TI/MD free energy calculations on ligands dissolved in bulk water and found in agreement with the experimental data. In the current study, we also calculate these relative free energies with the ligands occupying S1 of AmtB and constrained so as not to drift far from the binding site.

Equilibration of the protein with Na^+, K^+, or NH_4^+ in S1 of AmtB using our hybrid polarizable/conventional force field in the absence of restraint potentials is performed for 700 ps. The simulation shows that while Na^+ and K^+ in S1 spontaneously transfer to bulk periplasmic solution, a stable binding of NH_4^+ to S1 is observed. A weak potential was thus imposed on the ion to prevent large drifts from S1, in order to allow for reliable measurements of relative free energies. The measured relative free energies together with those calculated in bulk water[I] are reported in table 4.4. Relative binding free energies, calculated using eq 1, are also reported in table 4.4. On the basis of multiple runs (forward and backward transformations), the overall precision of the calculated relative binding free energies is in the order of ± 0.5 kcal/mol.

Table 4.4. Relative binding free energies (kcal/mol) of NH_4^+ at the external binding site of AmtB.

Mutation	ΔG_{mut}^{prot}	ΔG_{mut}^{wat}	$\Delta\Delta G_{bind} = \Delta G_{mut}^{prot} - \Delta G_{mut}^{wat}$
$H_2O \rightarrow NH_4^+$	–70.9	–61.7	–9.2
$NH_4^+ \rightarrow Na^+$	–9.4	–18.6	9.2
$NH_4^+ \rightarrow K^+$	7.0	–1.2	8.2

The computed relative binding free energies in Table 4.4 indicate that NH_4^+ is 9.2 kcal/mol more stable in S1 compared to bulk water. This value which translates into a sub-micromolar binding constant K = 0.18 μM confirms the high affinity of the external site to the ion. It is consistent with the fact that the protein is expressed when the bacterium is in a nitrogen-poor environment.[32,33] The binding free energies of ammonium ion relative to Na^+ and K^+, 9.2 and 8.2 kcal/mol, respectively, show that the later two ions do not bind S1 and thus do not inhibit the protein activity in agreement with the experimental results.[36–38] The observed relative binding free energies also confirm that S1 is selective for NH_4^+ toward Na^+ and K^+, in agreement with the experimental results.[36–38]

Compared to previous computational studies,[39,40] the observed affinity and selectivity of S1 (current study) provide the best agreement with experimental data. Using ab initio QM/MM simulations Nygaard *et al.*[39] showed that the binding affinity of S1 of AmtB toward Na^+, K^+, and NH_4^+ follows the order $NH_4^+ > Na^+ > K^+$. The authors however reported that only K^+ and NH_4^+ can reach S1, which disagrees with their observed binding affinity trend and disagrees with the fact that K^+ does not inhibit the activity of the protein[36–38] and thus should not reach S1. Luzhkov *et al.*[40] performed MD

and free energy perturbation simulations and reported that S1 is selective for NH_4^+ toward alkali metal ions. The authors however reported binding free energies of K^+, Rb^+, and Cs^+, relative to NH_4^+ that are almost the same, ~2.5 kcal/mol.[40] Their finding indicates that K^+ and Cs^+ possess the same binding affinity toward S1. This does not agree with Javelle *et al.* experimental study[37] in which, in contrast to K^+, Cs^+ is observed to inhibit MA conduction in AmtB, indicating that Cs^+ has higher affinity to S1 compared to K^+. Of all computational investigations on the binding affinity and selectivity of AmtB,[39,40] only the current study utilizes a force field calibrated for the interactions of ions with amino acids near S1 and S2. Calculated binding energies in the current study are thus more reliable as evidenced by the observed affinity and selectivity of S1, in agreement with experimental results.

4.3.5. Binding free energy of NH_4^+ in S2

Equilibration of the simulation system with NH_4^+ occupying S2 in the pore lumen of AmtB protein using the developed hybrid polarizable/conventional force field showed a stable binding of the ion in S2 during the equilibration time period (500 ps). The ion is observed to coordinate the side chains of the amino acids Phe215 and Trp212 through cation–π interactions.[I,46] H-bonding of NH_4^+ and NE2 of His168 and with a water molecule in S3 is also observed.

In order to calculate the binding energy of NH_4^+ to S2, we calculated the free energy accompanying the mutation $H_2O \rightarrow NH_4^+$ in S2. The results are reported in table 4.5. A value of −76.1 kcal/mol is obtained, compared to −70.9 kcal/mol for the mutation performed in S1, which indicates that ammonium ion is 5.2 kcal/mol more stable in S2 compared to S1.

Table 4.5. Relative binding free energies (kcal/mol) of NH_4^+ at the S2 binding site of AmtB.

Mutation	ΔG_{mut}^{prot}	ΔG_{mut}^{wat}	$\Delta\Delta G_{bind} = \Delta G_{mut}^{prot} - \Delta G_{mut}^{wat}$
$H_2O \rightarrow NH_4^+$	–76.1	–61.7	–14.4

This suggests that the ion can reach S2 without deprotonation. The stability of the ion in S2 observed in the equilibration of the system without potential restraints (500 ps) and its stable H-bonded complex with His168 observed in both the equilibration and the free energy simulations suggests that His168 is a probable proton acceptor as previously suggested by Lamoureux *et al.*[157] His168 together with His318 exists in the pore lumen of the AmtB transport channel with their side chains arranged such that a H-bond forms between their δ-nitrogen atoms.[157] These two amino acids are almost conserved in Amm transport proteins which supports the suggested functional role in deprotonation of the ion. The observed proton transfer from NH_4^+ to imidazole or 4-methylimidazole during ab initio optimization of the complexes is also supporting the fact that His168 is a probable proton acceptor and that deprotonation of the ion occurs at S2.

4.4. Conclusion

In this work, we have conducted ab initio QM geometry optimization and PESs calculations on the complexes of Na^+, K^+, and NH_4^+ with 9 compounds (ethanol, N-methylacetamide, toluene, phenol, p-methylphenol, indole, 3-methylindole, imidazole, and 4-methylimidazole). These compounds model the peptide backbone and the side

chains of the amino acids lining the section of the AmtB permeation pathway that is potentially accessible to charged species (Ser, Phe, Trp, and His). Polarizable models for the interaction of the three ions with the studied compounds are optimized based on the ab initio properties of the complexes. A Hybrid polarizable/conventional molecular dynamic simulation protocol has been described for reliable measurements of the binding affinity and selectivity of S1 toward the three ions as well as the binding affinity of S2 to NH_4^+. In the simulation protocol we describe the side chains of the amino acids as well as close water molecules by the parameterized polarizable force field while other interactions are described by a conventional force field. The free energy calculations are showing that S1 is highly selective toward NH_4^+ compared to Na^+ and K^+, in agreement with experiments. The usage of a polarizable force field that is calibrated for the interaction of ions with neighboring species (water or amino acid side chains) results in a reliable calculation of the selectivity of S1 compared to previous computational studies,[39,40] in which conventional noncalibrated force fields have been used. Free energy calculations on NH_4^+ in S2 are showing that the ion is 5.2 kcal/mol, more stable compared to S1, indicating preferable permeation of the ion to S2 rather than deprotonation at the periplasmic entry. The stability of NH_4^+ in S2, its tight coordination to His168, and the fact that ammonium ion readily transfers its proton to imidazole or 4-methylimidazole, suggests that His168 is the proton acceptor. Deprotonation of ammonium is thus suggested to occur at S2 and His168 is proposed as the most probable proton acceptor.

Summary and conclusion

In this work, we have applied ab initio (MP2/6-311++G(d,p)) QM calculations (geometry optimization and potential energy surfaces) in studying the interaction of Li^+, Na^+, K^+, and NH_4^+ with benzene monomer, dimer, and trimer and the interactions in the benzene dimer and trimer. The results are showing that cation–π interactions are strong in the gas phase and that their strength increases with increasing the number π systems.

Ab initio calculations have also been performed on the interaction of NH_3, Na^+, K^+, and NH_4^+ with different compounds (water, ethanol, NMA, toluene, phenol, p-methylphenol, indole, 3-methylindole, imidazole, and 4-methylimidazole) and the interaction of NH_3 with NH_3 and benzene. The optimum geometry of these complexes and their interaction energies are reported and discussed.

We parameterized novel polarizable models for NH_3 and NH_4^+ based on the ab initio calculations on the gaseous monomers and their complexes with water and benzene. Using the ab initio properties of the complexes, we also parameterized polarizable models for the interaction of NH_3, Li^+, Na^+, K^+ ,and NH_4^+ with benzene and for the interaction of NH_3, Na^+, K^+, and NH_4^+ with the other ligands (ethanol, NMA, toluene, phenol, p-methylphenol, indole, 3-methylindole, imidazole, and 4-methylimidazole). We also parameterized a model for NH_3–NH_3 interaction based on the density of liquid ammonia at its boiling point.

The optimized models for NH_3–H_2O and NH_4^+–H_2O interactions reproduce the experimental free energies of hydration of NH_3 and NH_4^+ without further adjustments. The NH_3–NH_3 potential model reproduces the enthalpy of vaporization of liquid

ammonia at its boiling point and the density as well as the structure of the liquid at other thermodynamic conditions without further adjustments. Our MD simulations on cation–π and π–π interactions in water show that of the four cations, only K^+, and NH_4^+ bind benzene in water and that the degree of π–π association increases in presence of the cation.

We applied our optimized models in studying the binding affinity of S1 and S2 of the bacterial ammonium transporter protein AmtB toward NH_4^+ and in studying the selectivity of S1 toward Na^+, K^+, and NH_4^+. For this purpose, we modeled water molecules and the side chains of the amino acids that exist near S1 and S2 by polarizable models. Free energy calculations in S1 show that the site is of high affinity to NH_4^+ and is selective to the ion compared to the biologically abundant Na^+ and K^+ ions. Free energy calculations at S2 showed higher binding energy of NH_4^+ compared to S1 suggesting that the ion does not undergoes deprotonation in S1 but reaches S2 where it can transfer its excess proton to residue His168. We thus suggest S2 as the deprotonation position and His168 as the proton acceptor.

Future work

This project opens various avenues of investigation, such as:

1) A survey of the PDB for cation–π_2 complexes. This aims to investigate the abundance of these complexes and their most probable geometrical arrangements in proteins. Our MD simulations results on NH_4^+(benzene)$_2$ complex in water showed that the most stable complex is one with cation–π–π binding motif. Cation–π_2 complexes in proteins however might adopt different geometries due to different possible environments around the complexes. The investigation of the preferable arrangements of two π systems around an ion and how widespread these complexes are in the protein structures can help to understand their functional roles in proteins and to improve refinement methods for experimentally unresolved protein structures.

2) Understanding the mechanism of salting-out of aromatic hydrocarbons by inorganic salts. Our calculations of the binding affinity between the four ions Li^+, Na^+, K^+, and NH_4^+ and benzene in water expects a decrease in the salting-out in the order $Na^+ > Li^+ > K^+ > NH_4^+$, compared to the experimentally reported order $Na^+ > K^+ > Li^+ > NH_4^+$. The anion might play roles in the mechanism of salting-out. Molecular dynamics simulations of benzene in aqueous solutions of different salts of different concentrations can provide a microscopic picture of the systems that can help investigating the mechanism of salting-out and explain the experimental trend in benzene salting-out.

3) Calculation of the binding free energy of NH_3 relative to that of NH_4^+ in S1. This calculation aims to investigate the selectivity of the periplasmic binding site of AmtB toward the two species. This calculation aims to confirm that NH_4^+ (not NH_3) is the species that binds S1.

4) Calculation of the binding free energy of NH_4^+ in sites S3 and S4 of AmtB. Computational free energy calculations showed that NH_4^+ has to deprotonate at some point in the transport pathway.[42,43] NH_4^+ at S3 or S4 will lose its stabilization due to cation–π interactions with the two stacked side chains of Phe107 and Phe215. The ion is thus expected to be more stable at S2 compared to S3 or S4, and S2 is the most probable position for deprotonation of the ion. Identification of the relative stability of the ion at the different crystallographically identified binding sites in the pore lumen of the channel (S2, S3, and S4) will help to confirm the deprotonation position and the identity of the proton acceptor.

References

(1) Dougherty, D. A. *Science* **1996**, 271, 163–168.

(2) Müller-Dethlefs K.; Hobza, P. *Chem. Rev*. **2000**, 100, 143–167.

(3) Schneider, H-J.; Yatsimirsky, A. *Principles and methods in supramolecular chemistry*, John Wiley & Sons Ltd, Chichester, England **2000**.

(4) Gromiha, M. M.; Santhosh, C.; Ahmad, S. *Int. J. Biolog. Macromol.* **2004**, 34, 203–211.

(5) Prajapati, R. S.; Sirajuddin, M.; Durani, V.; Sreeramulu, S.; Varadarajan, R. *Biochemistry* **2006**, 45, 15000–15010.

(6) Tayubi, I. A.; Sethumadhavan, R. *Biochemistry-Moscow* **2010**, 75, 912–918.

(7) Wintjens, R.; Lievin, J.; Rooman, M.; Buisine, E. *J. Mol. Biol.* **2000**, 302, 395−410.

(8) Lummis, S. C. R.; Beene, D. L.; Harrison, N. J.; Lester, H. A.; Dougherty, D. A. *Chem. Biol*. **2005**, 12, 993–997.

(9) Cheng, JG.; Luo, XM.; Yan, XH.; Li, Z.; Tang, Y.; Jiang, HL.; Zhu, WL. *Sci. China Ser. B: Chem*. **2008**, 51, 709–717.

(10) Zacharias, N.; Dougherty, D. A. *Trends Pharmacol. Sci*. **2002**, 23, 281–287.

(11) Bellsolell, L.; Prieto, J.; Serrano, L.; Coll, M. *J. Mol. Biol.* **1994**, 238, 489–495.

(12) Sussman, J. L.; Harel, M.; Frolow, F.; Oefner, C.; Goldman, A.; Toker, L.; Silman, I. *Science* **1991**, 253, 872–879.

(13) Mecozzi, S.; West, A. P.; Dougherty, D. A. *J. Am. Chem. Soc.* **1996**, 118, 2307−2308.

(14) Cubero, E.; Luque, F. J.; Orozco, M. *Proc. Natl. Acad. Sci. U.S.A.* **1998**, 95, 5976–5980.

(15) Soteras, I.; Orozco, M.; Luque, F. J. *Phys. Chem. Chem. Phys.* **2008**, 10, 2616−2624.

(16) Tsuzuki, S.; Yoshida, M.; Uchimaru, T.; Mikami, M. *J. Phys. Chem. A* **2001**, 105, 769–773.

(17) Sinnokrot, M. O.; Sherrill, C. D. *J. Phys. Chem. A* **2006**, 110, 10656–10668.

(18) Burley, S. K.; Petsko, G. A. *Science* **1985**, 229, 23–28.

(19) Hunter, C. A.; Singh, J.; Thornton, J. M. *J. Mol. Biol*. **1991**, 218, 837–846.

(20) Rebek, J., Jr. *Chem. Soc. Rev*. **1996**, 25, 255–264.

(21) Brana, M. F.; Cacho, M.; Gradillas, A.; Pascual-Teresa, B.; Ramos, A. *Curr. Pharm. Des*. **2001**, 7, 1745–1780.

(22) Frontera, A.; Quinonero, D.; Garau, C.; Costa, A.; Ballester, P.; Deya, P. M. *J. Phys. Chem. A* **2006**, 110, 9307–9309.

(23) Vijay, D.; Sastry, G. N. *Chem. Phys. Lett.* **2010**, 485, 235–242.

(24) Escudero, D.; Frontera, A.; Quinonero, D.; Deya, P. M. *Chem. Phys. Lett.* **2008**, 456, 257–261.

(25) Drude, P. *Lehrbuch der Optik*; S. Hirzel: Leipzig, **1900**. English translation: *The Theory of Optics*; Drude, P., translated from the German by C. Riborg Mann and Robert A. Mill; Longmans, Green and Co.: New York **1907**.

(26) Lamoureux, G.; Harder, E.; Vorobyov, I. V.; Roux, B.; MacKerell, A. D. *Chem. Phys. Lett.* **2006**, 418, 245–249.

(27) Rappe, A.; Casewit, C. J.; Colwell, K. S.; Goddard, W. A.; Skiff, W. M. *J. Am. Chem. Soc*. **1992**, 114, 10024–10035.

(28) Kaminski, G. A.; Stern, H. A.; Berne, B. J.; Friesner, R. A.; Cao, Y. X.; Murphy, R. B.; Ruhong Zhou, r.; Halgren, T. A. *J. Comput. Chem.* **2002**, 23, 1515–1531.

(29) Cieplak, P.; Dupradeau, F-Y.; Duan, Y.; Wang, J. *J. Phys.: Condens. Matter* **2009**, 21, 333102.

(30) Anisimov, V. M.; Lamoureux, G.; Vorobyov, I. V.; Huang, N.; Roux, B.; MacKerell, A. D. *J. Chem. Theory Comput.* **2005**, 1, 153–168.

(31) Lin, Y.; Cao Z.; and Mo, Y. *J. Phys. Chem. B* **2009**, 113, 4922–4929.

(32) Khademi, S.; O'Connell, J.; Remis, J.; Robles-Colmenares, Y.; Miericke, L. J. W.; Stroud, R. M. *Science* **2004**, 305, 1587–1594.

(33) Zheng, L.; Kostrewa, D.; Berneche, S.; Winkler, F. K.; Li, X. D. *Proc. Natl. Acad. Sci. U.S.A*. **2004**, 101, 17090–17095.

(34) Andrade, S. L. A.; Dickmanns, A.; Ficner, R.; Einsle, O. *Proc. Natl. Acad. Sci. U.S.A.* **2005**, 102, 14994–14999.

(35) Lamoureux, G.; Klein, M. L.; Berneche, S. *Biophys. J.* **200**7, 92, L82–L84.

(36) Ninnemann, O.; Jauniaux, J. C.; Frommer, W. B. *EMBO J.* **1994**, 13, 3464–3471.

(37) Javelle, A.; Lupo, D.; Ripoche, P.; Fulford, T.; Merrick, M.; Winkler, F. K. *Proc. Natl. Acad. Sci. U.S.A.* **2008**, 105, 5040–5045.

(38) Ludewig, U.; von Wiren, N.; Frommer, W. B. *J. Biol. Chem.* **2002**, 277 13548−13555.

(39) Nygaard, T. P.; Alfonso-Prieto, M.; Peters, G. H.; Jensen, M. O.; Rovira, C. *J. Phys. Chem. B* **2010**, 114, 11859–11865.

(40) Luzhkov, V. B.; Almlof, M.; Nervall, M.; Aqvist, J. *Biochemistry* **2006**, 45, 10807–10814.

(41) Fong, R. N.; Kim, K. S.; Yoshihara, C.; Inwood, W. B.; Kustu, S. *Proc. Natl. Acad. Sci. U.S.A.* **2007**, 104, 18706–18711.

(42) Lin, Y. Cao, Z. Mo, Y. *J. Am. Chem. Soc.* **2006**, 128, 10876–10884.

(43) Bostick, D. L.; Brooks, C. L. *PLoS Comput. Biol.* **2007**, 3, 0231–0246.

(44) Javelle, A.; Lupo, D.; Zheng, L.; Li, X-D.; Winkler, F. K.; Merrick, M. *J. Biol. Chem.* **2006**, 281, 39492–39498.

(45) Ma, J. C.; Dougherty, D. A. *Chem. Rev.* **1997**, 97, 1303–1324.

(46) Mecozzi, S.; West, A. P.; Dougherty, D. A. *Proc. Natl. Acad. Sci. U.S.A.* **1996**, 93, 10566–10571.

(47) Gallivan, J. P.; Dougherty, D. A. *Proc. Natl. Acad. Sci. U.S.A.* **1999**, 96, 9459−9464.

(48) Armentrout, P. B.; Rodgers, M. T. *J. Phys. Chem. A* **2000**, 104, 2238–2247.

(49) Amicangelo, J. C.; Armentrout, P. B. *J. Phys. Chem. A* **2000**, 104, 11420–11432.

(50) Amunugama, R.; Rodgers, M. T. *J. Phys. Chem. A* **2002**, 106, 5529–5539.

(51) Amunugama, R.; Rodgers, M. T. *J. Phys. Chem. A* **2002**, 106, 9092–9103.

(52) Amunugama, R.; Rodgers, M. T. *J. Phys. Chem. A* **2002**, 106, 9718–9728.

(53) Ruan, C. H.; Yang, Z. B.; Hallowita, N.; Rodgers, M. T. *J. Phys. Chem. A* **2005**, 109, 11539–11550.

(54) Amunugama, R.; Rodgers, M. T. *Int. J. Mass Spectrom.* **2003**, 227, 339–360.

(55) Amunugama, R.; Rodgers, M. T. *Int. J. Mass Spectrom.* **2003**, 222, 431–450.

(56) Amunugama, R.; Rodgers, M. T. *Int. J. Mass Spectrom.* **2003**, 227, 1–20.

(57) Ruan, C. H.; Yang, Z. B.; Rodgers, M. T. *Int. J. Mass Spectrom.* **2007**, 267, 233−247.

(58) Woodin, R. L.; Beauchamp, J. L. *J. Am. Chem. Soc.* **1978**, 100, 501–507.

(59) Ruan, C. H.; Rodgers, M. T. *J. Am. Chem. Soc.* **2004**, 126, 14600–14610.

(60) Wu, R. H.; McMahon, T. B. *J. Am. Chem. Soc.* **2008**, 130, 12554–12555.

(61) Yorita, H.; Otomo, K.; Hiramatsu, H.; Toyama, A.; Miura, T.; Takeuchi, H. *J. Am. Chem. Soc.* **2008**, 130, 15266–15267.

(62) Wouters, J. *Prot. Sci.* **1998**, 7, 2472–2475.

(63) Fedushkin, I. L.; Lukoyanov, A. N.; Hummert, M.; Schumann, H. *Russ. Chem. Bull.* **2007**, 56, 1765–1770.

(64) Meadows, E. S.; De Wall, S. L.; Barbour, L. J.; Gokel, G. W. *J. Am. Chem. Soc.* **2001**, 123, 3092–3107.

(65) Barbour, L. J.; De Wall, S. L.; Meadows, E. S.; Gokel, G. W. *Ind. Eng. Chem. Res.* **2000**, 39, 3436–3441.

(66) Meotner, M.; Deakyne, C. A. *J. Am. Chem. Soc.* **1985**, 107, 469–474.

(67) Deakyne, C. A.; Meotner, M. *J. Am. Chem. Soc.* **1985**, 107, 474–479.

(68) Hallowita, N.; Carl, D. R.; Armentrout, P. B.; Rodgerst, M. T. *J. Phys. Chem. A* **2008**, 112, 7996–8008.

(69) Caldwell, J. W.; Kollman, P. A. *J. Am. Chem. Soc.* **1995**, 117, 4177–4178.

(70) Aschi, M.; Mazza, F.; Di Nola, A. *J. Mol. Struct.Theochem* **2002**, 587, 177–188.

(71) Estarellas, C.; Escudero, D.; Frontera, A.; Quinonero, D.; Deya, P. M. *Theor. Chem. Acc.* **2009**, 122, 325–332.

(72) Xu, Y. C.; Shen, J. H.; Zhu, W. L.; Luo, X. M.; Chen, K. X.; Jiang, H. L. *J. Phys. Chem. B* **2005**, 109, 5945–5949.

(73) Marshall, M. S.; Steele, R. P.; Thanthiriwatte, K. S.; Sherrill, C. D. *J. Phys. Chem. A* **2009**, 113, 13628–13632.

(74) Mishra, B. K.; Bajpai, V. K.; Ramanathan, V.; Gadre, S. R.; Sathyamurthy, N. *Mol. Phys.* **2008**, 106, 1557–1566.

(75) Coletti, C.; Re, N. *J. Phys. Chem. A* **2006**, 110, 6563–6570.

(76) Feller, D.; Dixon, D. A.; Nicholas, J. B. *J. Phys. Chem. A* **2000**, 104, 11414−11419.

(77) Minoux, H.; Chipot, C. *J. Am. Chem. Soc.* **1999**, 121, 10366–10372.

(78) Crowley, P. B.; Golovin, A. *Proteins: Struct. Funct. Bioinf.* **2005**, 59, 231–239.

(79) Shi, Z. S.; Olson, C. A.; Kallenbach, N. R. *J. Am. Chem. Soc.* **2002**, 124, 3284−3291.

(80) Kumpf, R. A.; Dougherty, D. A. *Science* **1993**, 261, 1708–1710.

(81) Heginbotham, L.; Lu, Z.; Abramson, T.; Mackinnon, R. *Biophys. J.* **1994**, 66 1061–1067.

(82) Sunner, J.; Nishizawa, K.; Kebarle, P. *J. Phys. Chem.* **1981**, 85, 1814–1820.

(83) Sa, R. J.; Zhu, W. L.; Shen, J. H.; Gong, Z.; Cheng, J. G.; Chen, K. X.; Jiang, H. L. *J. Phys. Chem. B* **2006**, 110, 5094–5098.

(84) Costanzo, F.; Della Valle, R. G.; Barone, V. *J. Phys. Chem. B* **2005**, 109, 23016−23023.

(85) Chipot, C.; Maigret, B.; Pearlman, D. A.; Kollman, P. A. *J. Am. Chem. Soc.* **1996**, 118, 2998–3005.

(86) Brooks, B. R.; Brooks, C. L.; Mackerell, A. D.; Nilsson, L.; Petrella, R. J.; Roux, B.; Won, Y.; Archontis, G.; Bartels, C.; Boresch, S.; Caflisch, A.; Caves, L.; Cui, Q.; Dinner, A. R.; Feig, M.; Fischer, S.; Gao, J.; Hodoscek, M.; Im, W.; Kuczera, K.; Lazaridis, T.; Ma, J.; Ovchinnikov, V.; Paci, E.; Pastor, R. W.; Post, C. B.; Pu, J. Z.; Schaefer, M.; Tidor, B.; Venable, R. M.; Woodcock, H. L.; Wu, X.; Yang, W.; York, D. M.; Karplus, M. *J. Comput. Chem.* **2009**, 30, 1545–1614.

(87) Lamoureux, G.; Roux, B. *J. Chem. Phys.* **2003**, 119, 3025–3039.

(88) Frisch, M. J. T., G. W.; Schlegel, H. B.; Scuseria, G. E.; Robb, M. A.; Cheeseman, J. R.; Scalmani, G.; Barone, V.; Mennucci, B.; Petersson, G. A.; Nakatsuji, H.; Caricato, M.; Li, X.; Hratchian, H. P.; Izmaylov, A. F.; Bloino, J.; Zheng, G.; Sonnenberg, J. L.; Hada, M.; Ehara, M.; Toyota, K.; Fukuda, R.; Hasegawa, J.; Ishida, M.; Nakajima, T.; Honda, Y.; Kitao, O.; Nakai, H.; Vreven, T.; Montgomery, Jr., J. A.; Peralta, J. E.; Ogliaro, F.; Bearpark, M.; Heyd, J. J.; Brothers, E.; Kudin, K. N.; Staroverov, V. N.; Kobayashi, R.; Normand, J.; Raghavachari, K.; Rendell, A.; Burant, J. C.; Iyengar, S. S.; Tomasi, J.; Cossi, M.; Rega, N.; Millam, N. J.; Klene, M.; Knox, J. E.; Cross, J. B.; Bakken, V.; Adamo, C.; Jaramillo, J.; Gomperts, R.; Stratmann, R. E.; Yazyev, O.; Austin, A. J.; Cammi, R.; Pomelli, C.; Ochterski, J. W.; Martin, R. L.; Morokuma, K.; Zakrzewski, V. G.; Voth, G. A.; Salvador, P.; Dannenberg, J. J.; Dapprich, S.; Daniels, A. D.; Farkas, Ö.; Foresman, J. B.; Ortiz, J. V.; Cioslowski, J.; Fox, D. J. Gaussian, Inc., Wallingford CT *Gaussian 09, Revision B.01* **2009**.

(89) Boys, S. F.; Bernardi, F. *Mol. Phys.* **1970**, 19, 553–566.

(90) MacKerell, A. D.; Bashford, D.; Bellott, M.; Dunbrack, R. L.; Evanseck, J. D.; Field, M. J.; Fischer, S.; Gao, J.; Guo, H.; Ha, S.; Joseph-McCarthy, D.; Kuchnir, L.; Kuczera, K.; Lau, F. T. K.; Mattos, C.; Michnick, S.; Ngo, T.; Nguyen, D. T.; Prodhom, B.; Reiher, W. E.; Roux, B.; Schlenkrich, M.; Smith, J. C.; Stote, R.; Straub, J.; Watanabe, M.; Wiorkiewicz-Kuczera, J.; Yin, D.; Karplus, M. *J. Phys. Chem. B* **1998**, 102, 3586–3616.

(91) Lopes, P. E. M.; Lamoureux, G.; Roux, B.; MacKerell, A. D. *J. Phys. Chem. B* **2007**, 111, 2873–2885.

(92) Yu, H. B.; Whitfield, T. W.; Harder, E.; Lamoureux, G.; Vorobyov, I.; Anisimov, V. M.; MacKerell, A. D.; Roux, B. *J. Chem. Theory Comput.* **2010**, 6, 774–786.

(93) Ryckaert, J. P.; Ciccotti, G.; Berendsen, H. J. C. *J. Comput. Phys.* **1977**, 23, 327−341.

(94) Lamoureux, G.; Roux, B. *J. Phys. Chem. B* **2006**, 110, 3308–3322.

(95) Deng, Y. Q.; Roux, B. *J. Phys. Chem. B* **2004**, 108, 16567–16576.

(96) Souaille, M.; Roux, B. *Comput. Phys. Commun.* **2001**, 135, 40–57.

(97) Kumar, S.; Bouzida, D.; Swendsen, R. H.; Kollman, P. A.; Rosenberg, J. M. *J. Comput. Chem.* **1992**, 13, 1011–1021.

(98) Khavrutskii, I. V.; Dzubiella, J.; McCammon, J. A. *J. Chem. Phys.* **2008**, 128, 044106.

(99) Soper, A. K. *J. Chem. Phys.* **1994**, 101, 6888–6901.

(100) Bruge, F.; Bernasconi, M.; Parrinello, M. *J. Am. Chem. Soc.* **1999**, 121, 10883−10888.

(101) Marcus, Y. *J. Chem. Soc., Faraday Trans.* **1991**, 87, 2995–2999.

(102) Aqvist, J. *J. Phys. Chem.* **1990**, 94, 8021–8024.

(103) Tissandier, M. D.; Cowen, K. A.; Feng, W. Y.; Gundlach, E.; Cohen, M. H.; Earhart, A. D.; Coe, J. V.; Tuttle, T. R. *J. Phys. Chem. A* **1998**, 102, 7787–7794.

(104) Contreras, R.; Klopman, G. *Can. J. Chem.* **1985**, 63, 1746–1749.

(105) Klots, C. E. *J. Phys. Chem.* **1981**, 85, 3585–3588.

(106) Bennaim, A.; Marcus, Y. *J. Chem. Phys.* **1984**, 81, 2016–2027.

(107) Hallen, D.; Wadso, I.; Wasserman, D. J.; Robert, C. H.; Gill, S. J. *J. Phys. Chem.* **1988**, 92, 3623–3625.

(108) Mcdevit, W. F.; Long, F. A. *J. Am. Chem. Soc.* **1952**, 74, 1773–1777.

(109) Sanemasa, I.; Arakawa, S.; Araki, M.; Deguchi, D. *Bull. Chem. Soc. Jpn.* **1984**, 57, 1539–1544.

(110) Narten, A. H. *J. Chem. Phys.* **1968**, 49, 1692–1696.

(111) Narten, A. H. *J. Chem. Phys.* **1977**, 66, 3117–3120.

(112) Sette, F.; Ruocco, G.; Cunsolo, A.; Masciovecchio, C.; Monaco, G.; Verbeni, R. *Phys. Rev. Lett.* **2000**, 84, 4136–4139.

(113) Giura, P.; Angelini, R.; Datchi, F.; Ruocco, G.; Sette, F. *J. Chem. Phys.* **2007**, 127, 084508.

(114) Bencivenga, F.; Cunsolo, A.; Krisch, M.; Monaco, G.; Ruocco, G.; Sette, F. *J. Chem. Phys.* **2009**, 130, 064501.

(115) Bausenwein, T.; Bertagnolli, H.; David, A.; Goller, K.; Zweier, H.; Todheide, K.; Chieux, P. *J. Chem. Phys.* **1994**, 101, 672–682.

(116) Thompson, H.; Wasse, J. C.; Skipper, N. T.; Hayama, S.; Bowron, D. T.; Soper, A. K. *J. Am. Chem. Soc.* **2003**, 125, 2572–2581.

(117) Chieux, P.; Bertagnolli, H. *J. Phys. Chem.* **1984**, 88, 3726–3730.

(118) Ricci, M. A.; Nardone, M.; Ricci, F. P.; Andreani, C.; Soper, A. K. *J. Chem. Phys.* **1995**, 102, 7650–7655.

(119) Nelson, D. D.; Fraser, G. T.; Klemperer, W. *J. Chem. Phys.* **1985**, 83, 6201–6208.

(120) Tongraar, A.; Kerdcharoen, T.; Hannongbua, S. *J. Phys. Chem. A* **2006**, 110, 4924–4929.

(121) Janeiro-Barral, P. E.; Mella, M. *J. Phys. Chem. A* **2006**, 110, 11244–11251.

(122) Rajamaki, T.; Kallay, M.; Noga, J.; Valiron, P.; Halonen, L. *Mol. Phys.* **2004**, 102, 2297–2310.

(123) Boese, A. D.; Chandra, A.; Martin, J. M. L.; Marx, D. *J. Chem. Phys.* **2003**, 119, 5965–5980.

(124) Kiselev, M.; Kerdcharoen, T.; Hannongbua, S.; Heinzinger, K. *Chem. Phys. Lett.* **2000**, 327, 425–428.

(125) Spirko, V. *J. Mol. Spec.* **1983**, 101, 30–47.

(126) Spirko, V.; Kraemer, W. P. *J. Mol. Spec.* **1989**, 133, 331–344.

(127) Tassaing, T.; Soetens, J. C.; Vyalov, I.; Kiselev, M.; Idrissi, A. *J. Chem. Phys.* **2010**, 133, 214505.

(128) Diraison, M.; Martyna, G. J.; Tuckerman, M. E., *J. Chem. Phys.* **1999**, 111, 1096−1103.

(129) Almeida, T. S.; Coutinho, K.; Costa Cabral, B. J.; Canuto, S. *J. Chem. Phys.* **2008**, 128, 014506.

(130) Hannongbua, S.; Kiselev, M.; Heinzinger, K. *Cond. Mat. Phys*. **2000**, 3, 381–392.

(131) Paul, S.; Chandra, A. *J. Chem. Phys.* **2005**, 123, 174712.

(132) Dang, L. X.; Garrett, B. C. *Chem. Phys. Lett.* **2004**, 385, 309–313.

(133) Raushel, F. M.; Thoden, J. B.; Holden H. M. *Acc. Chem. Res.* **2003**, 36, 539–548.

(134) Wang, X. S.; Roitberg, A. E.; Richards N. G. J. *Biochemistry* **2009**, 48, 12272−12282.

(135) Marini, A. M.; Vissers, S.; Urrestarazu, A.; Andre, B. *EMBO J.* **1994**, 13, 3456−3463.

(136) Marini, A. M.; Urrestarazu, A.; Beauwens, R.; Andre, B. *Trends Biochem. Sci.* **1997**, 22, 460–461.

(137) von Wiren, N.; Gazzarrini, S.; Gojon, A.; Frommer, W. B. *Curr. Opin. Plant Biol.* **2000**, 3, 254–261.

(138) Ludewig, U.; von Wiren, N.; Rentsch, D.; Frommer, W. B. *Genome Biol.* **2001**, 2, 1010.

(139) Weiner, I. D. *Curr. Opin. Nephrol. Hy.* **2004**, 13, 533–540.

(140) Anisimov, V. M.; Vorobyov, I. V.; Roux, B.; MacKerell, A. D. *J. Chem. Theory Comput.* **2007**, 3, 1927–1946.

(141) Harder, E.; Anisimov, V. M.; Whitfield, T. W.; MacKerell, A. D.; Roux, B. *J. Phys. Chem. B* **2008**, 112, 3509–3521.

(142) Lopes, P. E. M.; Lamoureux, G.; Mackerell, A. D. *J. Comput. Chem.* **2009**, 30, 1821–1838.

(143) Nose, S. *J. Chem. Phys.* **1984**, 81, 511–519.

(144) Hoover, W. G. *Phys. Rev. A* **1985**, 31, 1695–1697.

(145) Martyna, G. J.; Tobias, D. J.; Klein, M. L. *J. Chem. Phys.* **1994**, 101, 4177–4189.

(146) Herzberg, G., *Electronic spectra and electronic structure of polyatomic molecules*,Van Nostrand,New York **1966.**

(147) Herbine, P.; Dyke, T. R. *J. Chem. Phys.* **1985**, 83, 3768–3774.

(148) Rodham, D. A.; Suzuki, S.; Suenram, R. D.; Lovas, F. J.; Dasgupta, S.; Goddard, W. A.; Blake, G. A. *Nature* **1993**, 362, 735–737.

(149) Hutchison, C. A.; O'Reilly, D. E. *J. Chem. Phys.* **1961**, 34, 163–166.

(150) de Oliveira, C. A. F.; Hamelberg, D.; McCammon, J. A. *J. Phys. Chem. B* **2006**, 110, 22695–22701.

(151) Osborne, N. S.; Dusen, M. S. V. *J. Am. Chem. Soc.* **1918**, 40, 14–25.

(152) Marini, A. M.; SoussiBoudekou, S.; Vissers, S.; Andre, B. *Mol. Cell. Biol.* **1997**, 17, 4282–4293.

(153) Soupene, E.; Chu, T.; Corbin, R. W.; Hunt, D. F.; Kustu, S. *J. Bacteriol.* **2002**, 184, 3396–3400.

(154) Soupene, E.; He, L. H.; Yan, D. L.; Kustu, S. *Proc. Natl. Acad. Sci. U.S.A.* **1998**, 95, 7030–7034.

(155) Fong, R. N.; Kim, K. S.; Yoshihara, C.; Inwood, W. B.; Kustu, S. *Proc. Natl. Acad. Sci. U.S.A.* **2007**, 104, 18706–18711.

(156) Siewe, R. M.; Weil, B.; Burkovski, A.; Eikmanns, B. J.; Eikmanns, M.; Kramer, R. *J. Biol. Chem.* **1996**, 271, 5398–5403.

(157) Lamoureux, G.; Javelle, A.; Baday, S.; Wang, S.; Berneche, S. *Transfus. Clin. Biol.* **2010**, 17, 168–175.

(158) Bostick, D. L.; Brooks, C. L. *Biophys. J.* **2007**, 92, L103–L105.

(159) Liu, Y. M.; Hu, X. H. *J. Phys. Chem. A* **2006**, 110, 1375–1381.

(160) Nygaard, T. P.; Rovira, C.; Peters, G. H.; Jensen, M. O. *Biophys. J.* **2006**, 91, 4401–4412.

(161) Cao, Z.; Mo, Y.; Thiel, W. *Angew. Chem. Int. Edit.* **2007**, 46, 6811–6815.

(162) Lopes, P. E. M.; Roux, B.; MacKerell, A. D. *Theor. Chem. Acc.* **2009**, 124, 11−28.

(163) Lamoureux, G.; MacKerell, A. D.; Roux, B. *J. Chem. Phys.* **2003**, 119, 5185−5197.

(164) Baker, C. M.; Lopes, P. E. M.; Zhu, X.; Roux, B.; MacKerell, A. D. *J. Chem. Theory Comput.* **2010**, 6, 1181–1198.

(165) Jorgensen, W. L.; Chandrasekhar, J.; Madura, J. D.; Impey, R. W.; Klein, M. L. *J. Chem. Phys.* **1983**, 79, 926–935.

(166) Jo, S.; Kim, T.; Iyer, V. G.; Im, W. *J. Comput. Chem.* **2008**, 29, 1859–1865.

(167) Brooks, B. R.; Bruccoleri, R. E.; Olafson, B. D.; States, D. J.; Swaminathan, S.; Karplus, M. *J. Comput. Chem.* **1983** 4, 187–217.

(168) Schlenkrich, M.; Brickmann, J.; Mackerell, A. D., Jr.; Karplus, M. "Biological membranes: A molecular perspective from computation and experiment" **1996**, 31–81.

(169) Darden, T.; York, D.; Pedersen, L. *J. Chem. Phys.* **1993**, 98, 10089–10092.